Geology and Origin of Mystery Cave

Forestville State Park, Minnesota

TECHNICAL REPORT

LCMR Mystery Cave Resources Evaluation

Arthur N. Palmer
Margaret V. Palmer
1993

Consultant's Report

ACKNOWLEDGMENT:

Funding for this project was approved by the Minnesota Legislature M. L. 91, Chapter 254, Article 1, Section 14, Subd. 3(1), as recommended by the Legislative Commission on Minnesota Resources, from the Future Resources Fund.

GEOLOGY AND ORIGIN OF MYSTERY CAVE

Technical Report

Arthur N. Palmer and Margaret V. Palmer
Department of Earth Sciences
State University of New York
Oneonta, NY 13820-4015

page

CONTENTS

Continued.....

INTRODUCTION

This is the technical portion of the final report for the Legislative Commission on Minnesota Resources (LCMR) project entitled **Mystery Cave Geology Resources Evaluation**, part of the Mystery Cave Resource Evaluation. This project concerns the geology, mineralogy, and origin of Mystery Cave. A summary of these topics in non-technical terms is given in a separate Interpretive Report, and recommendations for further study and management suggestions are given in a separate Management Report. This Technical Report contains a detailed discussion of the results of this study, along with information on quantitative methods, techniques and equipment, analysis of error and of scientific findings, and tables of data. It is intended to supplement the Interpretive Report, which covers many of the discussions in non-technical terms. Future publications (journal articles, etc.) will be based on both the Technical and Interpretive reports.

Two sets of units are used in this report: American and metric. Large distances are in American units because they are most familiar to the reader, and also because the USGS topographic maps of the area are in feet. Metric units are used for small features, for which there are no convenient American units.

Mystery Cave is the largest cave in Minnesota. The two entrances of the cave, as well as land around them, are administered by the state Department of Natural Resources at Forestville State Park, and interpretive tours are run for the public in both sections by DNR staff. The purpose of this report is to enhance the interpretive and management programs of the Park by providing a comprehensive reference to the geology and origin of the cave.

Acknowledgments: Funding for this project was approved by the Minnesota Legislature M. L. 91, Chapter 254, Article 1, Section 14, Subd. 3(l), as recommended by the Legislative Commission on Minnesota Resources, from the Future Resources Fund. Several people helped considerably in the field work for this project. Warren Netherton, Cave Specialist at Mystery Cave, provided inspiration, enthusiasm, and continual support throughout the project. He and his family did a great deal to make our visits memorable. Calvin Alexander and Roy Jameson of the Dept. of Geology and Geophysics at the University of Minnesota generously contributed their ideas and information about the cave. The Mystery Cave staff gave us much encouragement and guided us in searching out the questions that most needed answering. Our sincere thanks to them all.

GEOLOGIC SETTING

Mystery Cave is located in the Central Lowlands geomorphic province, in gently dissected plateaus with a local relief of only 150-200 feet. It has been developed in carbonate rocks of the Stewartville, Dubuque, and Maquoketa Formations of Ordovician age, which have been dissected by Quaternary stream erosion. The cave occupies an entrenched meander in the South Branch of the Root River. Nearly all the water in the river passes underground through the cave and other solution conduits. The region underwent Quaternary glaciation, although the most recent glacial advances fell short of this area. The latest glacial advance into southern Minnesota was the Des Moines ice lobe, whose eastern boundary fell about 40 miles to the west of Mystery Cave. Glacial effects have been significant in the cave area, however. Thick loess (wind-deposited material derived from unvegetated glacial drift) blankets the area to depths up to 25 feet. The cave contains many sediments that appear to have be glacial material carried underground by the South Branch.

The sedimentary rocks at Mystery Cave locally dip toward the west-northwest at about 0.5-0.6 degrees, Most of the underground water flow is against the dip, toward the east and northeast, with a great deal of discordance made possible by prominent joints and faults. The main outlet for water is Seven Springs, located east of the cave at the valley of the South Branch. About 13 miles of passages have been mapped in the cave, nearly all of which have been guided by fractures oriented mainly E-W and NE-SW. NW-SE orientations are also common in the northeastern part of the cave, and a few passages follow rare N-S joints.

FIELD AND LABORATORY METHODS

Interpretation of the cave required detailed geologic mapping, sampling of bedrock and cave deposits, and a variety of field and laboratory techniques. The major techniques are described in detail here, with the data listed in the appendices. Interpretations of the data are given later in this report. Brief summaries are given in the Interpretive Report.

Leveling Survey

For general orientation and preliminary observations, we used the existing map of the cave made by the Minnesota Speleological Survey (a plan view showing survey lines only). To obtain detailed geologic information, we leveled all the major passages in the cave (and some minor ones) with a tripod-mounted Nikon AZ-1 automatic surveyor's level and segmented metric rods. This survey provided very precise vertical measurements, which are essential for a valid geologic interpretation. To obtain horizontal coordinates, bearings were measured with a hand-held SUUNTO compass, and distances were calculated from stadia readings made with the level. The horizontal accuracy was no better than that of the original survey, as slight errors in location are not significant to the interpretation. The vertical accuracy with this method probably exceeds that of any other cave survey (see the following section on survey accuracy). Where it was not possible to use the tripod-mounted level, a hand level and rods were used, along with a fibreglass tape and SUUNTO compass. In the main part of Mystery III, where numerous junctions made precise locations possible from the original map, we obtained the horizontal coordinates directly from the map.

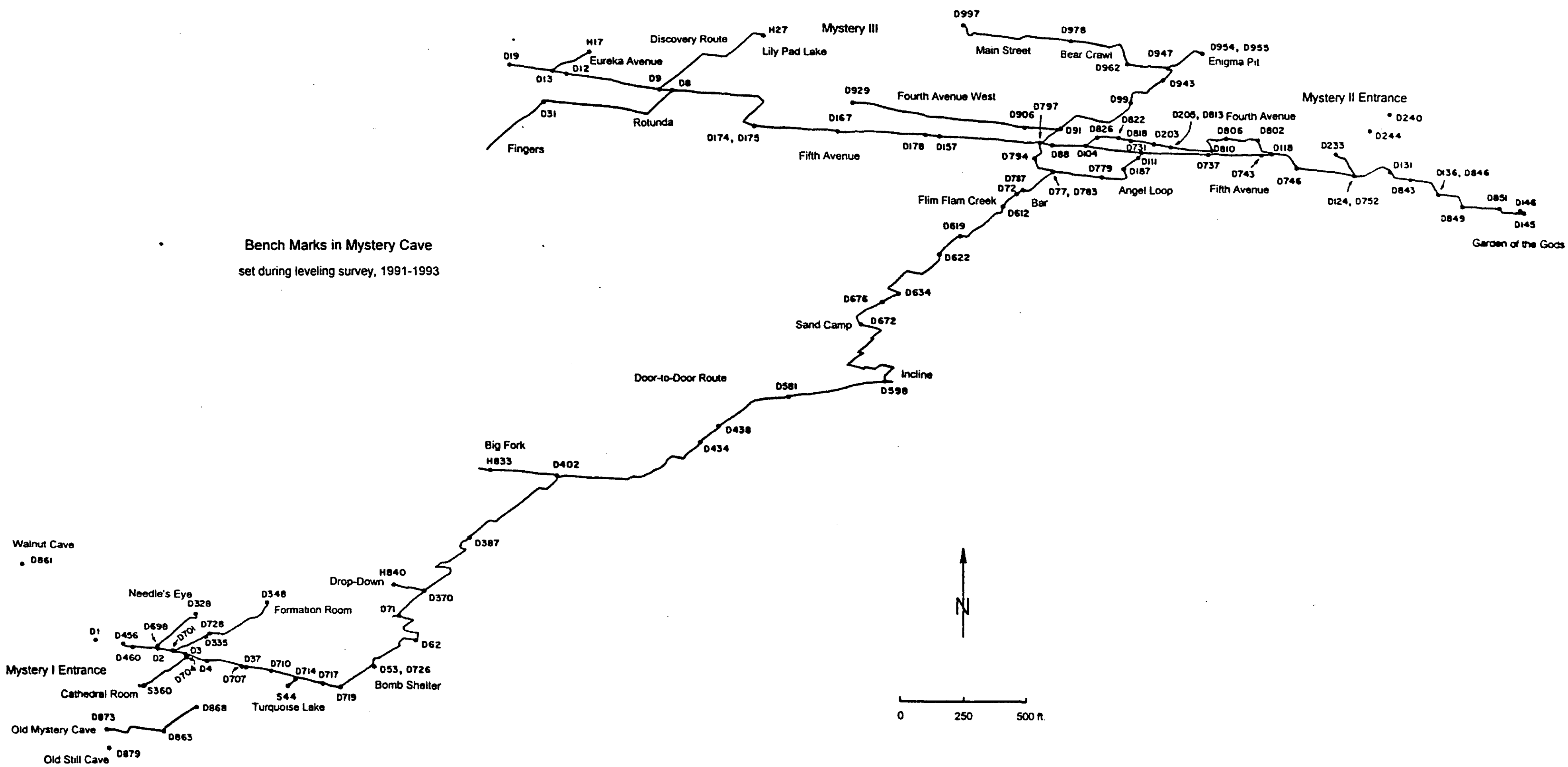

Figure 1: Map of passages included in leveling survey, showing location of bench marks.

Survey notes taken in the cave included sketches of continuous profiles, with pertinent cross sections and descriptive information. At each leveling station we measured upward or downward to the ceiling, floor, bedding planes, geologic contacts, sediment levels, water levels (past and present), and other noteworthy features. Where appropriate for future use, semi-permanent bench marks were established. Most of these were natural features that are unlikely to move, such as the tips of stalagmites. Where natural features were not available, an inconspicuous "+" was chiseled into the bedrock or on breakdown slabs, as requested by DNR. The 112 bench marks are listed in Appendix 1, along with a few other pertinent elevations.

The leveling survey extended through all the public trails in Mystery I and II, plus the Door-to-Door Route and the major passages of Mystery II and III. We also extended the survey to include Old Mystery Cave, other nearby cave entrances, various wells, Grabau Quarry, Seven Springs, and a roadcut along Route 5 that contains the same rocks as those in Mystery Cave. The leveling survey included 851 stations in the cave (not counting bench marks), with a total of 1405 measurements to geologic features. Including surface surveys, the total was about 1200 stations. Figure 1 shows the cave passages that were included in this survey, as well as the location of bench marks. The survey data are summarized in Appendix 2, which omits some of the surface surveys, for which only a summary of the end points is needed.

Accuracy of Leveling Survey

To provide maximum accuracy, the calibration of the tripod-mounted level was frequently checked with a closed loop between two immobile rods on the surface. The instrument was adjusted to eliminate nearly all deviation from the true horizontal (typically to within about 0.02 millimeter/meter), and any residual error was corrected for by multiplying the residual error by the shot length. The surveys consisted of alternate backsights and foresights with the instrument, which tended to cancel any calibration errors; but even so, the length-adjusted corrections were necessary, since the calibration error would cancel entirely only if the sum of the backsight lengths equaled the sum of the foresight lengths, which was not the case in this survey.

The hand level was also frequently calibrated on the surface, and its deviation from horizontal was adjusted to be as close to zero as possible. Although no length-adjusted correction was added, the alternation between foresights and backsights tended to eliminate most of the residual error.

The greatest potential for error is in mis-reading the instrument or forgetting to write down datum changes in the hand-level survey. Fortunately there was an internal check: since we were tying to the various strata in the cave walls, any significant deviations in bed elevations were clearly apparent. Two errors were detected in this way, one in Mystery I near the beginning of our survey (where we mis-read the rod by a whole meter) and one on the Door-to-Door Route, where a one-foot datum change was not recorded. These errors caused blatant discrepancies in the elevations of the beds, and so they were easily detected.

The SUUNTO compass was calibrated to true north by sighting between widely spaced points on the surface and comparing the reading with the actual direction as shown on the 1989 DNR topographic survey of the area. This discrepancy was subtracted from each compass reading. It represents both magnetic declination and compass calibration error.

The tripod-mounted level survey included two closed loops: those between Fifth Avenue and

Angel Loop, and between Fifth Avenue and Fourth Avenue. Closure error was 1.9 mm in the first loop and 0.5 mm in the second loop. There is not enough information to suggest a typical error per unit distance, because the longer loop produced the smaller error. The vertical error is negligible. The horizontal error was about 0.1 percent, which is well within normal cave-surveying tolerances and is quite sufficient for our purposes. Accuracy in the vertical data is critical to the interpretation of the geologic structure and cave origin, whereas the horizontal coordinates do not need such accuracy.

The ultimate test of accuracy was the entrance-to-entrance vertical discrepancy between our leveling survey through the cave and the 1989 DNR survey on the surface. Between the DNR bench marks BM10 by the ticket office at Mystery I and BM15 on a power pole near the Mystery II entrance, the vertical discrepancy between the two surveys was only 0.15 foot (4.6 cm). This close agreement was a surprise even to us, since about half of the underground distance was surveyed with a hand level.

Our calculated altitude for Seven Springs is about 6 feet higher than the DNR topographic survey seems to indicate. We need to repeat our survey, as it is likely that there was a mis-reading of the rod on one of the long-distance shots.

As a further check on the accuracy of the cave survey, we re-leveled many of the main passages in Mystery I and II while placing bench marks. This allowed us to note any discrepancies with the original survey. Replicated values are shown below:

Station	Original elevation (1991)	Resurveyed elevation (1992)	
D1	1230.37	-------	(used as base station)
D3	1218.54	1218.54	
D37	1220.87	1220.86	
D53	1219.15	1219.15	
D72	1212.57	1212.51	(awkward position on ledge)
D111	1217.67	1217.67	
D118	1217.83	1217.82	
D187	1214.32	1214.32	
D233	1251.49	1251.48	
D244	1273.60	1273.60	
D348	1222.96	1222.97	
D456	1228.92	1228.92	

The original figures are considered valid and are the ones shown in the listing of survey coordinates in the appendices.

Computer Analysis of Survey Data

Using a home-made computer program, the leveling surveys were converted to X-Y-Z coordinates (i.e., East-North-Vertical coordinates). Survey lines were plotted in plan views and in both extended and projected profile on a Hewlett Packard 7470A plotter, and details were added from the survey notes. The program also allowed plotting the elevations on specified beds and determining the mean dip and strike of the beds by extending a regression plane through the data. Residuals between the regression plane and the actual survey data could also be plotted. Structural contour maps were also made with the program SURFER (Golden Software, Inc., Golden, CO).

Sampling of Bedrock and Speleothems

Loose chips of bedrock and broken speleothems were obtained in a non-destructive way, leaving no observable damage. Collecting in a cave should be done in the most discrete way possible, and only for projects that will provide a clear benefit to the interpretation of the cave. In some places it was appropriate to break a small chip from a larger already-broken fragment within the cave; however, virtually no visible scars were left in the cave, even on breakdown blocks. Some bedrock samples were obtained by prying small loose blocks from the wall where fresh breakdown had already occurred. No sampling was done of unique or attractive features, or of features which we are not qualified to study (e.g., bacterial filaments).

The entire stratigraphic sequence within cave was sampled bed by bed -- a total of 76 beds. In addition, 57 speleothem chips (5 for radiometric dating) and 4 sediment samples were obtained; the latter are relatively few, as the sediments had already been studied extensively by Milske (1982), and by Milske, Alexander, and Lively (1983).

A few water samples were taken for chemical analysis to correlate with our mineralogical observations. Water chemistry was the main focus of the LCMR hydrology project, and so our geochemical sampling and measurements were done simply to clarify a few mineralogical questions.

Sampling sites for rocks, minerals, and sediments for this study are shown in Appendix 4. The sediment sampling sites of Milske (1982), the Speleothem samples used for U/Th dating by Lively (Milske, Alexander, and Lively, 1983) and for this report are shown in Appendix 9. One complication is that many of our speleothem samples were obtained from dump piles placed at the surface during excavation of fill from Mystery I during trail improvement in 1990-1992. This material consisted mainly of broken fragments that were used during early (pre-DNR) commercialization to fill the large depression at the base of Frozen Falls. However, it is clear that nearly all of that material originated from the floor of the route to the Bomb Shelter, which was excavated during early commercialization to allow easier access to that part of the cave. Figure 30 in Appendix 4 shows these samples in approximately their original location between Turquoise Lake and the Bomb Shelter.

Stratigraphic Mapping

A major purpose of the leveling survey and the bedrock sampling was to determine the stratigraphic section at Mystery Cave. Each bed in the exposed sequence was measured during the survey, and nearly all beds were sampled for analysis. The stratigraphic section (or column) is shown in Figure 2. The location of our bedrock samples in the column is also shown. A similar column containing formation descriptions is included in the Interpretive Report. The rock formations exposed in the cave (Stewartville, Dubuque, and Maquoketa Formations) are shown on the column with the most commonly accepted boundaries. Individual members within the Dubuque (Frankville, Luana, and Littleport) are difficult to distinguish in this area on the basis of field observation alone. The Luana contrasts with the other two members by having a much lower dolomite content (see details in the discussion of stratigraphy elsewhere in this report and in the Interpretive Report).

Individual beds are identified with code names. SX1 through SX3 are granular, crystalline beds near top of Stewartville. DT1 through DT4 are transitional beds at base of the Dubuque, with little or no shale between them. BP1 through BP3 are major bedding planes near the base of the Dubuque. DL1 through DL29 are limestone beds in the Dubuque sandwiched between thin shale beds. DS1 through DS30 are the thin shale beds that separate the limestones in the Dubuque. Individual beds and contacts between beds are identified on the geologic profile by these code names. Contacts are indicated as in the following example: DS11/DS10 = contact between shale bed DS11 and the underlying limestone bed, DL10.

The code names for the thin limestone and shale beds may seem awkward at first, but the advantage is that in the field it is possible to count quickly upward or downward from a known bed, using only the projecting limestones or the recessive shales, without having to keep track of every bed. It is appropriate to interpret each shale/limestone sequence as beginning with an influx of mud into the shallow sea, followed by a quiet period in which limestone is deposited. The alternation between shale and limestone therefore begins with DS1 (the first shale) followed by the corresponding limestone (DL1), then by the next sequence (DS2 and DL2), and so on.

Note that the terms "limestone" and "shale" are used rather liberally in this description. As explained in the sections on interpretation of the bedrock, most of the limestones are highly dolomitic, and most of the shales are a combination of limestone and shale and so are technically limy shales or shaly limestones.

Refraction Seismology

A Bison single-channel signal-enhancement refraction seismometer was used to determine depths to bedrock in the valley of the South Branch of Root River near the Mystery I entrance, as well as a few other locations (see data and interpretations in Appendix 3). To use the instrument, shock waves are generated at the surface in one of several possible ways (we used a sledge hammer on a 1"-thick 8" X 8" aluminum plate). These are detected by a seismometer (geophone) implanted in the soil at varying distances from the shock source. The travel time to the geophone for the first wave arrival is recorded on the cathode-ray tube of the seismograph. By graphing the travel time vs. horizontal distance between the shock source and the geophone, wave velocities through the various underlying materials can be determined (see Figure 3). Best-fitting straight lines are drawn through the data, and their slopes are equal to the inverse of the wave velocity in the various layers beneath the traverse site. Seismic waves travel directly from the hammer to the geophone through the uppermost layer (soil or topsoil). This provides the first straight-line segment on the graph. Wave energy that penetrates deeper into the ground refracts through the underlying layers back to the surface, providing the subsequent line segments on the graph. Layers can generally be detected to a depth no greater than about 1/3 the length of the seismic traverse. With a hammer, the maximum length is about 200 feet (representing a depth of about 60 ft). To detect all layers within this range, each successive layer must have a seismic velocity greater than that of the layer above. The most common sequence is: (a) dry soil, (b) slightly saturated soil, (c) saturated soil (perhaps not present), and (d) bedrock (several layers may be detectable). Each material is slightly more rigid and less compressible than the overlying layer, and so the seismic velocity increases downward.

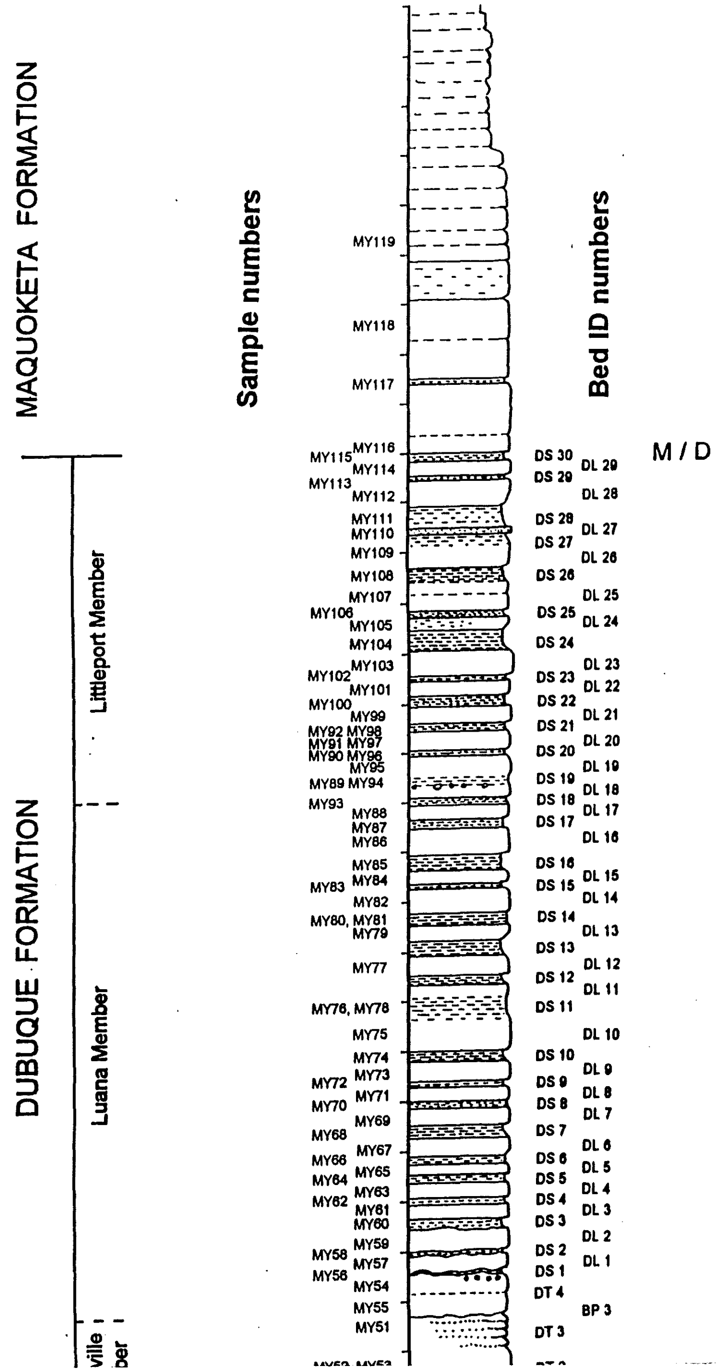
MAQUOKETA FORMATION
DUBUQUE FORMATION
Littleport Member
Luana Member
ville
ber
Sample numbers
Bed ID numbers
M / D
MY119
MY118
MY117
MY115 MY116
MY114
MY113
MY112
MY111
MY110
MY109
MY108
MY107
MY106
MY105
MY104
MY103
MY102
MY101
MY100
MY99
MY92 MY98
MY91 MY97
MY90 MY96
MY95
MY89 MY94
MY93
MY88
MY87
MY86
MY85
MY83 MY84
MY82
MY80, MY81
MY79
MY77
MY76, MY78
MY75
MY74
MY72 MY73
MY70 MY71
MY69
MY68
MY67
MY66 MY65
MY64
MY63
MY62 MY61
MY60
MY59
MY58
MY57
MY56
MY54
MY55
MY51
DS 30 DL 29
DS 29
DL 28
DS 28
DL 27
DS 27
DL 26
DS 26
DL 25
DS 25 DL 24
DS 24
DL 23
DS 23 DL 22
DS 22
DL 21
DS 21
DL 20
DS 20
DL 19
DS 19
DL 18
DS 18
DL 17
DS 17
DL 16
DS 16
DL 15
DS 15
DL 14
DS 14
DL 13
DS 13
DL 12
DS 12
DL 11
DS 11
DL 10
DS 10
DL 9
DS 9
DL 8
DS 8
DL 7
DS 7
DL 6
DS 6
DL 5
DS 5
DL 4
DS 4
DL 3
DS 3
DL 2
DS 2
DL 1
DS 1
DT 4
BP 3
DT 3

Typical seismic velocities are:

dry soil:	600-2000 ft/sec
saturated soil or sediment:	5000 ft/sec
shale or sandstone:	6000-12,000 ft/sec (depending on compaction or cementation)
limestone:	12,000-17,000 ft/sec
igneous rock:	16,000-22,000 ft/sec
metamorphic rock:	varies a great deal, depending on type of rock
weathered bedrock:	generally about 50-80% of the values for unweathered rock

The depth to the second layer can be determined by the following equation:

$$Depth = \frac{Xc}{2}\sqrt{\frac{V_2 - V_1}{V_2 + V_1}}$$

where X_c = the horizontal position on the graph where the two lines of data intersect, V_1 = velocity of upper layer, and V_2 = velocity of lower layer.

Where more than two layers are present, the above equation is valid only if the top layer is relatively thin. Otherwise a more complicated approach is needed. In nearly all the seismic profiles for this report, only two distinct layers were observed: dry unconsolidated river sediment (or loess) overlying limestone bedrock. The contrast in seismic velocities between these two materials is extreme, and so there was little doubt as to the depth to bedrock, except where the bedrock surface appeared to be disrupted by collapse material or had a highly irregular contact with the overlying unconsolidated material. Irregular contacts (if not too irregular) can be detected as scatter in the data beyond the first line segment. Delays in arrival times represent hollows and early arrivals represent high areas.

Reverse profiles (reverse "shots") are used to detect lateral variations in geology. For example, dipping or sloping contacts can be detected by noting discrepancies in the wave velocities between forward and reverse shots. The contact dips in the direction of the apparent lower velocity. The true velocity is roughly the average of the two apparent velocities, and the dip angle is found by:

$$Dip = 0.5\ [\arcsin\frac{V_1}{V_{2a}} - \arcsin\frac{V_1}{V_{2b}}]$$

where V_{2a} and V_{2b} are the apparent velocities of the lower layer measured in the down-dip and up-dip directions respectively.

The example in Figure 3 shows the results for profile #3, which was in the picnic area across from Mystery I, perpendicular to the South Branch, with the forward shot oriented toward the west. Arrival times for the forward shot are shown as triangles, and for the reverse shot as pluses. Note the prominent break in slope in each of the two sets of data. The initial steep portion represents the direct waves that travel only through the soil or sediment. The more gently sloping portion represents the waves that have refracted through the next layer down (in this case, limestone). Straight lines are drawn through the data. Their point of intersection is X_c, the critical distance, where both the direct and refracted waves arrive simultaneously. For the forward shot, $X_c = 50.5$ ft. For the reverse shot, $X_c = 120 - 70.5 = 49.5$ ft. The slope of the initial line is 0.0009 sec/ft, and the seismic velocity of the upper layer is the inverse of this, or 1110 ft/sec. Using the same technique, the reverse shot gives an upper-layer velocity of 1105 ft/sec. The fact that they are almost exactly the same is not surprising, since they represent the same layer. This is a typical seismic velocity for dry soil or sediment.

The slope of the second line in the forward shot is 0.00009 sec/ft, which gives a bedrock velocity of 11,110 ft/sec. (The numerical similarity to V_1 is coincidental.) The reverse shot gives a slightly lower velocity (8695 ft/sec) for the same layer, apparently because of a slight slope on the sediment/bedrock interface. The average of the two values (9900 ft/sec) is a little low for limestone, but this is undoubtedly a weathered surface that should not have as high a velocity as unweathered limestone. The dip of the interface is only about a degree toward the east.

The depth to bedrock is found in the following way:

$$\textit{Forward shot: Depth} = \frac{50.5}{2}\sqrt{\frac{11110-1110}{11110+1110}} = 22.8\,\textit{ft}$$

The corresponding depth from the reverse shot is 21.8 ft. The calculated depth actually represents the depth at about 0.5 X_c, so the shallower depth for the reverse shot agrees with the fact that the bedrock surface slopes very gently toward the east..

Point A deviates significantly from the straight line. This could be caused simply be scatter, but the regularity of all the other data argues that it is a valid point. This was apparently caused by a slight depression in the bedrock surface, which caused the seismic waves to be delayed by having to travel through a greater distance of low-velocity sediment. The delay is only 0.002 sec, which, with an upper-layer velocity of 1110 ft/sec, represents a depression of only two feet or so (taking into account the fact that the wave is traveling at an angle to the surface). The irregularities on the bedrock surface are not large enough to warrant special attention.

Vibration Study

The same Bison seismometer used in the surface seismic study was also used in the cave to measure the effect of surface disturbances compared to the background level of vibration. This study was not very conclusive because of limited equipment, but in general it showed that normal traffic over the cave produces almost undetectable vibration in comparison with background vibration from drips and other natural sources.

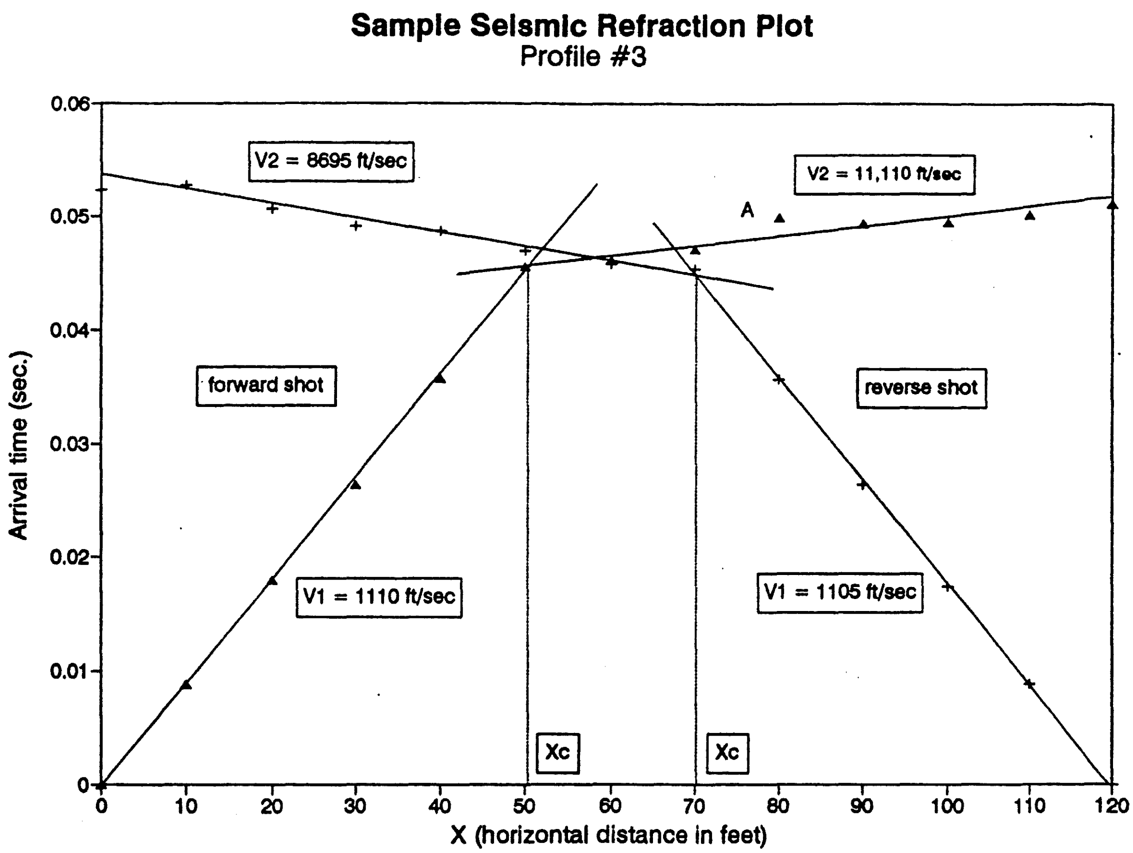

Figure 3: Example of travel-time graph for seismic refraction profiles.

Photography

Black-and-white photographs were made of significant features in the cave, as well as close-up views of samples and photomicrographs of thin section. Kodak T-Max 100 and Tech Pan film were used for all photos. Cave scenes were photographed with a rangefinder Leica M2, and outdoor scenes, close-ups, and microscopic samples were photographed with a single-lens-reflex Leica R4. Only a few of the photos are included in this preliminary version of the LCMR report. The complete collection will appear in the June 1994 version.

Laboratory Preparation of Samples

Rock and mineral samples were first sketched, photographed (if appropriate), and described under binocular microscope at magnifications up to 40X. Fossils, basic structure, and most minerals could be identified by this method. Where appropriate (for about 80% of the samples) the samples were cut by diamond saw into thin slabs and mounted on glass slides with epoxy resin (Buehler epoxide), then sent to a professional lab for thin-section preparation. Delicate samples were first impregnated and embedded in epoxy to prevent disintegration. Mounted slabs are ground by the thin-section laboratory to about 30 microns (0.03 mm) thickness, at which where they are transparent and can be viewed by transmitted light through a microscope.

Thin-Section Analysis

Thin sections were interpreted and photographed with the aid of a petrographic microscope (Leitz model 11, with magnification up to 630X), which provides the option of using polarized or cross-polarized light, which enhances certain images to help in the identification of minerals and their associations. Under the polarizing microscope nearly all minerals could be identified and their interrelationships were clarified. The chemical history of the sample could be fairly clearly interpreted.

A simple but effective method for identifying certain minerals in rock slabs or thin sections is to color them with mineral-specific stains. This is not always necessary, but it provides a quick and easy way of distinguishing the relative abundance and distribution of mineral types within a sample. Alizarine red staining for calcite was used on all thin sections of bedrock to aid in making preliminary distinctions between minerals.

Seventy-three thin sections of rock samples from the cave were made in order to interpret the environment in which the various beds formed, as well as their effect on the cave. Point counts were made to determine the major constituents of each sample. These are done with a mechanical slide holder that moves the sample a given distance in either of two perpendicular directions, so that the entire surface (or a selected portion of it) is divided into a rectangular grid. At each point on the grid, the mineral is noted and recorded. Summing the results gives the percentage of each mineral in the sample.

X-Ray Diffraction

Minerals that are too small to recognize under the polarizing microscope, or whose identity is ambiguous, can be identified by powdering a small sample and determining its X-ray diffraction pattern. A thin layer of powder is placed on a microscope slide and is slowly rotated within an X-ray diffractometer while it is exposed to a beam of X-rays. The rays are scattered by diffraction at given angles (2-theta), and each mineral has a distinctive set of peaks at which the outgoing radiation is most concentrated. Mineral identification is usually quite unambiguous, although certain mineral groups, such as clay, can prove difficult to distinguish. The relative abundance of elements in certain minerals, such as the Mg/Ca ratio in calcite or dolomite, can also be determined. For this study most of the samples were analyzed with a Philips model XRG-3100 X-ray diffractometer.

Scanning Electron Microscopy and Energy-Dispersive X-Ray Analysis

The scanning electron microscope (SEM) is used to examine the surface characteristics of a sample. It produces exquisite photomicrographs. The problem is that only the surface can be viewed, in contrast to the petrographic scope, which allows internal structures to be viewed. Combined with the SEM is an EDX (energy-dispersive X-ray) unit that identifies individual elements within selected parts of the sample. This information complements that from the X-ray diffraction unit. It does not identify the minerals but helps to narrow the range of possibilities and gives information about their impurities. We used an ISI DS-130 scope with Tracor-Northern EDX unit, courtesy of Rick Olson of the Electron Microscopy Laboratory at University of Illinois. So far only two samples have been analyzed in this way: MY 98, a shale in the Dubuque (DS21), to verify the chemical content determined by X-ray analysis, and MY219, a black flowstone chip from the Tar pits, to identify the source of the black stain.

Geochemistry

Water chemistry was not one of the primary goals of this project, since detailed information on the subject is available from the group undertaking the LCMR Hydrology project. However, the major geochemical concepts are described here, and a few measurements of water chemistry were made for this study, because they concern the origin of the cave and its speleothems.

The pH and temperature were measured in selected pools, streams, and drips, as well as in the South Branch of Root River during a moderate flood (April 19, 1993). Calcium and magnesium were measured in the lab by EDTA titration (repeatability to 1-2%). From these four measured variables it is possible to calculate the saturation index (SI) for calcite, aragonite, and dolomite, the equilibrium P_{CO2} of the water, and the molar Mg/Ca ratio. Without a full analysis of the dissolved components the SI and P_{CO2} are not exactly accurate, but the major karst-related attributes of the water and comparisons between water samples are apparent. Data from the thesis by Shiela Grow (1986) were also used to calculate the SI of calcite and dolomite, to show how saturation levels in the river water could affect rates of cave enlargement.

The home-grown Pascal program "SI" was used to determine saturation index with respect to calcite, aragonite, and dolomite, as well as molar Mg/Ca ratio and equilibrium P_{CO2}. Our figures differ slightly from those of the hydrology team because we use slightly different equilibrium constants, and because the SI calculations are more accurate (as shown by significant discrepancies in mass balance with the PC WATEQ program normally used). However, in practice the difference is negligible.

The following sections describe in detail the results and conclusions from the field mapping and laboratory analysis. Only the quantitative and technical aspects are discussed here. A more general discussion is given in the Interpretive Report.

GEOLOGIC PROFILE OF MYSTERY CAVE

The profile of the cave that accompanies these reports consists of 20 11" X 17" sheets. This is an **extended profile**, which stretches out all the bends and allows the surveyed passages to be viewed from the side without the confusion of having segments arranged at various angles to the surface of the page. Each profile sheet contains a plan-view index map of the cave to show where that particular segment of the profile is located. The profile sheets are unbound because of their large format. This facilitates comparison between sheets and also makes it possible to piece them together if desired. Ceilings, floors, major cave features, survey stations, and permanent bench marks are shown, as well as geologic contacts that appear in the cave walls. Only a few selected contacts are shown on the profiles to avoid clutter, but all beds, contacts and bedding planes are shown on the cross sections that accompany the profile. Survey stations are shown as round dots. To avoid clutter, fewer than half are labeled, but the sequence of the unlabeled stations is clear. Survey data and geologic measurements at each station are shown in Appendix 2, along with an explanation of the notation.

The vertical scale of the profile is exaggerated 5 times, to emphasize differences in elevation between various parts of the cave. The cross sections have a 1:1 vertical to horizontal scale -- i.e., they look just the way they do in the cave. The vertical exaggeration of the profile prevents it from looking like a strand of spaghetti, but it does cause some strange effects on local features -- breakdown that looks like the Tower of Pisa, needle-like stalactites, side passages that look far thinner than they really are, and descending fissures that look terrifyingly deep and narrow (an impression that seems all too real to the explorer). For this reason some of the features (particularly breakdown) are drawn with a certain amount of artistic license, reducing their vertical exaggeration to provide a better feel for how they look in the cave.

The vertical exaggeration of the profile also exaggerates the dip of the beds. Do not measure the dip directly from the profile! To find the actual dip between two points, measure the horizontal distance between the points, as well as the elevation difference on a given contact or bedding plane between the same two points. Divide the elevation difference by the horizontal distance and take the arctangent (inv tangent or $\tan^{-1}$ on a calculator) to obtain the true dip. For example, between stations R24 and D37 on Sheet 1 (Mystery I), the horizontal distance is 411 ft and the elevation change on contact DS13/DL12 is 2.3 ft. The apparent angle of dip exposed in this section of the cave is therefore arctan (2.3/411) = 0.32 degrees. Warning: the dip shown on the profile is only an *apparent* dip. That is, where a passage cuts across the beds at some angle other than the true dip direction, the beds exposed in the walls will exhibit a dip, but it will not be the full amount of the dip. For example, if the true dip is to the northwest and a passage is oriented east-west, it cuts across the structure at an angle of 45 degrees to the true dip. The apparent dip (exposed in the walls of the passage) will be only half as great as the actual dip. If the passage is oriented northeast-southwest, as is much of the Door-to-Door Route, the apparent dip will approach zero. In passages that zig-zag in many directions, such as the passage near the Bomb Shelter and toward Enigma Pit, the apparent dip will vary considerably. The apparently radical changes in dip on the section between Fifth Avenue and Enigma Pit (Sheet 15) are caused more by changes in the passage direction than by changes in the dip itself.

STRATIGRAPHIC INTERPRETATION

The rock strata at Mystery Cave and their origin are described in detail in the Interpretive Report. The following section includes the results of the rock analysis, interpretations about the environments in which the rocks were deposited, and their effect on the cave. Refer to Figure 2 and Appendices 4-7 for quantitative details.

Bedrock Composition

The descriptions and map in Appendix 4 show where the bedrock samples were obtained in the field. Their descriptions are given in Appendix 5. Insoluble residue percentages were determined by dissolving part of each sample in dilute hydrochloric acid, weighing the residue, and calculating the weight ratio of the residue to the original sample. This information is also shown in Appendix 5. The grain composition of each bedrock sample was then determined by making point counts of the thin section of each sample (Figure 4). The relative percentages of calcite spar, calcite mud (micrite), dolomite, fossils (mainly calcite), and non-carbonate material (mainly silt and clay) are listed in Appendix 6. Alizarine red stain was used to differentiate calcite from other minerals. Because it was difficult to differentiate stained grains in clay-size material, the percent insoluble residue is a better approximation of the shale content. In a few samples the insoluble residue does not agree with the percent insoluble material measured in thin sections, as shown in Appendix 5, because of local variations in composition within the sample and lower accuracy of identifying insoluble material in thin sections. The insoluble percentage of the Dubuque shale beds varies from 34% in bed DS6 to more than 70% in beds DS14 and DS18 (Figure 5). The Dubuque "shales" are actually limy shales at best, and many of them are simply shaly limestones. This is to be expected, because limestone deposition did not stop when the detrital sediment was being carried into the Ordovician sea. The insoluble content of the limestone beds is much lower. In the Stewartville it ranges from nearly zero up to about 10%. In the Dubuque limestones it ranges from nearly zero up to about 30%. The Maquoketa had a consistently significant insoluble percentage from about 8 to more than 50%. There is one discrepancy in the bed names: the bed we labeled in the field as DL27 (implying that it is a limestone), because of its resistance to weathering compared to the surrounding shales, turned out to have a very high insoluble percentage and is probably better identified as a limy siltstone.

X-ray analysis of insoluble material from the shale beds in the Dubuque shows that it consists mainly of illite (a clay mineral), muscovite (mica), and quartz. The results are shown in Appendix 7. EDX spectra of sample MY98 (bed DS21) showed the presence of Mg, Al, Si, K, Ba and Fe. This corroborated the X-ray analysis. The uniformity of most of the results shows that the erosional source area was rather constant. Montmorillonite, a clay mineral that might indicate the presence of former volcanic ash beds or bentonite, was not found, although some samples have yet to be analyzed. It is possible that accessory minerals will have to be used to identify the bentonites.

Three beds show a significant difference from the others: DS16, DS20, and DS25 (samples MY85, MY90, and MY106). They contain chlorite and kaolinite (also clay minerals) in addition to the other three. It is interesting to note that both DS16 and DS20 have a distinctly gummy texture, weathering almost to the consistency of soft chewing gum. Both are exposed in many places (see geologic profile). Our samples came, respectively, from near the ceiling of the western extension of Fifth Avenue and from the connection in Fourth Avenue between Fat Man's Misery and the Smoking

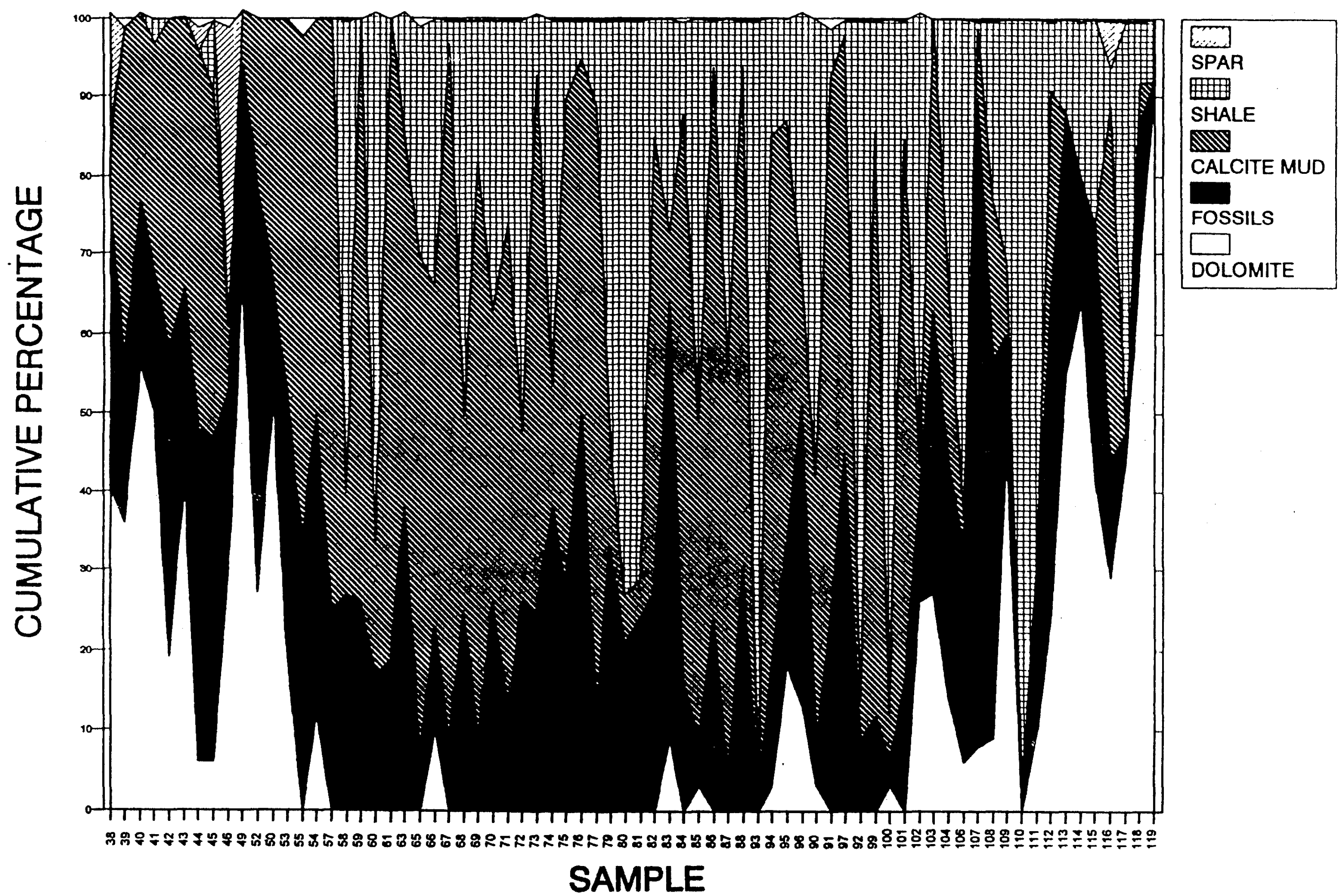

Figure 4: Petrographic characteristics of bedrock samples, based on point-count analysis of thin sections.

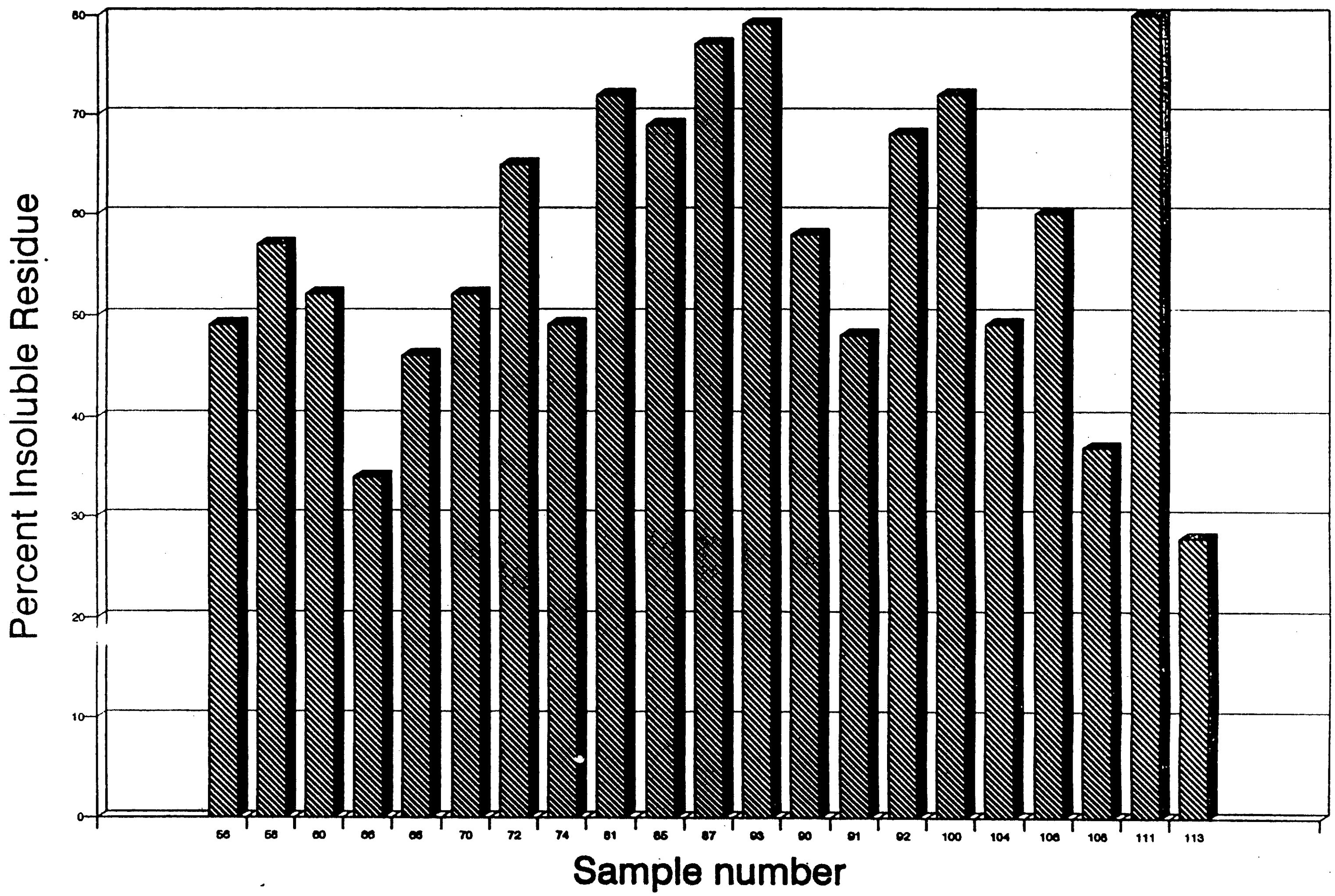

Figure 5: Insoluble residue in shale samples from the Dubuque Formation.

Chamber. Bed DS25 was not sampled only at the cave entrance, but it probably behaves in a similar manner in the moist cave environment.

Interpretation of Environments of Deposition of Bedrock

Figure 6 and Appendix 6 show that dolomite forms a high percentage of the Stewartville Formation and the Frankville Member of the Dubuque Formation. Dolomite crystal sizes average 200 microns (0.2 mm). There is a sharp drop in dolomite percentage at the Luana/Frankville contact at the first distinct shale (DS1). There continues to be a trace amount of dolomite in the Luana and a small amount of rhombic porosity that represents dolomite that has been dissolved from the sample by weathering. Dolomite becomes significant again in the Littleport Member. Dolomite content adds to the meager rationale for subdividing the Dubuque into members. The Maquoketa is even more dolomitic than the Stewartville, with some beds that have been almost completely dolomitized.

Little of the dolomite in the section is detrital (i.e., deposited as sediment grains). Most of it has replaced preexisting limestone carbonate beds. However, some dolomite rhombs at the tops of beds in the Littleport Member appear to be detrital. For example, bed DL26 (as shown by sample MY109) overlies a wave-scoured surface, from which material was ripped off by storm activity and which acquired a wavy surface. Non-dolomitic angular clasts of siliceous clay float in a matrix of dolomite rhombs above the wavy bedding. This juxtaposition suggests that the dolomite was a detrital residue from the eroded layer. A photomicrograph of a typical storm deposit is shown in Figure 7.

The most obvious depositional trend, of course, is the appearance of shale interbeds at the Luana/Frankville contact. Phosphate grains and phosphatized fossils, especially conodonts, appear for the first time and coincide with the influx of shale. Shale and phosphate continue to be common upward through the lower Maquoketa. Fossils are located rather uniformly throughout the column, suggesting that any changes in the geochemical environment controlling the precipitation of dolomite were subtle enough that the fauna were not disrupted. Carbonate mud is also fairly constant, although it gives way to shale in the Maquoketa.

Fossils are one of the chief clues to interpreting the depositional environment. Details are given in the Interpretive Report. The most characteristic feature of the Stewartville is the numerous burrows of the worm *Paleosynapta flaccida*. They are tubular structures about a centimeter in diameter and have been dolomitized. The dolomite is very susceptible to weathering and often leaves holes in the surrounding limestone. However, in many places the burrows protrude into the cave instead of weathering inward. The difference is shown in photographs in the Interpretive Report. Projecting burrows invariably lie below those that weather to holes. This difference is not controlled by stratigraphy, because the transition point migrates up or down following the contours of what seem to have been banks of sediment. Burrows that project outward appear to have been covered at one time by sediment that has since been removed by erosion. The sediment apparently protected the dolomite from weathering. Remnants of sediment can be traced up to the level at which the burrows stop projecting. The cave walls are usually more recessed where the burrows protrude. Burrows stick out on the surface of undercut ledges, implying that water may have been more aggressive to limestone than to dolomite below the sediment cover, where erosional effects would be absent.

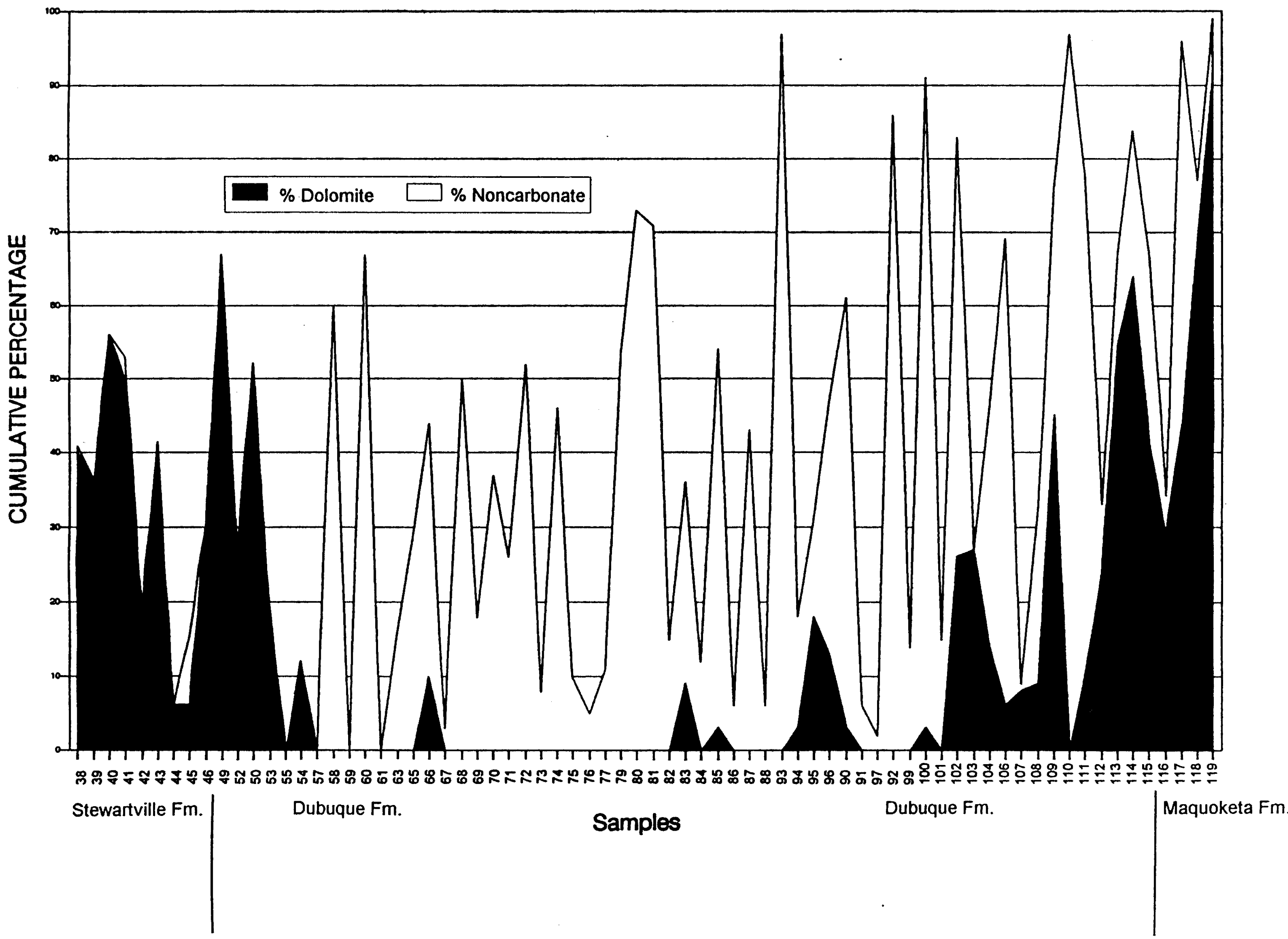

Figure 6: Pecentage of dolomite and non-carbonate fractions in bedrock samples, based on point-count analysis of thin sections.

The burrows tell a great deal about the depositional environment in the Stewartville. Biological disruption of sediment (bioturbation) is typical of quiet water in which nutrients are available. The Stewartville samples contain very little noncarbonate sediment. This corroborates the idea that the Transcontinental Arch to the west of Minnesota lay under water during Stewartville time (see Interpretive Report). The bedrock was initially calcite mud with scattered fossil fragments floating in it -- a texture called wackestone (pronounced "wackystone"!). The burrows are secondary and have disturbed the original texture of the sediment. Bedding-plane partings are rare in the Stewartville and those that do occur they are discontinuous, probably because of the burrowing activity.

Although the dolomite is concentrated in the burrows, its contact with the surrounding calcite mud is gradational. The dolomite clearly cuts across mud and fossil fragments alike (Figure 8). It not only occurs in the burrows but also is found associated with small clusters of other fossils. It is common for dolomite rhombs (parallelogram-shaped crystals) to cut across both fossils and surrounding limestone matrix, with the edge of the crystal faces perfectly intact where they project into the matrix. This shows that the dolomite was not transported into the area (which would have abraded the grains) but instead formed soon after the burrows, after the sediment was completely deposited. All of the dolomite is rich in iron oxide derived from former pyrite. Most of the iron oxide is amorphous (has no crystal structure), but in a few places it is pseudomorphic after pyrite cubes (i.e., it takes on the shape of former pyrite crystals). Weathering caused the burrows to become yellow-brown as the pyrite was oxidized to the iron oxide minerals limonite and hematite. In weathered samples, many of the dolomite crystals are surrounded by porous zones that allow the crystals to fall out easily, which makes the burrows less resistant than the surrounding rock (Figure 9). Dolomite in the burrows is cloudy with dark filamentous inclusions which appear to be organic. The burrows apparently represented a stagnant reducing environment. It is highly probably that sulfate in the seawater within them was reduced in the presence of organic material to hydrogen sulfide, which combined with iron to produce pyrite. A byproduct of the reduction process was the precipitation of dolomite:

$$\underset{}{\text{Organic carbon}} + \underbrace{SO_4^{=}}_{\text{sulfate}} + Ca^{++} + Mg^{++} \Longrightarrow \underbrace{CaMg(CO_3)_2}_{\text{dolomite}} + \underbrace{H_2S}_{\text{hydrogen sulfide}} \text{ etc.}$$

$$H_2S + Fe^{++} \Longrightarrow \underbrace{FeS_2}_{\text{pyrite}} \text{ (by a couple of intermediate steps)}$$

In fresh water, in the presence of gypsum, dolomite tends to be replaced by calcite. Dolomite forms in the presence of gypsum only in sea water, which has a very high Mg/Ca ratio.

Many of the fossils in the Stewartville are conspicuously bored, probably by endolithic boring algae, although fungi, sponges, barnacles and bryozoa can produce similar structures (Figure 10). ("Endolithic" means within the rock.) The boring implies that the shells lay in the photic zone penetrated by sunlight. Both the Stewartville and the Dubuque contain a large amount of mud-sized carbonate material and scattered fossils. Fossil fragments in the Stewartville are randomly oriented, implying that storm erosion had little effect on sorting them or aligning them (for example, parallel to wave motion), or that bioturbation destroyed any such effects. Sedimentation was probably very slow, allowing time for boring and bioturbation to take place undisturbed.

Figure 7: Thin section of a lag deposit of shells overlain by carbonate mud that settled out after a storm (MY100a). Enlargement = 5.5X (non-polarized light).

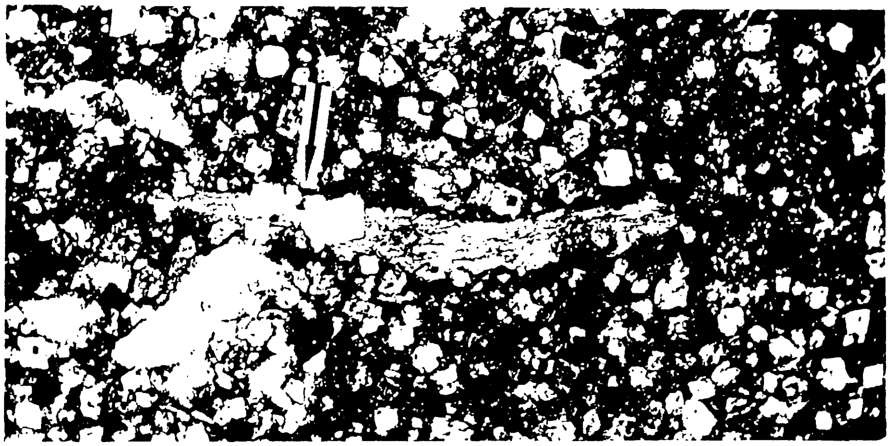

Figure 8: Dolomite rhombs typically cross the bedrock matrix, grains, and fossils, showing that the dolomite post-dates the original sediment (sample MY109). Elargement = 40X (polarized light).

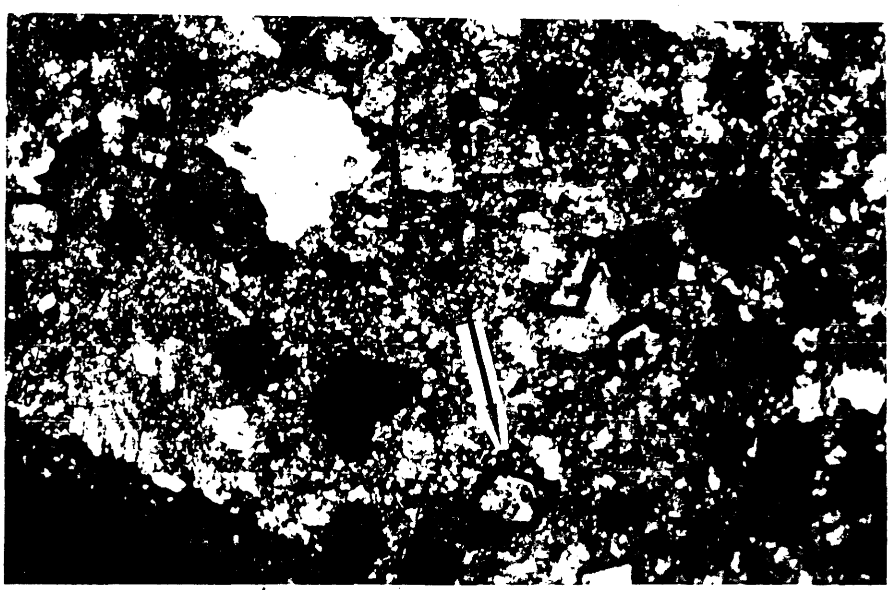

Figure 9: Porous zones (dark areas) outlining corroded dolomite crystals in weathered samples (MY2). Enlargement = 67X (polarized light).

Figure 10: Thin section showing organic borings in a fossil fragment, typical of Stewartville Formation (MY38). Enlargement = 50X (polarized light).

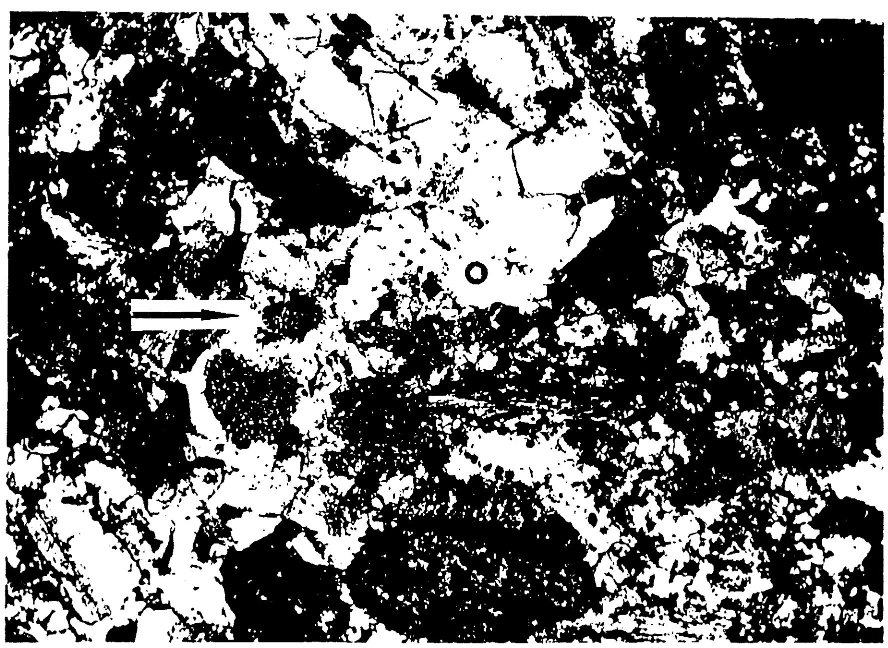

Figure 11: Bedrock grains partly replaced by gypsum that has since been replaced by calcite spar (MY 45). Enlargement 50X (polarized light)

Some fossils in the rocks exposed in Mystery Cave have been recrystallized to calcite spar. Many of these fossils were completely dissolved and their molds were filled with spar. This is typical of fossils whose shells were originally composed of aragonite. Because aragonite is usually unstable in fresh groundwater, it easily dissolves. The tendency for former aragonite shells to dissolve in the upper Stewartville was noted by Delgado, (1983), although his observations show that the dissolved shells were filled with sediment instead. Evidence of boring activity in some of these calcified fossils indicates that calcite replacement took place in the marine environment, in which the aragonite would presumably have still been stable, and not at a later date after the rocks had been exposed to fresh groundwater by uplift. Calcite nodules scattered throughout the Stewartville, especially near the top, are another indication that calcite was stable at the time of dolomite precipitation. Calcite vugs are also concentrated along joints and cracks at about eye level in the Angel Loop. Near the top of the Stewartville, calcite spar fills the burrows but is surrounded by a hazy zone of dolomite. The spar does not have a sharp contact with the surrounding rock but partially digests it, leaving bits of unassimilated dolomite and inclusions floating in the spar. Dolomite rhombs are irregular and corroded, with many holes and ragged edges. In sample MY45 (near the top of the Stewartville) partly assimilated fossil fragments "float" in spar. Edges of the fragments are broken into small crystals that have become assimilated by the spar. Iron oxide occurs at the edges. Slightly larger spindle- or lozenge-shaped càlcite crystals float nearby within the spar along with tiny remnants of almost completely assimilated fossil grains. In one place the inclusions are dark, very small networks of what appear to be filaments. It is clear that dolomite formed in the low-energy reducing environment and that the spar formed soon afterward.

Textures like these are common in areas of gypsum replacement of limestone or dolomite. Gypsum wedges the bedrock apart as the gypsum crystallizes in cracks and gradually replaces the fragments by assimilation (Figure 11). Bedrock fragments appear to "float" in the gypsum. Breccias (conglomerates with angular fragments) are commonly produced. Such a breccia occurs at the Stewartville/Dubuque contact. We have observed similar features in bedrock replacement zones behind gypsum crusts in many areas, including Lechuguilla Cave, New Mexico. Another indication that gypsum was present is the presence of stylolites, which are irregular interpenetrations of one bed into the underlying one. Stylolites represent zones of compaction, often where a void space has collapsed. Gypsum is very soluble and its former presence is frequently represented by stylolites. Sample MY46 (bed SX3) is lined with spar that has filled cracks formed by gypsum growth. The spar in MY 46 (bed SX3) ends laterally in a wavy disconformity, as described in the Interpretive Report.

Besides the worm burrows in the Stewartville, other organic remains can tell us about the environment. Scavenging organisms such as snails and nautiloids are common, indicating yet again a high level of organic material in the sediment. Fossils are similar to those found in the Dubuque. Sloan (1987) reported that an extinction event reduced the fauna by 90 percent in the lower Stewartville, which he thought was caused by shallowing of the water (see graph of water depths in the Interpretive Report). If our interpretation is correct that sulfate reduction was common in the Stewartville, could an alternate explanation be that salinity rose as the sea became shallower, killing many organisms? According to Sloan and Webers (1987), the few species of snails that dominated the upper Stewartville lived under very harsh conditions. We found fewer intact shells in the Stewartville than in the Dubuque, but the overall percentage of fossil debris does not vary much between formations, and the fossil types were much the same.

Large fossil fragments are easily recognized in thin sections from the Dubuque. The most common include brachiopods, trilobites, ostracods, conodonts, and echinoderms. Brachiopod shells are layered, with thin, subparallel laminations that are inclined at angles to the shell surface like shingles on a roof. The laminations are usually slightly wavy or crinkled. A trilobite shell consists of a single crystal. Extinction under polarized light (i.e., the sample turns dark) does not occur sharply or all at once, but instead a dark extinction band travels as a wave across the crystal as the microscope stage is rotated. In cross section, trilobite shells have bent ends that look like shepherd's crooks. The two shells of an ostracod are usually nearly spherical and only about a millimeter wide. Conodonts are tiny (1/2 mm) tooth-shaped features usually replaced by phosphate. Echinoderms are made up of monocrystalline plates. The echinoderm is easily broken up, leaving many round-to-square plates having sharp extinction under polarized light. Chitinozoans, of uncertain affinity, became common in the Upper Dubuque and Maquoketa. They are tiny (1/2 mm) opaque, thin walled, black organic bodies shaped like vases but squashed flat in our samples so that the two walls lie against each other.

Phosphate is associated with the shale beds in the upper Dubuque Formation and continues upward into the Maquoketa. Phosphate is also encountered in one of the lowest shales (sample MY58 = bed DS2). At this same horizon, dolomite decreases to a trace amount. Phosphate is often associated with nondepositional intervals or periods of slow sedimentation and can imply high biological production (Scholle, 1978). Experiments suggest that organic matter provides phosphate to pore water and will not form if the substrate is sterile (Southgate, 1986). Burrowing becomes less common upward into the Dubuque, and layers of large fossil fragments separated by calcite mud are common. These fossils are probably remnants from episodic storms, when high-energy waves reworked the bottom sediment. Fine-grained material went into suspension, while the heavier fossils were aligned along the bottom as a lag deposit and were covered with mud again when the fine-grained material settled out. Sparse calcite spar in the upper Dubuque shows evidence of having replaced evaporites. Conditions seem to have returned to those of the upper Stewartville. Dolomite crystallized in a reducing environment near the top of the Dubuque where organic carbon was present.

The Dolomite Question

How does dolomite form? This is a question that has plagued geologists for many years. There is an immense amount of literature devoted to this topic and no real end in sight (Hardie, 1987). There are many hypotheses on the subject, and a good discussion can be found in Blatt, Middleton and Murray (1980). But when applied to the field, usually no single theory seems to fit. Most geologists in the midcontinent favor the model that invokes mixing of freshwater with seawater for the Galena dolomites. It was thought that fresh water from land areas mixed with magnesium-rich saline water to form a mixture that would precipitate dolomite. Even though the idea is supported by the fact that the Galena dolomites formed in shallower water than limestone, there are exceptions where this hypothesis does not hold true (Witzke, 1983).

Friedman (1980) recognized that dolomite is associated with gypsum (Friedman, 1980), and that its reduction might form dolomite (Mullins and others, 1988). Compton (1988), who studied dolomite in the Monterey Formation in California, found so much evidence for the coincidental decay of organic matter, the reduction of sulfate, and the origin of dolomite, that he called this dolomite "organogenic." Evidence that sulfate reduction produced the large bodies of dolomite that formed in the shallow continental seas of the past has been largely overlooked. Although the evidence in the Mystery Cave samples is subtle, we strongly support this origin for the dolomite in the Stewartville.

GEOLOGIC STRUCTURE

The enclosed geologic profile of the cave clearly shows the local northwesterly dip of the rocks in which the cave is developed. The mean dip of any particular geologic contact or bed (i.e., the angle at which it is tilted) can be found by calculating the regression plane through all the measured points on that contact. The results differ according to the contact chosen because the dip is not uniform, and each contact is exposed in somewhat different parts of the cave.

The 87 points measured in the cave on the Dubuque/Stewartville contact have the following regression plane:

elevation above sea level = 0.0071 E - 0.0050 N + 1198.95 ft.

where E = feet east of station D1 and N = feet north of station D1 (use negative values for west and south respectively). The standard error of estimate is 2.08 feet -- that is the mean deviation in elevation between the regression planes and the actual measured points. The regression plane dips 0.50 degree in the direction 304.9 degrees.

A summary of the dip attitude of various contacts is given below:

Contact	Dip angle	Ft./mile	Dip direction	Std. error	No. of points
D/S	0.50 deg	46 ft/mi	304.9 deg	2.08 ft	87
BP2	0.68	62	307.4	1.55	56
DS1/DT4	0.77	71	312.6	1.91	19
DL9/DS9	0.55	51	302.1	1.27	38
DS10/DL9	0.68	63	308.0	1.46	21
DL10/DS10	0.72	66	308.1	1.24	34
DL14/DS14	0.50	46	307.4	1.55	18

The average dip of the rocks in the cave is therefore about 50-60 feet per mile, with a rather uniform dip direction of about 307 degrees (i.e., 53 degrees west of north). The smaller mean dips are on contacts that are partly exposed in low-dip parts of the cave. For example, D/S is exposed in Fifth Avenue and the route to the Garden of the Gods, where the dip is less than in the other parts of the cave. The standard error is understandably large, because a single regression plane cannot represent very well all the points on a contact that varies in dip. Those contacts with both low standard error and low dip are exposed mainly in those parts of the cave in which the dip is low.

In detail, there are many small structures superimposed on the average dip, some due to erosional/depositional irregularities or differential compaction, and some due to structural deformation. From the standpoint of water flow, there is little difference in effect.

To reveal the variations in dip in the area, the Dubuque/Stewartville contact was contoured using the contouring program SURFER (Golden Software Co., Golden, CO). To provide rather uniform coverage throughout the cave, several other higher stratigraphic contacts were included in the data, with their elevations adjusted downward to the Dubuque/Stewartville contact. In other words, measurements on DL10/DS10 are 15.25 feet above the D/S contact, and so this interval was subtracted from the original values to represent the underlying D/S contact at that location. Stratal thickness is nearly uniform throughout the cave, so this technique was valid for this purpose. All such adjusted values were then contoured using the minimum curvature routine, which fits the data points with a contoured surface having the smallest possible curvature. The resulting structural contour map is shown in Figure 12. Survey points are shown as asterisks.

Contours in Figure 12 are least accurate in the northwest, northeast, and southeast corners of the map, where there are no measured points. The contouring routine assigned unlikely warped structures to these areas to fulfill the minimum-curvature requirements, and to avoid this a few arbitrary points were added in these areas to make the structure more realistic, although still obviously not correct. Unless actual data points are available for these areas, no amount of statistical manipulation can interpret what is going on there.

Contouring by hand is often better for geologic interpretations, as the computer program has no intuitive feel for the way geologic structures behave in real life. The adjustment of the contours in the corners described above is an example of the intuitive approach. However, the contours produced by the program were left intact in the cave area, where there were abundant data points, to avoid any bias in contouring. This impartial approach was important at Mystery Cave, because regardless which contouring routine was used, a distinct change in dip angle was observed in the vicinity of the junction between Fifth Avenue and the Angel Loop that seems to account for northwest-southeast passage trends in that part of the cave.

The northwest-southeast fissure passages in the cave are all located along or just east of the steepening of dip (compare Figure 12 with the cave maps included in the Appendices). Joints having this NW-SE trend appear throughout the cave, but they are enlarged to cave size by solution only in the northeastern part of the cave. Local stress in the rock must have been greater along the hinge line where the dip changes, widening the joints to the point where the cave could utilize them as easily as the other joint sets. Therefore, this flexure in the beds appears to have had a significant impact on the orientation of fissure passages in the cave.

The structural contour map shows a dip change from west-northwest at Mystery Cave to southwest at Grabau Quarry, which is located north of the South Branch of Root River. The map shows a strike direction of 310 degrees (N 50° W) at the quarry. During the leveling survey to the quarry, we measured the local strike by positioning the tripod-mounted level at a distinct contact and rotating the instrument until its cross-hairs were superimposed on the same contact in the opposite wall of the quarry. This indicated a strike direction of 328 degrees (N 38° W). No attempt was made to account for the slight calibration error in the instrument over that distance (several hundred feet), so this strike estimate is imperfect. However, the local southwesterly dip on the structural contour map was verified.

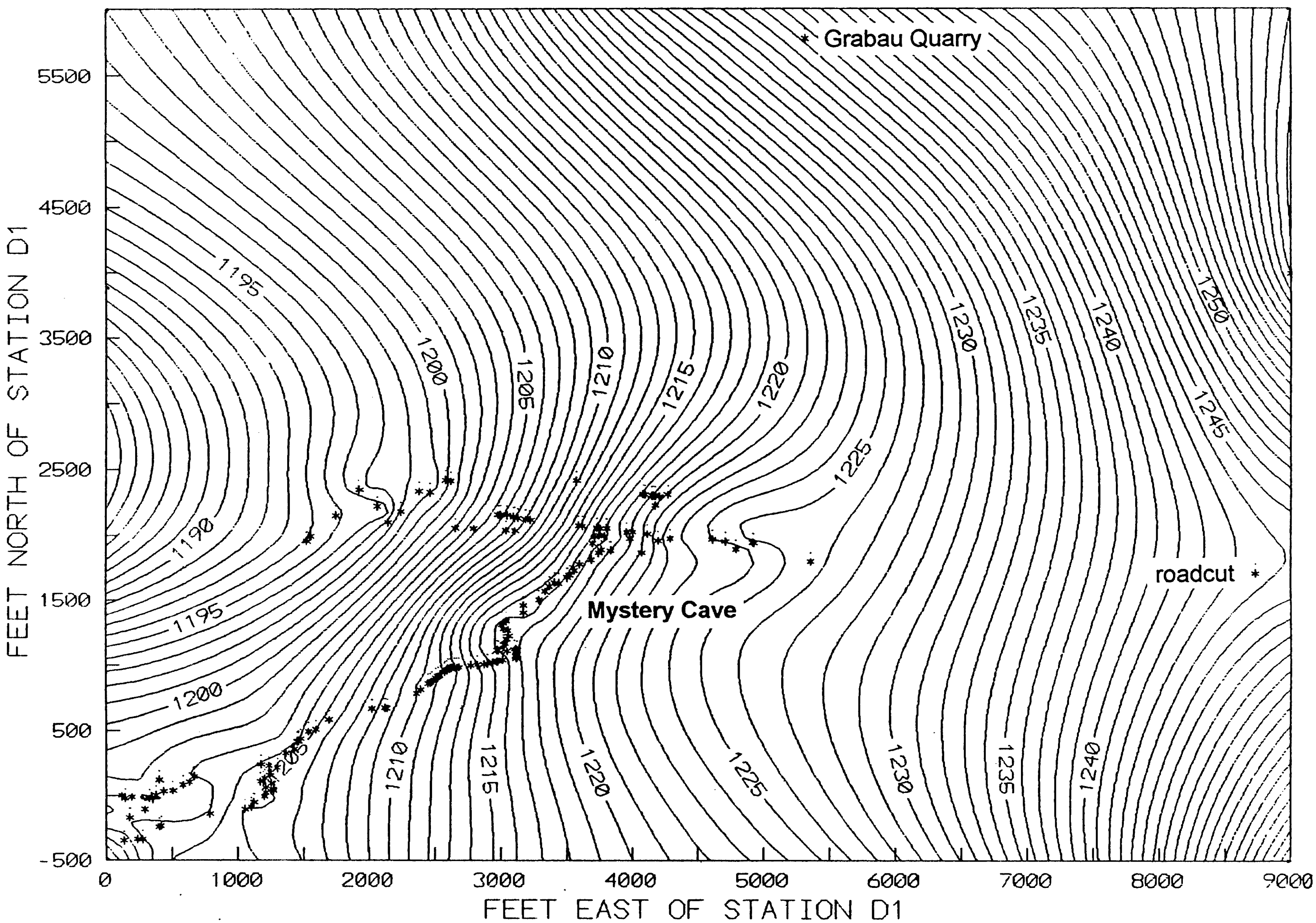

Figure 12: Structural contour map of the Dubuque / Stewartville contact in Mystery Cave and surrounding areas. * = surveyed points. Refer to Figure 1 for passage relationships.

GEOMORPHIC INTERPRETATION

The main discussion of the origin and developmental history of Mystery Cave is given in the Interpretive Report. The following section contains a summary of quantitative information that supports our conclusions. A summary of this interpretation is that the cave originated as an underground bypass for the South Branch of Root River, and that the passages developed in several stages: (1) an early west-to-east series of passages, including Fourth and Fifth Avenues; (2) passages in Mystery I and the Door-to-Door Route, with a general northeasterly trend; (3) lower levels that formed as the river level cut downward in its channel, allowing deeper cave development. This eveolution did not take place in discrete stages, as they overlap in time, and many of the original paths are still active in the lower levels, as well as periodically at all levels during floods. We view the cave as a dynamic floodwater cave that is intimately tied to the entrenchment history of the South Branch valley, rather than an enlarged remnant of a region-wide system of solutional fissures, although early solutional enlargement previous to the entrenchment of the river probably did contribute to the initial enlargement of some fractures. Entrenchment of the South Branch, and therefore the origin of Mystery Cave, depended on the entrenchment of the Mississippi River into the low-relief pre-glacial landscape. The Root River is tributary to the Mississippi and could not cut downward independently. This entrenchment began in the early or middle Quaternary Period, probably between 500,000 and 1,000,000 years ago, as indicated by the presence of old glacial deposits of presumed "Kansan" age in the valley. (The terms Nebraskan, Kansan, Illinoian, and Wisconsinan have long been used to designate what were thought to be four main glaciations in North America, but recent evidence makes this interpretation and these names a bit obsolete, although they are still used for general reference.) That would make the deepening of the river channel more than about 500,000 years ago.

Speleothem Dating

One of the few methods for obtaining absolute ages for cave features is radiomentric dating of calcite speleothems. Speleothem dates using $^{234}U/^{230}Th$ disequilibrium methods (Milske, Alexander and Lively, 1983), have made it possible to outline the more recent events in the cave's history. Most of the speleothem groups have already been sampled by Lively (of the Minnesota Geological Survey), and so only 5 additional dates were obtained as part of this LCMR project. These dates are summarized in Appendix 9.

A frequency plot of speleothem ages (Figure 13) shows several time intervals when caclite deposition was favored (mainly around 10-5 ka and 100-150 ka) with intervening periods of little or no deposition (*ka* = age in thousands of years -- a convenient abbreviation used mainly by those involved in geologic age dating). Some dates exceed the range of the method, and are therefore older than 350 ka. In accordance with earlier workers, Milske, Alexander and Lively (1983) interpreted this pattern with the view that speleothems form during interglacial periods, when vegetated soil is abundant and contributes CO_2 to the infiltrating water. During cold periods, when the area is either covered with ice or in the zone of permafrost, both the infiltration rate and the CO_2 production in the soil are low. Some caves were also deactivated by nearly complete filling with glacially derived sediment. Speleothem dates from Europe and elsewhere in North America (Hennig and others, 1983) show peaks of speleothem growth at 0-20 ka and around 100 ka. Beyond that there are no significant peaks or breaks in the dates. The data of Harmon and others (1977) for speleothems from caves in the Canadian Rockies show the first two peaks, but also two older around 200 and 300 ka. Because ice-free and ice-covered conditions seem to have no sharp divisions in the midcontinent, it is impossible to

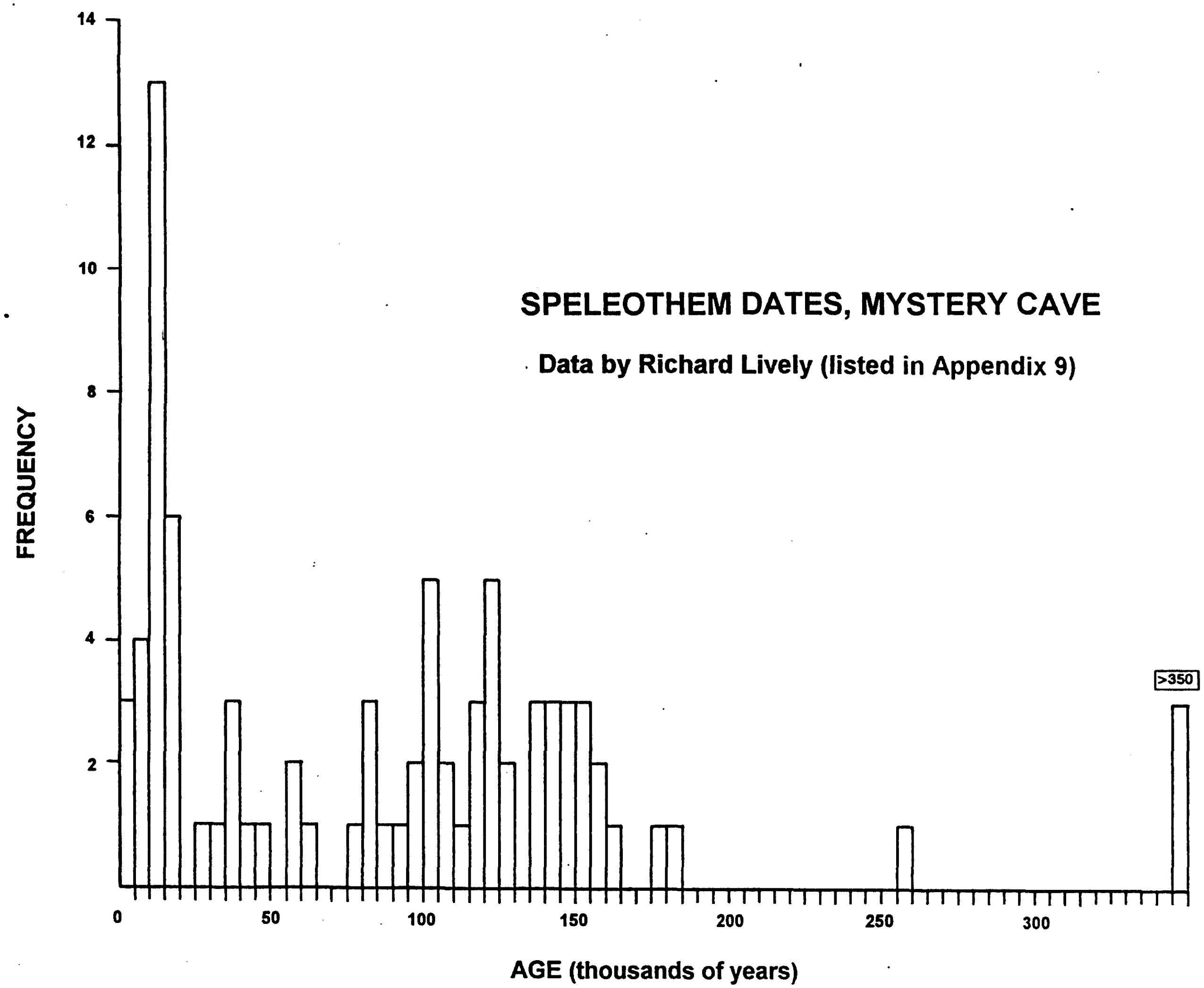

Figure 13: Distribution of speleothem ages, from Milske, Alexander, and Lively (1983) and from samples collected for this project.

make sharp distinctions between cold and warm periods, and the the speleothem record reflects the haziness of the climatic boundaries.

The lack of clear peaks beyond about 150 ka in Mystery Cave is probably due to the fact that many of the older speleothems have been so recrystallized that their U/Th composition has been disrupted, and no dates could be obtained from them. Another factor of particular significance at Mystery Cave is that flooding tends to destroy speleothems, and so those that are preserved are mainly the younger ones that post-date the deeper levels in the cave.

Cave Sediment

The sediment study by Milske (1982) and the summary by Milske, Alexander, and Lively (1983) shows that the typical sediment distribution in Mystery Cave consists of thick silt overlain by thin layers of sand and gravel. They found that most of the sediment in the cave was derived from pre-Illinoian glacial deposits outside the cave. It was rarely derived from the bedrock. Both the cave sediment and the glacial material contain varying amounts of feldspar, montmorillonite and kaolinite; whereas the shale in the Dubuque does not contain these minerals. They interpreted the silt to have been deposited during the transition from deep phreatic to shallow phreatic conditions (*phreatic* means below the water table, where all openings are filled with water year round), and that the sand and gravel were deposited by swiftly flowing streams late in the history of the cave. Our interpretation, based partly on the seismic data from the South Branch valley, is that silt is derived from the thick loess that covered the land surface late in the glacial history of the area, and that this material was carried in by the river and choked all the lower levels. The rapidly flowing streams that deposited the sand and gravel represented the same water, but flowing swiftly more or less at grade with the river and perched on the older silt.

On the basis of the speleothem dates, however, there appears to have been more than one stage of filling. Sediment in Enigma Pit is capped by old speleothems (up to 180 ka), but those on the Door-to-Door Route are much younger (about 12 ka on the average). This age distribution may be misleading, because the Door-to-Door Route is still subject to flooding, and it is possible that early speleothems have been removed or were unable to form in the first place. These topics are discussed in detail in the Interpretive Report.

The last glacial advance, the Des Moines Lobe, is probably represented by the break in speleothem deposition between 12-20 ka, and outwash from this lobe may have furnished the Door-to-Door sand and gravel, which was then overlain by thin silt and finally calcite dated at 8-12.6 ka. During the waning stages of the Des Moines Lobe, a series of large lakes ponded behind remnant ice in the Mississippi valley (Wright, 1985). When the ice dams broke, the river scoured its valley about 150 feet below its present floodplain. This channel has since filled with sediment back to about its original level. The South Branch of Root River at Mystery Cave apparently did not experience this short phase of entrenchment.

Past Water Flow in Mystery Cave

Scallop Data

Scallops are asymmetrical hollows in soluble bedrock formed by turbulent eddies in rapidly moving solvent water. They indicate two things of importance to interpreting cave origin: the direction and velocity of the last flow to significantly enlarge a given cave passage. This is convenient, because the scallops persist after the passage has been abandoned by the flow that formed it.

The direction of flow is indicated by the asymmetry of the scallops. The steep side of the divide between scallops is on the downstream side, as it is in a sand dune or current ripple mark. Running a hand along the wall, one finds that the sharp edges of the scallops feel rougher in the upstream direction than in the downstream direction. It helps to imagine the asymmetry to be like the teeth in a saw.

The velocity of flow is inversely proportional to the scallop length, measured in the direction of flow (Curl, 1974). A one-inch-long scallop represents twice the velocity of a two-inch-long scallop. Since the scallops in a passage exhibit a variety of lengths, a weighted mean is used that emphasizes the larger (and presumably better-developed) scallops. Measure the maximum crest-to-crest length of all scallops in a given area, cube each measurement, then square each measurement. The weighted mean recommended by Curl is the Sauter mean, in which the sum of all the cubed values is divided by the sum of all the squared values. In practice, there is little need for this amount of rigor, since we are interested in rough comparisons between different parts of the cave. Furthermore, if one selects just the well-developed scallops, a simple arithmetic mean (average) length is sufficient (Palmer, 1976).

The scallops indicate the flow velocity right near the wall. However, the velocity of turbulent water increases logarithmically away from the walls. Thus the velocity at a distance of two inches from the wall would be twice as great as the velocity at a distance of one inch from the wall. To obtain the average velocity within the passage, it is necessary to integrate the velocity across the entire passage radius. Curl (1974) provides solutions for two end members: tubes of circular cross section and narrow fissures. Considering the uncertainty of scallop preservation and interpretation, and the irregularity of passages, it is convenient simply to use the average scallop length to find the velocity near the wall and to consider that to be a representative velocity for the entire passage, or a particular part of the passage. Using the experimental results of Curl (1974), it is possible to simplify the otherwise complex calculation by using the following expression (Palmer, 1981):

$$\text{velocity (cm/sec)} = 350 / L$$

where L = scallop length in centimeters. Thus a passage containing scallops with an average length of 5 cm was last enlarged by water with a velocity of at least 70 cm/sec, or about two feet per second. Calculations can be easily made right in the cave and compared from one place to another.

The apparent origin of Mystery Cave by underground piracy of the South Branch of Root River would seem to provide an ideal setting for scallop development. However, the mottled texture of the Stewartville Formation is not conducive to scallop development. Projections caused by differential solution interfere with the eddies that would otherwise form scallops. In addition, scallops require rather uniform bedrock texture to achieve their natural form. The best strata for preserving scallops are the transitional beds between the Stewartville and Dubuque and the limestone units within the

Dubuque. However, most of the Dubuque is exposed in high-level passages subject only to relatively static ponding during floods, and so scallops are largely absent from the Dubuque as well. As a final complicating factor, even well-developed scallops are scattered among many alternate paths of flow, so it is difficult to draw together their individual characteristics into a single cave-wide interpretation. We are left with relatively few interpretable scallops.

Scallops are best preserved in the Door-to-Door Route and in Mystery III. In both locations the Dubuque and transitional beds are exposed in passages low enough in elevation to allow invasion by high-velocity floodwaters. During the leveling project, scallops were observed in the following locations (calculated velocities are rounded off slightly):

Station	Location	Scallop Length	Min. Velocity
H377	between Bomb Shelter and Big Fork	1.5 cm	230 cm/sec
H401-403	crawl beyond Big Fork	3 cm	115 cm/sec
H416	fissure beyond Big Fork	1 cm	350 cm/sec
H429	fissure near Little Fork	9 cm	40 cm/sec
H646	Culverts	1.5 cm	230 cm/sec
H655	fissures northwest of Culverts	3-6 cm	60-115 cm/sec

All of the above indicate flow away from Mystery I toward Mystery II.

H22	Discovery Route (Mystery III)	12-15 cm	25-30 cm/sec H16
	passage to 1st Triangle Room	2.5 cm	140 cm/sec
H32	passage to Fifth Ave. West	2.5-10 cm	35-140 cm/sec
H29	passage to Rotunda Room	15 cm	25 cm/sec
H27	above Lily Pad Lake	2.5 cm	140 cm/sec
H33	Fingers area	2.5 cm	140 cm/sec

All of the above indicate flow toward the north, northeast, or east (depending on orientation of passage).

Rather high velocities are indicated by these scallop measurements. During floods, water moves very rapidly through narrow passages where there is no alternate route. Such passages commonly contain coarse sediment such as sand and gravel, although these coarse sediments may be concealed beneath a cover of fine-grained sediment deposited on top during ponding events. In places, water ponds up in nearly static lakes where a downstream constriction prevents it from exiting a given passage at the same rate that it enters. Such areas of static ponding do not contain scallops and are recognized only by fine-grained sediment (clay and silt) and by injection floodwater features such as ceiling pockets and joint-controlled dead-end fissures.

Sediment Grain Size as a Velocity Indicator

From the above discussion, it is clear that sediment is an important indicator of flow velocity and should be used in conjunction with scallops in interpreting the hydraulics of the cave. There are various ways to estimate flow velocity from the grain size of sediment. The most commonly used method is the experimental graph of Hjulström (1935), which shows the minimum velocities at which sediment grains of a given size are eroded and deposited (Figure 14). This graph is obviously generalized, because these critical velocities depend on many other factors besides grain size, such as channel size and gradient, temperature, and density and shape of grains. Yet it is ideal for rough estimates of comparable accuracy to scallop data.

The silt deposits in the cave have an average grain size of about 0.05 mm indicates that incoming water required a velocity greater than about 20 cm/sec to erode the silt, at least 0.2 cm/sec to transport it, and less than 0.2 cm/sec to deposit it. Cobbles of at least 10 cm diameter are also found in the gravels on the Door-to-Door Route. These required velocities of more than 300 cm/sec to be eroded, at least 200 cm/sec to be transported into the cave, and less than 200 cm/sec to be deposited.

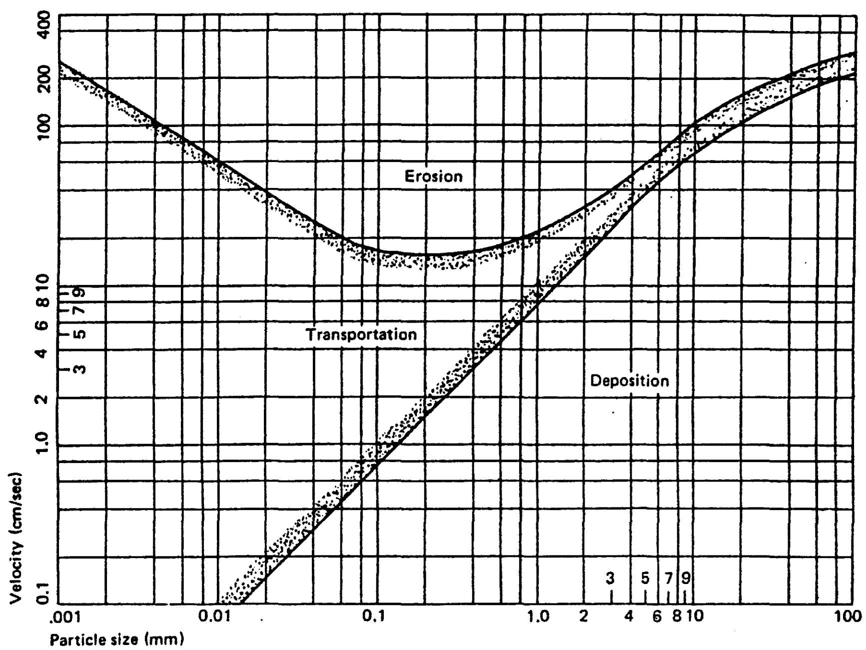

Figure 14: Diameter of sediment grains vs. the approximate current velocities needed to erode, transport, and deposit them (Hjulström, 1935).

Velocity estimates like this are tantalizing, but it is difficult to make much quantitative headway beyond the obvious fact that silt and clay represent relatively stagnant water and sand and gravel represent fast-moving water. For example, the presence of gravel in the cave requires a supply of gravel on the surface. This may not have been available at all times during the history of the cave. The thick silt may represent widespread availability of windblown material at the surface during glacial events, rather than special aspects of cave development. Much can be done on this subject, but any gains will be hard won.

Sediment Thickness and Bedrock Configuration at Mystery Cave

Seismic profiles were conducted mainly to determine the depth to bedrock in the valley adjacent to the cave. Seismic data, locations, and interpretations are given in Appendix 3. The cross section of the valley fill in the valley of the South Branch of Root River at the Mystery I entrance is shown in Figure 15. The average depth of sediment fill in the valley is 20-23 feet, increasing to a maximum measured value of 27 feet below Grabau Quarry. Depth to bedrock appears to be comparable in the uplands. It is 22 feet above Garden of the Gods in Mystery II, and between 10 and 20 feet in the field west of Walnut Cave. Walnut Cave is located in a residual bench of limestone over which the soil depth is only about 10 feet. Apparently the South Branch had cut its channel about 20-27 feet deeper in the past than it is at present, and has since been partly filled with sediment.

The seismic velocity of the surficial material (evidently the entire thickness) is surprisingly uniform over the entire area at about 1000 ft/sec, which indicates dry unconsolidated material. The water table is at or below the bedrock surface. This means that the South Branch is perched above the water table on rather impermeable material and loses its water only where it encounters limestone or similar permeable material in its bed. The uniformity of this material in both thickness and seismic velocity over the entire area suggests that it is wind-deposited silt (loess). Further discussion of the topic is given in the Interpretive Report.

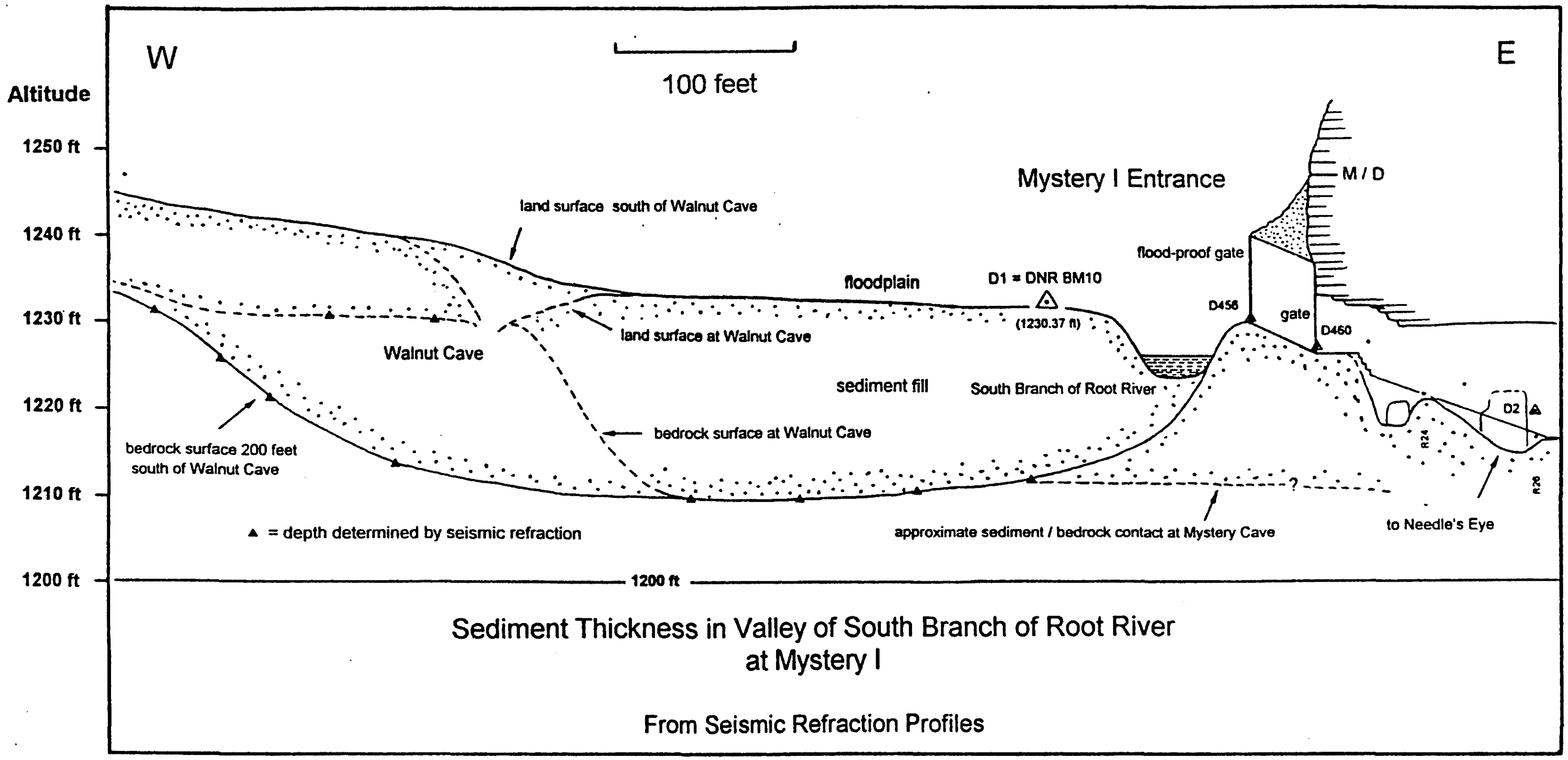

Figure 15: Sediment thickness in the valley of the South Branch of Root River at the Mystery I entrance, as determined by refraction seismology.

WATER CHEMISTRY

Although water chemistry is covered in a separate report by Calvin Alexander and Roy Jameson, two aspects of the subject are of concern to the geologic interpretation of the cave: (1) the nature of the water that formed the cave, and (2) geochemical factors that control the mineral types and crystal habits of cave deposits. We made a few measurements specifically to investigate these questions, but our conclusions are based mainly on reports by others.

Chemistry of Cave-Forming Water

The location of Mystery Cave in a meander loop of the South Branch suggests that the cave originated by underground diversion of the river water, forming a sort of subsurface meander cutoff with the cave as a byproduct. Today the river is usually supersaturated with calcite and dolomite, except during floods. The maze pattern of the cave can be attributed at least in part to flooding, where high-gradient, aggressive flow enlarges many different passages at comparable rates (Palmer, 1975). This view is supported by the fact that the river water is most aggressive during flood stage -- and in fact may not be able to enlarge the cave at all at other times. Streams in the cave are generally supersaturated during all but the highest flow (see report on the LCMR Hydrology Project).

From the field and lab data of Shiela Grow (1986), we calculated the saturation indices of calcite and dolomite (square-root version) and the P_{CO2} and plotted this information vs. river stage. Several points had to be deleted because of obvious inaccuracies or instrumental problems; but the remainder, despite considerable scatter, showed a strong inverse relationship between river stage and saturation index. The data showed no significant relationship between river stage and P_{CO2}, although such a relationship is of little concern here.

River stage was measured on the metric staff gauge that was formerly located near the Mystery I entrance. Unfortunately the staff gauge was removed before it could be tied to our leveling survey. However, typical stage at base flow was about 40 cm, and this gives a rough idea of how the old values compare with more recent measurements.

The data pairs (stage vs. SI) were fit best by straight lines (Figures 16 and 17). The regression lines shown on the graphs do not include our 4-19-93 data point, as its relationship to the stage readings of Grow (1986) is uncertain. The correlation coefficient for the linear regression is -0.84 and the standard error is 0.24, showing a distinct inverse relationship. For dolomite the correlation coefficient is -0.84 and standard error is 0.27.

This information suggests that the river water today is aggressive with respect to either limestone or dolomite only when the stage exceeds about 62 cm, which represents a flood of only about 22 cm -- less than a foot. Such floods occur many times each year, and although they account for only about 10-20% of the time, they represent periods of significant cave enlargement under the conditions most favorable to the origin of a network maze.

During a moderate flood on April 19, 1993, the South Branch rose 3-4 feet, covering the floodplain around the Mystery I ticket office. A water sample obtained no more than half an hour after the crest showed the river to have the following values: SIc = -0.52, SId = -0.79, and $P_{CO2} = 0.0011$ atm. Although these points fall considerably above the regression lines, the aggressive nature of the floodwater was verified.

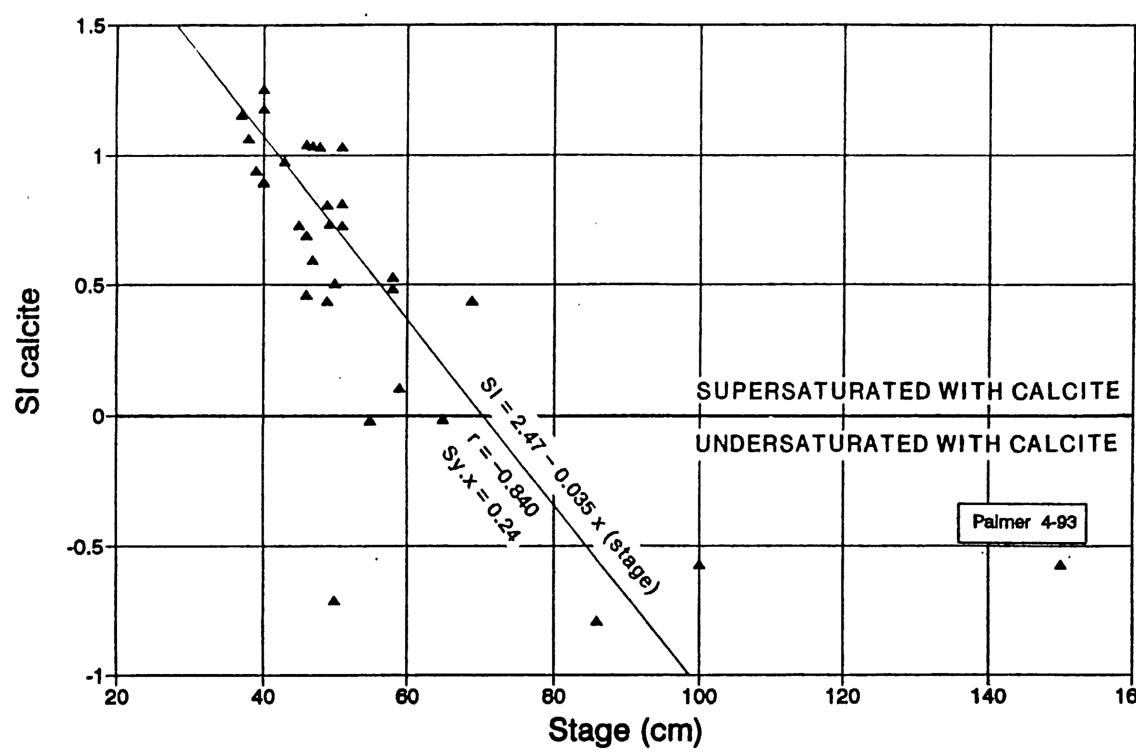

Figure 16: Calcite saturation values (SI) vs. river stage in South Branch of Root River at Mystery I, calculated from chemical measurements by Grow (1986).

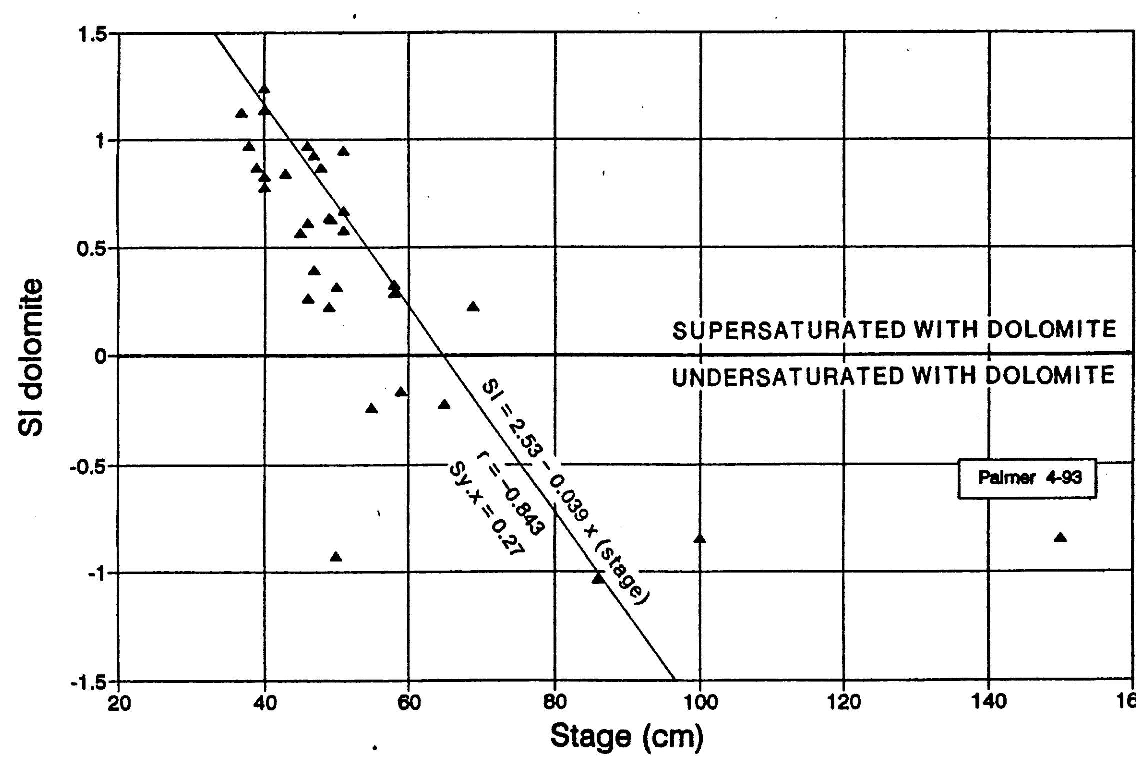

Figure 17: Dolomite saturation values (SI) vs. river stage in South Branch of Root River at Mystery I, calculated from chemical measurements by Grow (1986).

At nearly the same time, a sample was obtained from a floodwater pool below the Dome Room in Mystery I that yielded the following values: SIc = -0.22, SId = -0.46, and PCO2 = 0.00255 atm. The cave water was distinctly aggressive with respect to both limestone and dolomite during the flood. The aggressiveness had diminished slightly because of mixing with supersaturated cave water and probably with solution of bedrock, but the rise in P_{CO_2} (because of mixing with cave water and uptake of CO_2 from the cave atmosphere) helped to maintain the aggressiveness. The concept of cave enlargement under floodwater conditions is clearly supported by the data. There is no reason why the initial stages of cave origin cannot be attributed to similar waters.

What is the solution rate of the limestone? During low flow the water is nearly always supersaturated with respect to both calcite and dolomite. However, it is unlikely that there is any net deposition of either mineral because of solution during high flow, and because of the erosive power of the streams and the presence of sediment on the floors and walls. However, active solution can take place during high flow.

The saturation index of calcite can be converted to degree of saturation (or saturation ratio), C/C_S. The relationship is $C/C_S = \{\text{antilog (SI)}\}^{0.35}$. From the resulting values, the limestone solution rate can be determined (Palmer, 1991):

$$\text{Solution rate} = 11.7\, k\, (1 - C/C_S)^n \text{ cm/year},$$

where k is approximately 0.008 for typical limestone and n is approximately 2.2.

Therefore, on Figure 16, when the SI of calcite is -0.5, C/Cs = 0.67 and the approximate solution rate is 0.008 cm/yr (80 microns/yr) -- although that rate of solution lasts only a few days or weeks during a normal year. At SI = -1.0, C/C_S = 0.45, and the approximate solution rate is 0.025 cm/yr (250 microns/yr). These estimates are probably high, because they are for non-dolomitic limestone, and they do not take into consideration shielding of the bedrock walls and floors by sediment. Still, the importance of low SI values is very clear. It is important to realize that this solution rate can be diminished by sediment armoring of the walls and floor. However, erosion by stream-borne sand during high-velocity flow can increase the rate of cave enlargement, although not significantly at the slow velocities observed in Mystery Cave.

Variation of pH with Time and Depth in Cave Pools

We were curious to see whether there was any change in pH with depth in the cave pools. Our pH meter can be read to the nearest 0.001 pH unit, although this degree of precision is not necessary (or even desirable) for most water-chemistry studies, since the pH is so sensitive to environmental changes that two decimal places is all that can be counted on. For detailed monitoring of fluctuations, however, the more precise instrument is ideal.

The results were surprising. Within the uppermost few centimeters in each pool the pH changed rapidly with depth. In pools agitated by drips or waterfalls the pH also fluctuated greatly with time, especially near the surface, but much less so with depth.

Most interesting was the fact that pH decreased with depth in some pools and increased with depth or remained constant in others. The Rock Garden and Turquoise Lake decreased in pH downward; Sugar Lake was nearly constant in pH, with only a slight downward increase. The pH probe was waterproofed and held in place by a stiff wire to avoid motion. Measurements were repeated on three different days in Turquoise Lake and two different days in the Rock Garden. Measurements were made in three different places in Sugar Lake, with similar results.

In the Rock Garden (April 22, 1993) at a depth of 2 cm the pH stabilized at 8.307. At a depth of 5 cm it stabilized at 8.122. A large drip from the ceiling caused the pH to drop suddenly by 0.008 pH units, followed by slow recovery over the next few minutes back to 8.122. On an earlier day (April 12, 1993), the pH ranged from 8.222 at 2 cm to 8.045 at 5 cm.

In Turquoise Lake (April 22, 1993) at a depth of 2 cm the pH rose to 7.966 over the first 12 minutes, then dropped to 7.868 over the next 6 minutes, rose to 7.931 in 2 minutes, then dropped in an irregular pattern until the test was terminated at 25 minutes. Waves were visible from the waterfall at the far end of the pool, and turbulent eddies apparently caused the pH to fluctuate with a period of approximately 10 minutes (much less frequent than the waves, which had a period of less than a second). Soon afterward, at a depth of 60 cm, following recalibration, the pH rose gradually to 7.890 over the first 28 minutes, dropped suddenly to 7.882, then stabilized at 7.884 for 10 minutes. Apparently an eddy of slightly lower pH had moved into the area of measurement.

Earlier measurements in Turquoise Lake confirmed these findings: On April 12, 1993, the pH was observed to decrease from 7.930 at 2 cm to 7.815 at 15 cm. On April 20, 1993, the pH stabilized at 7.810 at 2 cm and 7.771 at 70 cm. The water entering the lake had a pH of 7.51. Apparently a great deal of CO_2 is lost from the surface of the water in the lake. On April 21, 1993, over a period of 20 minutes, the pH at 2 cm was observed to rise slowly to 8.020, drop to 7.954, then rise to 7.968, and finally drop to 7.887. At a depth of 30 cm the pH remained rather stable between 7.862 and 7.867. At a depth of 60 cm the pH remained rather stable between 7.883 and 7.886. Note that while the overall pH decreased with depth, there was a slight increase between 30 and 60 cm. The difference is minimal and could have been induced by agitation of the water by insertion of the pH probe.

In Sugar Lake on April 21, 1993, at the western end, the pH stabilized at 7.930 at a depth of 2 cm, 7.967 at 5 cm, and 7.996 at 10 cm. Measurements elsewhere in the pool showed the same trend, but the differences were much smaller due to mixing caused by agitation during probe movement. The pH was monitored over a 23-minute period on April 23, 1993, showing an asymptotic rise to 7.928 at a depth of 2 cm and 7.945 at 7 cm.

Mystery Pool (in Mystery II) showed decreasing pH with depth, from 8.062 at 2 cm and 8.051 at 15 cm. Repeating the shallow measurement yielded 8.063. The change with depth was distinct but not very substantial. Agitation of the water caused a rapid drop in pH to below 8, followed by a rapid rise to the former value when the water was allowed to stand.

Testing for drift with buffers showed a maximum of +0.02 units drift over 37 minutes. This is significant at the level of precision used in the monitoring, but the measured pH variations with time and depth were much greater. Furthermore, it does not affect the basic observations that pH varies with depth and over short time periods.

Water samples were taken at two depths in Turquoise Lake. At the surface, the water had a calculated P_{CO2} of 0.006 atmospheres and a calcite saturation index of +0.77. At a depth of 2.5 feet, the P_{CO2} was 0.007, with a calcite saturation index of +0.74. The stream feeding Turquoise Lake had a P_{CO2} of 0.013 and a calcite saturation index of 0.51. This brief test supported the view that the lake is rapidly degassing, so it is more highly supersaturated at the surface than at depth. A more rigorous approach will be used in the future.

The preliminary interpretation is as follows: The water at the pool surfaces approaches CO_2 equilibrium with the local cave atmosphere fairly rapidly, whereas the chemistry of the relatively stagnant water below responds much more slowly. A downward decrease in pH could mean one of two things: either the surface has responded to a recent decrease in CO_2 in the cave atmosphere, or CO_2 is being generated at depth by biologic activity (oxidation of organic compounds, etc.). A downward increase in pH is most easily explained by a recent decrease in atmospheric CO_2, but a valid interpretation must await water and air analyses. Interestingly, the downward increase in Sugar Lake was observed on the same day that a downward decrease was observed in Turquoise Lake.

These observations do not invalidate the measurements made during normal water chemistry studies, where a single pH and water sample are taken. Mixing of the water during this process usually provides an average pool chemistry. The variations in pH that we have measured with time and depth have only a slight effect on the saturation index and overall interpretations.

LABORATORY ANALYSIS OF SPELEOTHEMS

Influence of Water Chemistry on Crystal Shapes in Pool Deposits

In general there are three major types of calcite crystals in Mystery Cave: needles, blades, and rhombs (parallelogram-shaped crystals). Examples are shown in Figures 18-20. The rate of CO_2 degassing in the pools correlates with the shape of the crystals forming there. Some pools in Mystery Cave are lined with needle-shaped crystals and some with rhombs. The needles form in the pools where there is rapid degassing of CO_2. Blades form below water drips that are degassing, in shrub-like clusters (described in the Interpretive Report as "calcite shrubs"). Rhombs form in standing pools with very low water input. One potential problem is that water chemistry that we measure at any given time may not represent the conditions present when precipitation occurs. The close association between water chemistry and the crystal shapes of pool deposits suggests that this is not a great problem in Mystery Cave.

Turquoise Lake is fed by a small stream that is high in CO_2, and degassing in the lake causes the pH to rise near the surface, where the CO_2 content is lowest. The stream is floored with tiny needles, and, at the inlet side of the lake, calcite pool fingers grow from the wall. Tiny calcite needles coat the calcite crust on the walls of the pool itself. The folia in Mystery Cave are found above the level of Turquoise Lake and represent a higher stand of the lake. Folia are found in only a few other caves associated with rapidly degassing CO_2 or H_2S in caves such as Lechuguilla Cave, New Mexico, and are considered by some people to be hydrothermal in origin. These subhorizontal fins consist of layered, fibrous, subparallel crystals building outward like successive awnings as the water level changed. Precipitation at the former water surface has left a litter of calcite rafts, abundant shelfstone, and raft cones all the way to the Bomb Shelter.

Considering the rate of CO_2 degassing, calcite precipitation in pools like Turquoise Lake must be rapid. It appears that needle-shaped calcite crystals represent rapid precipitation. Needle-like or fibrous crystals can form either above or below water if precipitation is rapid. Most vadose speleothems formed by degassing or evaporation are characterized by a fibrous texture of long, narrow crystals and probably have the same fast growth. For example, needle-shaped calcite crystals have formed on the pipe and catch basin near the end of Old Mystery Cave at a known rate of about 1 mm per 30 years. Apparently Turquoise Lake is rapidly degassing most or all of the time, because all its crystals are needle-shaped.

Shrubs consist of bladed crystals that grow in V-shaped twins whose arms are typically oriented at approximately 45 degrees to the main axis of the speleothem (and where they form at a pool surface, at 45 degrees to that surface). Shrubs often alternate either with flowstone, cave ice or botryoidal fibrous clusters (MY135). They consist of layered bundles of radiating needles that have coalesced into blades (Figure 21). Each layer is only about 50 microns (0.05 mm) thick (Figure 22). If the rate of deposition is similar to that in Old Mystery Cave, each layer could represent an annual cycle, and the change from needles to blades could be caused by seasonal or slightly longer-term variations in the rate of CO_2 input. The needles are called crystallites, which are smaller unit crystals with discrete crystal faces (Kendall and Broughton, 1978). Evidence for the former needle-shaped crystal structure is commonly present as long narrow inclusions of incompletely cemented void space around the former crystals (MY138). Kendall and Broughton used the inclusions as evidence for the presence of precursor crystallites that coalesced to former the larger fibrous crystals in stalactites. The 45-degree angle corresponds with the orientation of the faces of a unit rhombohedron rather than

Figure 18: Calcite needles in folia above Turquoise Lake (MY30). Enlargement = 6X (polarized light).

Figure 19: Bladed calcite crystals coating calcite raft (MY33a). Enlargement = 100X (polarized light).

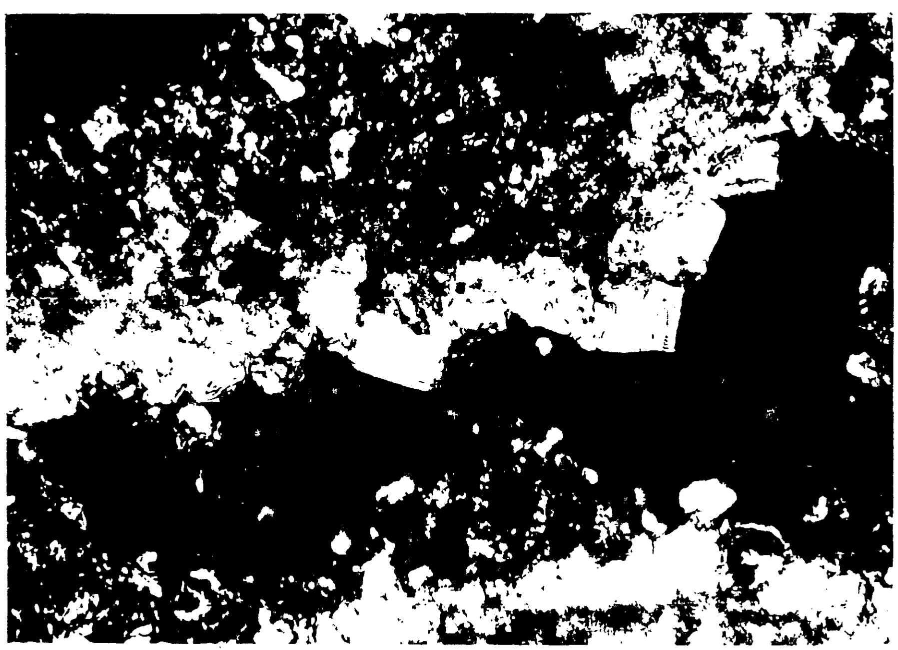

Figure 20: Calcite rhombs lining a pore in non-carbonate sediment (MY152). Enlargement = 200X (polarized light).

Figure 21: Bladed calcite crystals contain inclusions that outline the shapes of former needles (MY138). Enlargement = 20X (non-polarized light).

Figure 22: Layering within blades in calcite shrubs (MY11). Enlargement = 50X (polarized light).

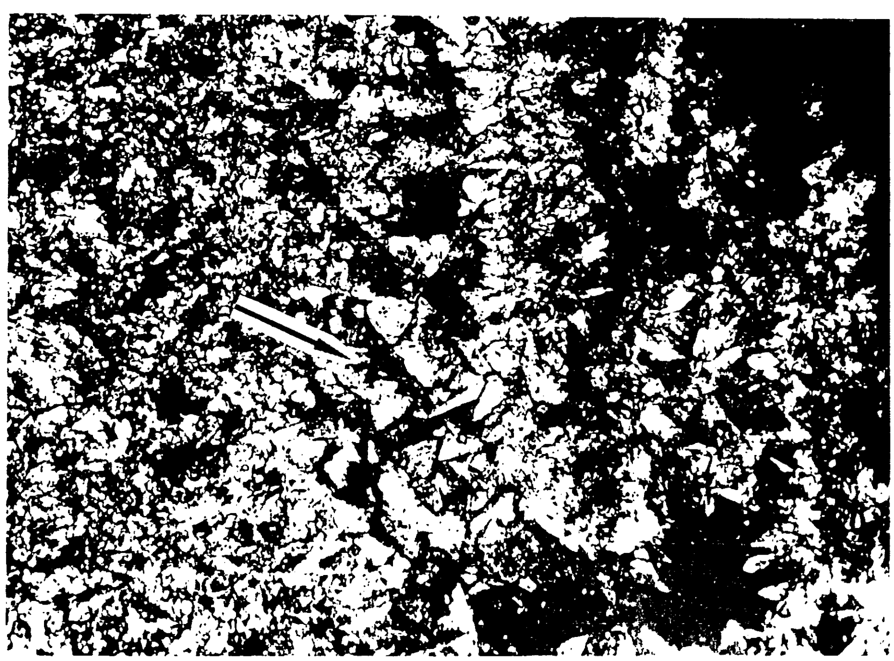

Figure 23: Triangular cross sections of bladed crystals (MY10). Enlargement = 20X (polarized light).

a scalenohedral form of calcite (Dickson, 1978). Sometimes a central crystal grows with twinned crystals branching out on either side, forming a single stem with upward-facing, v-shaped crystals superimposed on the central crystal. In cross section, a single bladed crystal is triangular and consists of parallel rows of smaller triangles (Figure 23).

Fibrous calcite in pools that are rapidly degassing commonly contain organic filaments of unknown affinity. The organics are either carried in from outside or thrive on chemical reactions in the cave. Filaments less than a micron (.001 mm) wide meander through shelfstone deposits in pools that also contain calcite shrubs, both in Mystery Cave and in New York caves. Pool fingers cover the wall opposite the dam at Turquoise Lake. Pool fingers in New Mexico caves contain bundles of filaments in their centers. The filaments provided a substrate for calcite precipitation. Chenille spar, which consists of drape-like calcite deposits in pools, appears to be simply a thick, coalesced version of pool fingers.

In contrast, crystals with rhombic terminations form the calcite surface that lines standing pools like Sugar lake, Dragon's Jaw Lake, and the Tar Pit pools (see Figure 20). The chemistry of these pools is quite different from that of Turquoise Lake. In Sugar Lake the pH rises very slightly, if at all, with depth. This little pool contains bladed raft material and raft cones, like Turquoise Lake, but some of the rafts are coated with rhombs. Sugar Lake has no apparent recharge most of the time, but raft cones show that drips once entered it, or do so periodically. The chemistry of pools of this sort remains relatively constant. They are fed by water that has already degassed and precipitated flowstone. In places, thick, bladed flowstone coats sediment, in which the pores are lined by small calcite rhombs. This is an example of how rhombs are favored by a static chemical environment. In most cave pools in which degassing of carbon dioxide is minimal, the blades or rhombic crystal terminations are coated with very thin calcite sheets that diminish in area of coverage, so that the overall crystal appears to be shingled.

Current Hypotheses on Calcite and Aragonite Crystal Growth

There is a lively debate about what controls the shape of calcite crystals, and why aragonite precipitates in some areas instead of calcite. (This is obviously one of the burning issues of our time.) The following questions have never been satisfactorily answered: why is aragonite the dominant carbonate mineral precipitated in seawater, and what causes the variation in calcite crystal morphology from needle-shaped to rhombic? Experiments by Bischoff and Fyfe (1968) showed that the Mg ion inhibited calcite crystal growth. In an elegant paper expanding on this theme, Folk (1974) proposed that the Mg ion "poisoned" the surfaces of calcite crystals, preventing lateral growth and promoting the growth of needle-shaped calcite crystals and aragonite. The Mg/Ca ratio was therefore thought to be important in controlling the shape of calcite crystals. Taking a different approach, Given and Wilkinson (1985) pointed out that the local degree of supersaturation controls the shapes of calcite crystals and that the Mg/Ca ratio has only an indirect effect. They hypothesized that needle-shaped crystals would form where precipitation is driven by rapid degassing of CO_2 and/or evaporation, leading to high degrees of supersaturation. They showed that aragonite or needle-shaped calcite could grow in any environment irrespective of the Mg/Ca ratio, as long as the supply of $CO_3^{=}$ ions is high enough.

Gonzalez, Carpenter, and Lohmann (1992), for the first time, presented actual chemical data from cave water in which different types of calcite crystals were forming. Like Given and Wilkinson, they found that the calcite crystal shapes are controlled primarily by the degree of supersaturation. At less than 6 times supersaturation, rhombs formed, whereas elongated crystals formed at greater values of supersaturation. At more than 12 times supersaturation, crystal faces became curved. They also noted that water chemistry was not completely responsible for crystal shapes, because needles and rhombic crystals form in water with overlapping chemical variables. They suggested that the rate of water flow was also essential in forming needle-shaped crystals because crystal growth is supposedly faster when the flow is fast. Apparently laying the magnesium theory to rest, they pointed out that needle-shaped calcite or rhombs can occur as either high- or low-Mg calcite. (Although calcite consists of $CaCO_3$, it incorporates various amounts of magnesium as an impurity.) X-ray data on speleothem fragments from Mystery Cave also show that the shape of calcite crystals is unrelated to the magnesium content (Figures 24 and 25, and summary of data in Appendix 8). All were low-magnesium calcite.

Our observations tend to support those of Gonzalez, Carpenter and Lohmann, in that growth rate seems to be the most important control over crystal morphology. However, we doubt that flow rate is significant. Needles and rhombs both form in pools in Mystery Cave, and the factor that controls them is clearly the rate of degassing. Supersaturation is the result of degassing of high-CO_2 water, which governs the growth rate and crystal structure. Comparing water chemistry in Mystery Cave with other caves in the United States, we found that needles can form in pools with either high or low magnesium content (see Tables 2 and 3, and Figures 26 a-c). The New Mexico cave pools have low levels of total Mg and Ca, with Mg distinctly higher than Ca becasue it is concentrated by evaporation. Water splashing onto fibrous-textured flowstone containing curved crystal terminations in Mammoth Cave, Kentucky, had the highest Ca/Mg ratio, while degassing pools with needles and shrubs were characterized by high Ca/Mg ratios. Static pools coated with shingled rhombs had the lowest Ca/Mg ratios.

In Mystery Cave, as in other caves, speleothems formed by the initial growth of numerous tiny crystallites that eventually coalesced. As suggested by Jones (1989) and Walkden and Berry (1984), crystal growth begins as either an aggregate of tiny needles oriented perpendicular to the substrate, or as sheets parallel to the substrate, depending on the growth rate. Needles form more rapidly. We did not address the aragonite problem, because to our knowledge aragonite is not precipitating in any of the cave pools. However, we have observed pools lined with aragonite in Carlsbad Cavern that are high in Mg but low in Ca. This was the only aragonite we have ever seen precipitating in cave water. It almost always forms by evaporation in contact with air and usually forms on dolomite bedrock. This is true in Mystery Cave, where aragonite is found on the Stewartville dolomite. This tends to support Folk's hypothesis that aragonite is favored by the presence of Mg ions.

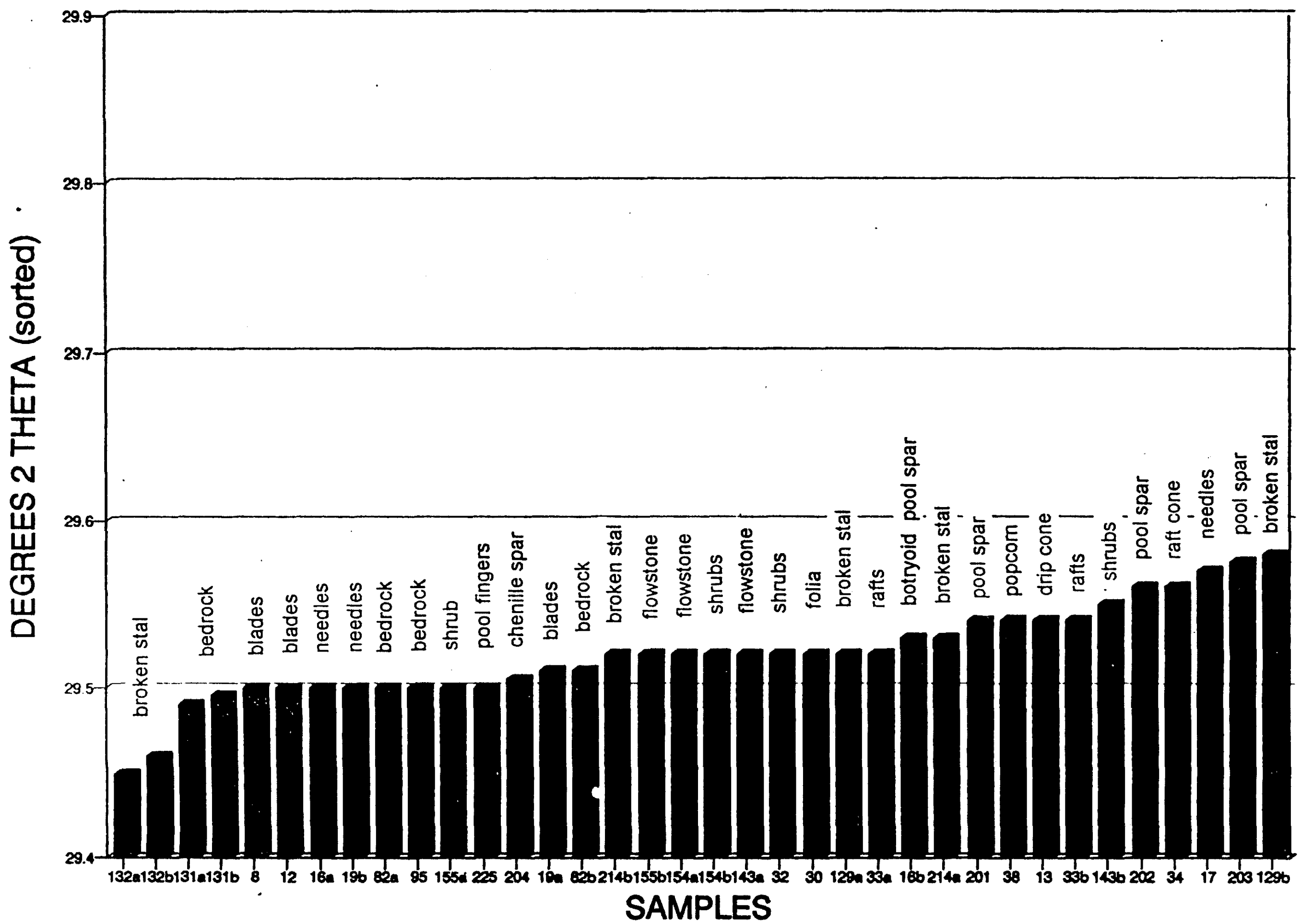

Figure 24: Maximum peak values (2-theta) for different kinds of calcite speleothems in Mystery Cave. Higher values of 2-theta indicate greater amounts of magnesium in the calcite structure (see Figure 25).

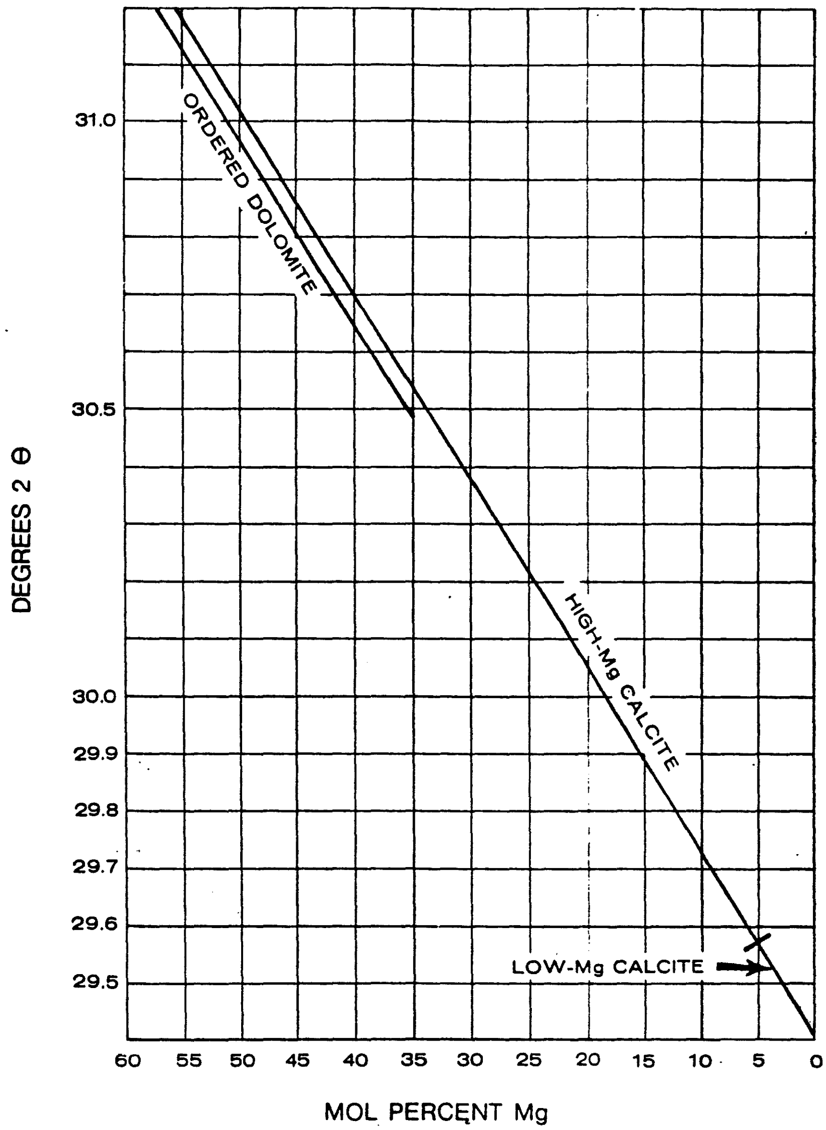

Figure 25: Molar percentage of magnesium in calcite vs. 2-theta angle of X-ray diffraction peak (from Scholle, 1978, modified from Goldsmith, Graf, and Heard, 1961).

Table 2: Summary of typical cave-water chemistry, sorted by total Ca + Mg. Analyses by A.N. and M.V. Palmer, except where otherwise noted. J+A = Roy Jameson and Calvin Alexander, LCMR Hydrology Project (1993); Oelker = Gregg Oelker, Pasadena, Calif. (1991). Average values are shown where more than one measurement is available for the same site.

Samples	**I.D. No.**	**Ca** mmol/L	**Mg** mmol/L	**Total** mmol/L
Overlook, pool #1, Mammoth Cave KY	MC1	0.80	0.41	1.21
Camp Pit, Mammoth Cave KY	MCC	0.84	0.45	1.29
Keller Shaft, Mammoth Cave KY	MCK	1.36	0.10	1.46
Lake Lebarge, Lechuguilla Cave, NM (Oelker)	LLB	0.83	0.88	1.71
Pelucidar drip, Lechuguilla Cave NM	LP2	0.64	1.15	1.79
Deep Secrets, mammillary pool, Lechuguilla Cave NM	LDS	0.61	1.28	1.89
Lake of Clouds, Carlsbad NM	CLC	0.62	1.36	1.98
Mary's Vineyard, Mammoth Cave KY	MCV	0.88	1.14	2.02
Lake Louise, Lechuguilla Cave NM	LLL	1.00	1.13	2.13
Liberty Bell drip, Lechuguilla Cave NM (Oelker)	LBD	0.78	1.35	2.14
Sugarlands chenille pool, Lechuguilla Cave NM	LS1	0.57	1.67	2.24
New Mexico Room, aragonite pool, Carlsbad Caverns NM	CM6	0.48	1.84	2.32
South pool, Dreamland, McFail's Cave NY	MF2	1.39	0.95	2.34
North pool, Dreamland, McFail's Cave NY	MF3	1.49	0.87	2.36
New Mexico Room, aragonite pool, Carlsbad Caverns NM	CM2	0.45	1.99	2.44
Sulfur Shores, Lechuguilla Cave NM (Oelker)	LSS	1.10	1.34	2.44
New Mexico Room, Carlsbad Caverns NM	CM3	0.42	2.03	2.44
New Mexico Room, chenille pool, Carlsbad Caverns NM	CM1	0.42	0.42	2.47
New Mexico Room, aragonite pool, Carlsbad Caverns NM	CM5	0.49	2.01	2.50
Sugarlands, mammillary pool, Lechuguilla Cave NM	LS2	0.82	1.77	2.59
New Mexico Room below chenille pool, Carlsbad Caverns NM	CM4	0.49	2.13	2.62
Tar Pits, Mystery Cave MN (J+A)	MYT	1.17	1.47	2.64
Pelucidar lower pool Lechuguilla Cave NM	LP3	1.60	1.20	2.80
Oasis Pool, Lechuguilla Cave NM (Oelker)	LOP	0.82	2.12	2.95
Dragon's Jaw Lake, Mystery Cave MN (J+A)	MYD	1.34	1.69	3.03
Blue Lake, Mystery Cave MN (J+A)	MYB	1.65	1.39	3.04
Rock Garden, Mystery Cave MN (J+A)	MYR	1.11	1.94	3.05
Sugar Lake, Mystery Cave MN (J+A)	MYS	1.61	1.49	3.10
Overlook, pool #2, Mammoth Cave KY	MCO2	0.94	0.31	3.19
Blue Lake drips, Mystery Cave MN (J+A)	MYD1	1.74	1.45	3.19
Dreamland drip, McFail's Cave NY	MF1	2.48	0.93	3.41
Lily Pad Lake, Mystery Cave MN (J+A)	MYP	1.68	1.81	3.49
Frozen Falls pool, Mystery Cave MN (J+A)	MYF	2.00	1.79	3.78
Frozen Falls drip, Mystery Cave MN	MYFD	2.52	2.24	4.48
Frozen Falls drip, Mystery Cave MN (J+A)	MYD5	2.39	2.16	4.55
Broken stal drip MCI-2, Mystery Cave MN (J+A)	MYD4	2.54	2.25	4.79
Rte. to Lake of Clouds, Carlsbad Caverns NM	CC	1.95	2.93	4.88
Turquoise Lake, Mystery cave MN (J+A)	MYT	2.62	2.30	4.93
Ceiling stal, MCI-4, Mystery Cave MN (J+A)	MYD3	2.68	2.35	5.03
Bedrock drips with syringe, Mystery Cave MN (J+A)	MYD2	4.22	2.33	6.55
Granddad, Mammoth Cave KY	MCD	4.42	9.09	13.51
Dilithium Pool, Lechuguilla Cave NM (Oelker)	LDP	14.15	2.00	16.15
Bitter Water Pool, Lechuguilla Cave NM (Oelker)	LBT	1.14	240.62	241.76

Table 3: Description of carbonate crystals forming in analyzed water. See Table 2 for location and water chemistry.

Samples	**Description**
MC1	Fibrous, dogtooth spar + shrubs
MCC	Twinned shrubs
MCK	Fibrous, dogtooth crystals
LLB	Curved fibrous
LP2	Dogtooth, stacked plates
LDS	Nonwarped fibrous
CLC	Fibrous
MCV	Warped, stacked rhombs
LLL	Aragonite + hydromagnesite
LBD	Rafts, cones, mammillary pool, dogtooth, fibrous
LS1	Stacked rhombs
CM6	Chenille spar, rafts, warped, stacked rhombs
MF2	Needles with tiny rhombs on tips
MF3	Shrubs
LSS	Aragonite, huntite fell into pool also
CM3	Non-warped blades on ice, dogtooth spar
CM1	No aragonite, some chenille, stacked rhombs
LS2	Aragonite, hydromagnesite nearby
CM4	Warped, stacked rhombs
MYT	No crystals in pool
LP3	Stacked rhombs
LOP	Fibrous, warped, some aragonite
MYD	Some rafts, non-warped stacked rhombs
MYB	Fibrous
MYR	Blades
MYS	Blades to rhombs
MCO2	Warped rhombs
MYD1	Dogtooth to needles
MYP	Needles to blades
MYF	Stacked blades to needles
MYFD	Shrubs with pyramidal crystals
MYD4	Twinned stalks
CC	Stalks with stacked blades
MYT	Needles
MCD	Warped rhombs
LDP	Gypsum blades
LBT	Hydromagnesite balls, non-warped and non-stacked pyramids

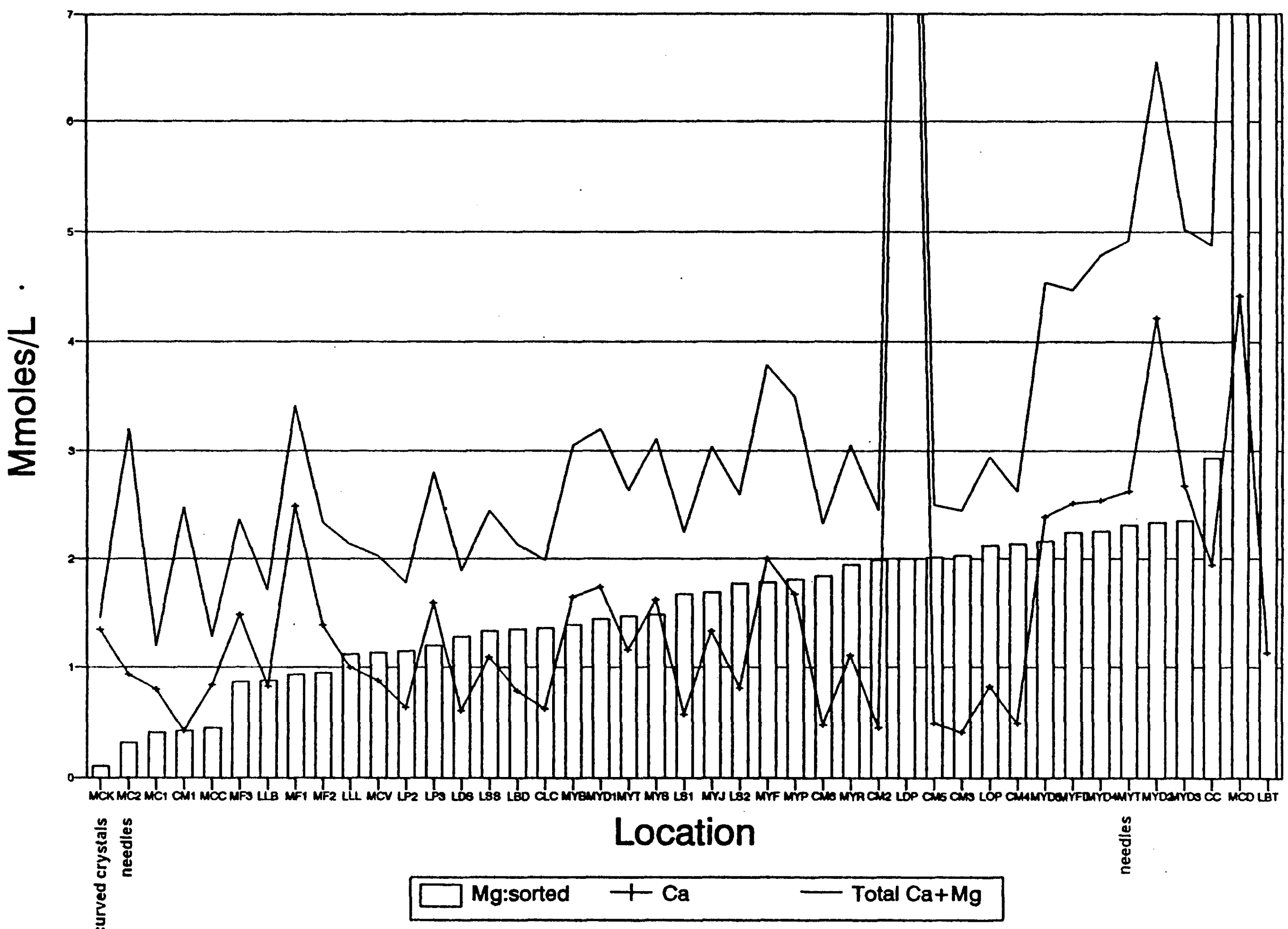

Figure 26A: Water analyses from a variety of caves including Mystery Cave, sorted by magnesium content. See Tables 2 and 3 for sample locations and description of speleothems.

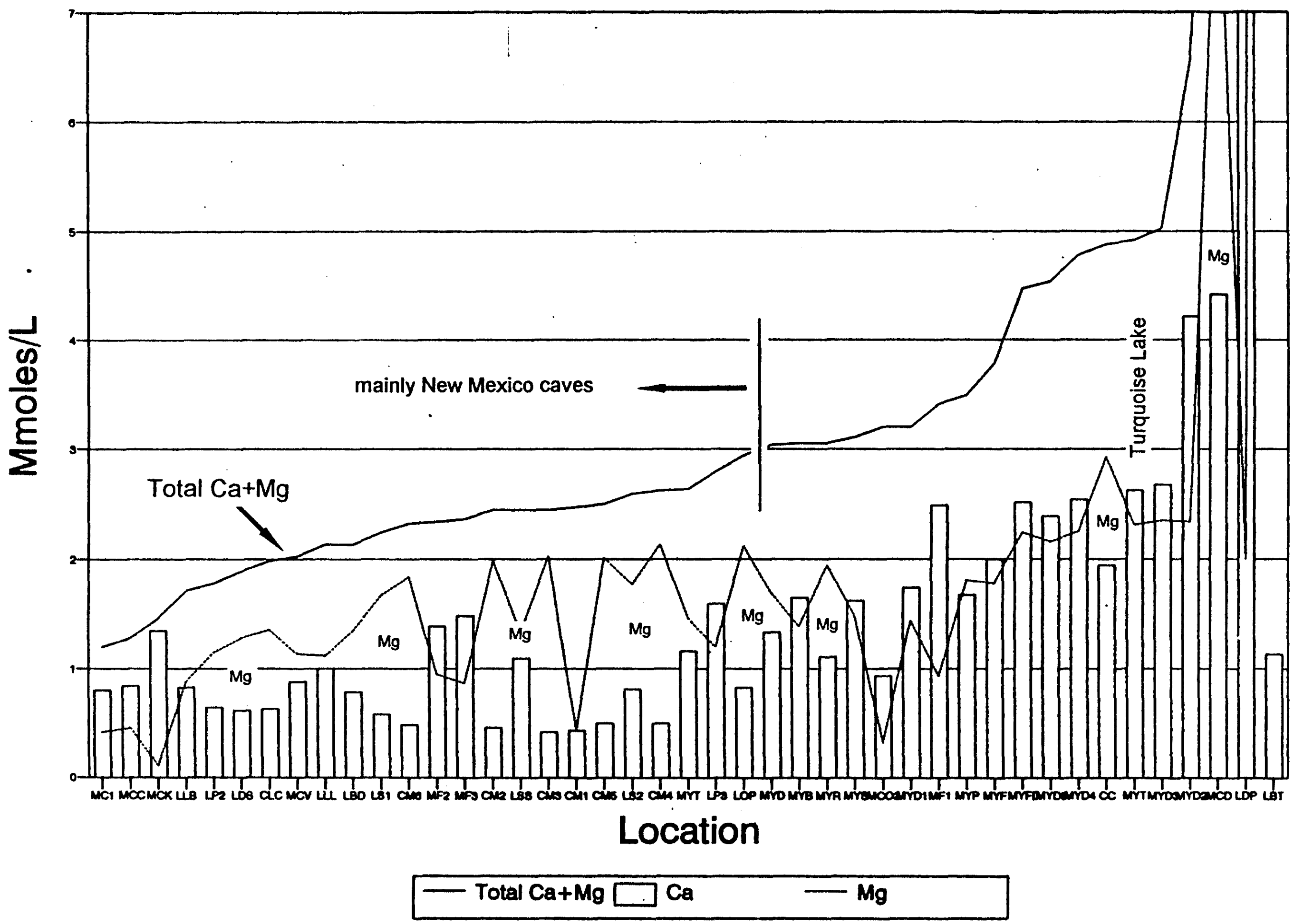

Figure 26B: Cave water analyses, sorted by total Ca + Mg content. See Tables 2 and 3 for sample locations and description of speleothems.

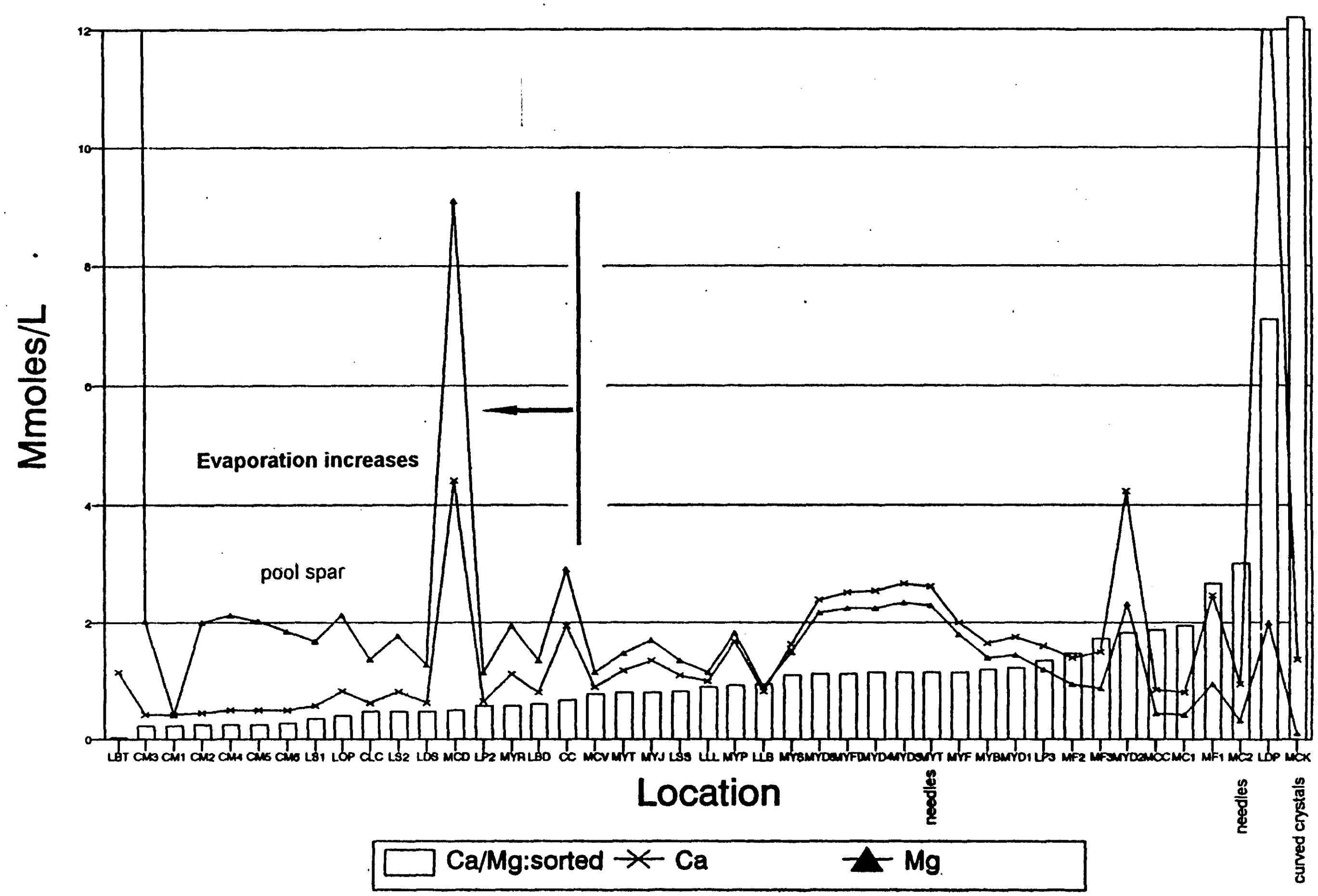

Figure 26C: Cave water analyses, sorted by Ca/Mg ratio. See Tables 2 and 3 for sample locations and description of speleothems.

A Few Observations about Speleothems in Mystery Cave

Stalactites and stalagmites

The stalactites in Mystery Cave have a pattern typical of most stalactites in having a primary thin (soda straw) core surrounded by layers of radial fibrous crystals. A stalactite fragment from near Dragon's Jaw Lake is a typical example. The initial drips that formed the stalactite deposited a thin sheet of calcite plates. By making a number of microscopic offsets, the plates of the soda straw have grown downward and outward and become the radial fibrous crystals perpendicular to the soda-straw walls. This suggests an outside attraction such as evaporation, with wicking of intercrystalline water from the inside. In other stalactites the inner soda straw plates do not bend outward. Instead, layers of fibrous crystals grow perpendicularly from the outside of the initial soda straw, but their outer edges are truncated at various angles (Figure 27). The surface may have been dissolved periodically by floodwater or by condensation of water from air. Some stalactites have silt and clay clastic sediment between the outer layers, showing that water from outside the stalactite tube coated it with sediment, possibly during flood events.

The central tube of a stalactite fragment from the Tar Pits is almost completely blocked by monocrystalline calcite, except for a tiny central hole (Figure 28). This may have been caused by a decrease in the drip rate. In a closed system, with only a small amount of recharge, the central tube can act like a tiny pool environment and acquire crystals similar (but on a much smaller scale) to pool deposits. Such monocrystalline cores are common in many of the older stalactites in the cave and may represent a climate change from wet interglacial to dryer glacial conditions.

The Door to Door route contains many areas of naturally broken speleothems. For example, MY 214 from the Culverts area probably represents a typical stalagmite. Dripping water formed thin layers of fibrous spar perpendicular to the floor. The layering represents periods of growth with periodic interruptions, as shown by the fact that certain layers cover the truncated surfaces of the layer beneath, as in the Dragon's Jaw Lake stalactite. Because the layers of spar in stalagmites form in thin films of water, the crystals have the same morphology as those in flowstone. Sample MY214 contains layers that are very porous. The pores were once water filled and behaved as tiny pockets that were roofed over by later calcite.

Iron-rich speleothems

Shaly limestone from bed DS11 (MY76) in the western part of Fifth Avenue contains patches of hematite (iron oxide) and gypsum (Figure 29). Both the hematite and the gypsum were derived from the oxidation of former pyrite. Most of the gypsum forms concentric balls of crystals surrounded by a rim of hematite pushed outward by the gypsum.

Another sample is a small iron-rich stalactite that peeled off flush with the ceiling. Its upper end is flared so that its broken top is flat where it once was attached to the ceiling. The stalactite appears to have originated as a thin film of calcite on the ceiling, and as water eventually consolidated into a drip, it formed a soda straw with walls surrounding a narrow central canal. Layers of radial fibrous crystals formed around the central soda-straw core. The calcite layers are separated by layers of iron oxide deposited by the water from the bedding plane above. This is apparently a miniature version of the iron-oxide-rich stalactites in the Formation Room.

Figure 27: Cross section of stalactite fragment MY130, showing truncated layers (arrow). Enlargement = 60X (non-polarized light).

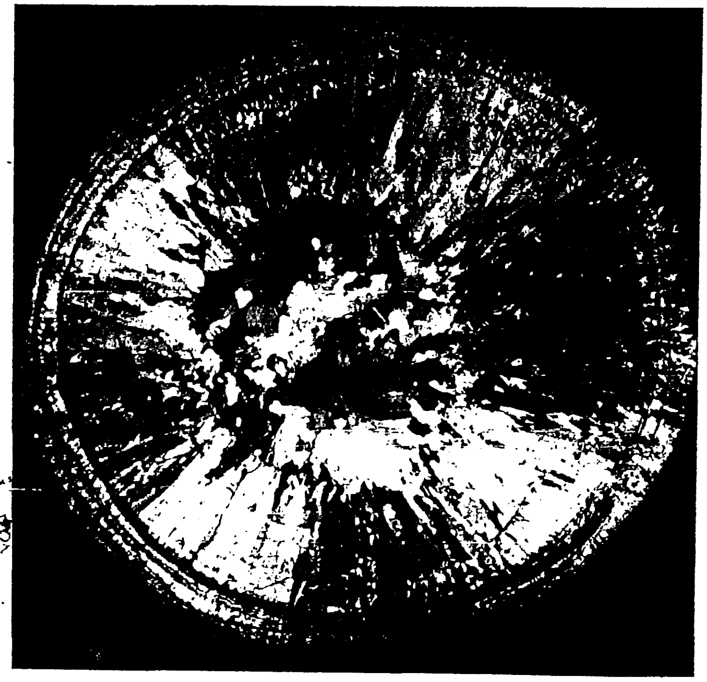

Figure 28: Cross section of stalactite fragment in which the central tube is nearly filled with calcite (MY130). Enlargement = 8X (polarized light).

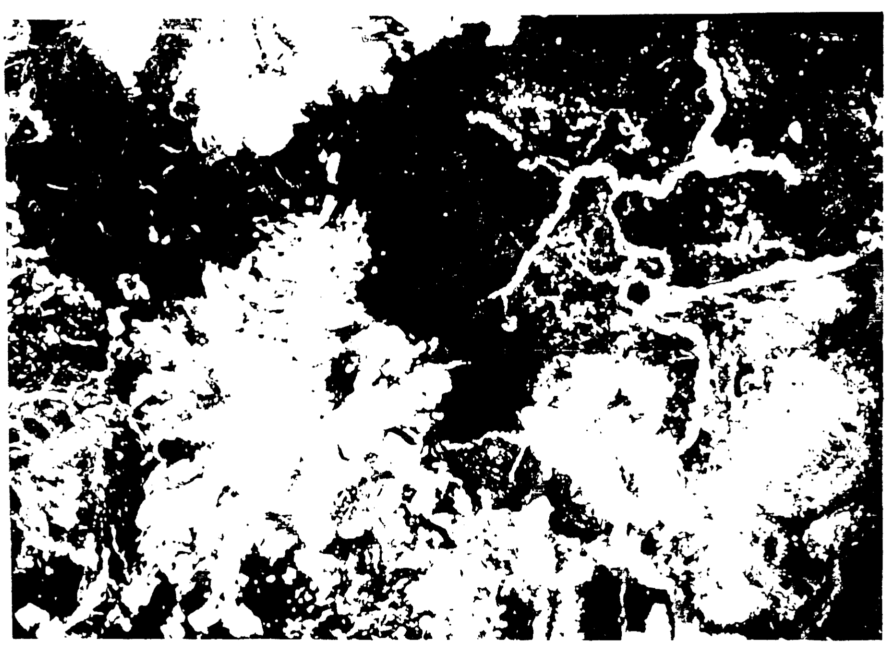

Figure 29: Gypsum clusters (white) surrounded by hematite (black) from the weathering of pyrite (MY78). Enlargement 3X (polarized).

Levels of Static Ponding

There are well-defined levels of deposition that represent old water levels -- mainly shelfstone and rimstone. These were carefully measured during the leveling project. It is quite clear from their disparate elevations that almost none of them correlate with each other! Ponding is controlled entirely by local conditions, such as breakdown and sediment fill. Former water levels, as shown by shelfstone, can be traced for short distances with very little if any change in elevation. However, from one passage to another there is no correlation in elevation. They do not represent widespread ponding levels but are local pools fed by infiltrating water from the surface, as at Blue Lake, Dragon's Jaw Lake, and Turquoise Lake. Many are still actively forming, although some have been covered by later sediment, as in the Bomb Shelter area. In Mystery I much shelfstone was removed from the route between Turquoise Lake and the Bomb Shelter to help open the area to visitors during the early days of commercialization. This broken material was dumped into the low area below Frozen Falls to build up the trail in that area. This dump site was re-excavated in the early 1990s, and the fragments of shelfstone took yet another trip, this time to a dump pile by the driveway. Some of the better-looking pieces were moved to the Cathedral Room or to the old outhouse across the river. We salvaged some of the material from the dump pile and outhouse for analysis.

VIBRATION MEASUREMENTS

The Bison seismometer was used in the Garden of Gods and nearby passages to determine the effect of surface-induced vibrations on the cave. This study was intended to shed light on the following: (1) possible damage to the cave as the result of future blasting in Grabau Quarry and movement of heavy trucks on the north-south road that passes over the cave near Garden of the Gods; (2) prolonged creaking or groaning noises in Mystery II, suggesting the movement of rocks; (3) vibrations felt in the cave when a bulldozer was operating near the Mystery II entrance.

Vibration energy from a shock source diminishes greatly with distance -- roughly with the square of the distance. Therefore a disturbance that produces a certain vibration at 10 feet will produce only about 25% as much vibration at 20 ft. Local disturbances in the cave, such as footsteps and drips, can produce large vibration amplitudes over short distances, but their overall energy is tiny compared to shocks that disperse energy throughout large areas, such as quarry blasts.

The seismometer was first tested with normal footsteps near the geophone, which was planted in the gravel pavement of the trail near Garden of the Gods. At full gain, mean vibration level from normal sneakered footsteps at 10-ft distance was used as a personal standard (amplitude = 1.0 units). Background vibration in the dry parts of the route was undetectable.

The geophone was then planted in a crack in flowstone in contact with the bedrock wall of Garden of the Gods. The background vibration was 0.07 units because of much dripping water. There were occasional 5-10 sec episodes of intensified low-frequency vibration of 0.1 - 0.17 units, possibly because of disturbance of tree roots by gusts of wind, which were intensifying at the time. A moderately loaded Ford Econoline van was then repeatedly driven over the driveway near the entrance gate to the Mystery Cave property, closest to the Garden of the Gods. There was no measurable increase in vibration. The van was then repeatedly driven over a 6"-diameter log at the same location. During this time, short bursts of vibration up to 0.1 unit were observed in the cave, barely exceeding the background level. Finally, a 1"-thick aluminum plate was repeatedly struck with a sledge hammer at the same surface site. This produced short vibration bursts of 0.3 - 0.5 units. The hammering therefore produced vibration intensities about 3 to 5 times greater than that of the truck driven over the log. Neither was detectable without the seismometer.

The geophone was then moved to the sediment on the floor of Garden of the Gods. Vibration increased considerably because of the many nearby drips of water from the walls and ceiling. The greatest amplitude was caused by a drip from a height of 10 ft. into a slightly concave pocket in the sediment floor. At a distance of one inch, it drove the meter right off the scale -- at least twice the amplitude of the standard footfall. However, because of the close proximity to the geophone, the drip represented much less energy than the footfall.

These vibration measurements shed a little light on the questions posed above. However, much more sophisticated analyses and vibration sources are needed for a full evaluation. Apparently normal traffic on the surface has minimal effect on the cave. Intense shocks, such as quarry blasts, would have a much greater effect. A drop of water or a footfall can send the meter off the scale at short distances, but the energy level is considerably smaller than vibrations generated by larger remote sources. Measurements within the cave are useful only in providing interesting comparisons. Widespread low-frequency, high-energy vibration is potentially the most damaging. Unfortunately it is difficult to estimate how much vibration energy the cave can tolerate before rockfall occurs. The structural attributes of the cave are very complex compared to those of artificial structures.

A few observations may help to clarify the situation. In general, the cave passages are extremely stable. They have not been blasted out of the native rock, but enlarged by solution, with natural rockfall stabilizing otherwise unstable spots. The high, narrow fissure passages are most stable, but some of the wide flat-ceilinged passages in the Dubuque are rather unstable, and occasional rockfall in such areas is likely.

Sediment fill in the cave vibrates discontinuously with the bedrock. The amplitude of vibrations increases when shock waves encounter the sediment, and the overall potential for damage is greater for anything situated on the sediment (walls, stalagmites, etc.). In general the bedrock moves more or less as a unit, so the bedrock structure of the cave is relatively stable. Stalactites and stalagmites oscillate at different frequencies and can snap off if the vibration is exceptionally great. This is unlikely. The many naturally broken speleothems in the cave probably met their fate during freeze-thaw cycles during the last glaciation, rather than as the result of an earthquake. Earthquakes, which represent the largest probable source of energy in the area, rarely have any significant effect on caves. Likewise, surface sources, although potentially closer, would have little effect; most of their energy is dissipated as surface waves that die out rapidly with depth below the surface.

The source of the creaking and groaning in the cave is enigmatic, and it is impossible to identify them without first-hand experience. However, similar sounds have been heard in other caves. Groaning Cave in Colorado was named for similar sounds whose source could not be identified. We have heard short-duration sounds of this sort in the vicinity of breakdown piles, particularly those cemented with a matrix of sediment. Settling and shifting of blocks in such areas is common, especially during relatively wet periods.

In addition, water flowing into the west end of Fourth Avenue beyond the Yellow Flow during periods of high discharge produces a reverberating pounding sound reminiscent of the sounds reported by the guides. It is likely that many of the reported noises can be attributed to water movement, especially since there is such a large fluctuation of water levels in the cave.

The source of natural disturbances in the cave is an interesting area for further study -- although not necessarily a fruitful one. A triple array of continuously recording seismometers could be set up to identify the location of vibration sources, the nature of the vibrations, and possibly the direction of displacement that causes the vibrations, much like earthquake seismology.

CONCLUSIONS

Several lines of research have proved useful in the interpretation of Mystery Cave. Although this is only a preliminary report, to be updated and expanded in 1994, results to date include the following: (1) A geologic profile was made in the main passages of the cave. This apparently represents the most detailed survey of its kind in any cave. (2) Bench marks were placed in many locations in the cave and on the surface and were tied to the 1989 DNR survey bench marks. Discrepancy between our underground survey and the DNR surface survey was within 5 cm. (3) Analysis of bedrock samples has provided information about the environment of deposition of the rocks, explains the texture of the rocks as they appear in the cave, and gives new criteria (mainly dolomite content) for subdividing the Dubuque Formation into members. (4) Analysis of speleothems and water chemistry relate the crystal structure of the speleothems to pool chemistry. This information will help interpret past conditions in caves that are no longer active. (5) Seismic profiles show that the bedrock floor of the valley of the South Branch of Root River lies 20-27 feet below the present valley floor and is more or less at grade with the passages in Mystery Cave. The silt in the cave appears to be the same material (apparently mostly loess) that fills the valley. (6) The origin of the cave seems to have been intimately controlled by the entrenchment history of the South Branch and probably 500,000 - 1,000,000 years old. (7) Structural mapping shows that the northwest-southeast fissure passages in the northeastern part of Mystery Cave appear to be controlled by a sharp steepening of dip. (8) Normal traffic over the cave, including truck traffic, has little vibrational effect on the cave.

Mystery Cave proves to be a significant natural laboratory for scientific study. Few caves in the United States contain as much information about glacial history, structural control of passages, crystal growth, and water flow. Minnesota is fortunate to have a cave of this calibre.

REFERENCES

Bischoff, J.L., and Fyfe, W.S., 1968, Catalysis, inhibition, and the calcite-aragonite problem: American Journal of Science, v. 266, p. 65-79.

Blatt, H., Middleton, G., and Murray, R., 1980, Origin of sedimentary rocks (2nd ed.): Englewood Cliffs, NJ, Prentice-Hall, Inc., 782 p.

Compton, J.S., 1988, Sediment composition and precipitation of dolomite and pyrite in the Neogene Monterey and Sisquoc Formations, Santa Maria Basin area, California, **in** Sedimentology and geochemistry of dolostones, Shukla, V., and Baker, P.A. (eds.): Society of Economic Petrology and Mineralogy Special Publication 43, p. 53-64.

Curl, R.L., 1974, Deducing flow velocity in cave conduits from scallops: National Speleological Society Bulletin, v. 36, p. 1-5.

Delgado, D.J., 1983, Deposition and diagenesis of the Galena Group in the Upper Mississippi Valley **in** Ordovician Galena Group of the Upper Mississippi Valley - deposition, diagenesis, and paleoecology, Delgado, D.J. (ed.): Guidebook for the 13th Annual Field Conference, Great Lakes Section, SEPM, p. A1-A17.

Dickson, J.A.D., 1978, Length-slow and length-fast calcite: a tale of two elongations: Geology, v. 6, p. 560-561.

----, 1993, Crystal growth diagrams as an aid to interpreting the fabrics of calcite aggregates: Journal of Sedimentary Petrology, v. 63, p. 1-17.

Easton, W.H., 1960, Invertebrate paleontology: New York, Harper and Row, 701 p.

Folk, R.L, 1974, The natural history of crystalline calcium carbonate: effect of magnesium content and salinity: Journal of Sedimentary Petrology, v. 44, p. 40-53.

Friedman, G.M., 1980, Dolomite is an evaporite mineral: evidence from the rock record and from sea-marginal ponds of the Red Sea, **in** Fossil algae, recent results and developments, Flugel, Erik (ed.): Springer-Verlag, N.Y., p. 66-73.

Given, R.K., and Wilkinson, B.H., 1985, Kinetic control of morphology, composition, and mineralogy of abiotic sedimentary carbonates: Journal of Sedimentary Petrology, v. 55, p. 109-119.

Gonzalez, L.A., Carpenter, S.J., and Lohmann, K.C., 1992, Inorganic calcite morphology: roles of fluid chemistry and fluid flow: Journal of Sedimentary Petrology, v. 62, p. 382-399.

Grow, S.R., 1986, Water quality in the Forestville Creek karst basin of southeastern Minnesota: M.S. thesis, University of Minnesota, Minneapolis, MN, 229 p.

Hallberg, G.R., Witzke, B.J., Bettis, E.A., and Ludvigson, G.A., 1985, Observations on the evolution and age of the bedrock surface in eastern Iowa in Pleistocene geology and evolution of the Upper Mississippi Valley, Lively, R.S. (ed.): Abstracts and Field Trip Guide, Minnesota Geological Survey, St. Paul MN, p. 15-19.

Hardie, L.A., 1987, Perspectives dolomitization: a critical view of some current views: Journal of Sedimentary Geology, v. 57, p. 166-183.

Harmon, R.S., Ford, D.C., and Schwarcz, H.P., 1977, Interglacial chronology of the rocky and Mackenzie Mountains based on $^{230}Th/^{234}U$ dating of calcite speleothems: Canadian Journal of Earth Science, v. 14, p. 2543-2552.

Hennig, G.J., Grun, R., and Brunnacher, K., 1983, Speleothems, travertines and paleoclimates: Quaternary Research, v. 29, p. 1-29.

Hill, C.A., and Forti, P., 1986, Cave minerals of the world: Huntsville, Ala., National Speleological Society, 238 p.

Hjulström, F., 1935, Studies of the morphological activity of rivers as illustrated by the River Fyris: Univ. of Uppsala, Geological Institute Bulletin 25, p. 221-557.

Hobbs, H.C., 1985, Quaternary history of southeastern Minnesota, **in** Pleistocene geology and evolution of the Upper Mississippi Valley, Lively, R.S. (ed.): Abstracts and Field Trip Guide, Minnesota Geological Survey, St. Paul MN, p. 11-14.

Jones, B., 1989, Syntaxial overgrowths on dolomite crystals in the Bluff Formation, Grand Cayman, British West Indies: Journal of Sedimentary Petrology, v. 59, p. 839-847.

Kendall, A.C., and Broughton, P.L., 1978, Origin of fabrics in speleothems composed of columnar calcite crystals: Journal of Sedimentary Petrology, v. 48, p. 519-538.

Levorson, C.O., and Gerk, A.J., 1983, Field recognition of stratigraphic position within the Galena Group of northeast Iowa (limestone facies), **in** Ordovician Galena Group of the Upper Mississippi Valley, deposition, diagenesis and paleoecology, Delgado, D.J. (ed.): Guidebook for the 13th Annual Field Conference, Great Lakes Section, SEPM, p. C1-C11.

Lively, R.S., and Alexander, E.C., 1985, Karst and the Pleistocene history of the Upper Mississippi River Valley **in** Pleistocene geology and evolution of the Upper Mississippi Valley, Lively, R.S. (ed.): Abstracts and Field Trip Guide, Minnesota Geological Survey, St. Paul MN, p. 31-32.

Mason, J.A., 1992, Loess distribution and soil landscape evolution, southeastern Minnesota: M.S. thesis, University of Minnesota, St. Paul, MN, 407 p.

Milske, J.A., 1982, Stratigraphy and petrology of clastic sediments in Mystery Cave, Fillmore County, Minnesota: M.S. thesis, University of Minnesota, St. Paul, MN, 111 p.

Milske, J.A., Alexander, E.C., and Lively, R.S., 1983, Clastic sediments in Mystery Cave, southeastern Minnesota: National Speleological Society Bulletin, v. 45, p. 55-75.

Mullins, H.T., Dix, G.R., Gardulski, A.F., and Land, L.S., 1988, Neogene deep-water dolomite from the Florida-Bahama platform **in** Sedimentology and geochemistry of dolostones, Shukla, V., and Baker, P.A. (eds.): SEPM Special Publication 43, p. 235-243.

Oelker, G.L., 1991, The Lechuguilla Cave water study: unpublished report.

Palmer, A.N., 1975, The origin of maze caves: National Speleological Society Bulletin, v. 37, p. 36-56.

----, 1981, A geological guide to Mammoth Cave National Park: Teaneck, N.J., Zephyrus Press, 210 p.

----, 1991, Origin and morphology of limestone caves: Geological Society of America Bulletin, v. 103, p. 1-21.

Palmer, M.V., 1976, Ground-water flow patterns in limestone solution channels: MA thesis, State University of New York, College at Oneonta, 150 p.

Phillips,. W.R., and Griffen, D.T., 1981, Optical mineralogy, the nonopaque minerals: San Francisco, W.H. Freeman and Co., 677 p.

Scholle, P.A., 1978, Carbonate rock constituents, textures, cements, and porosities: American Association of Petroleum Geologists Memoir 27, 241 p.

Seyfert, C.K., and Sirkin, L.A., 1979, Earth history and plate tectonics: New York, Harper and Row, 600 p.

Sloan, 1985, Pleistocene fluvial geomorphology of southeastern Minnesota, **in** Pleistocene geology and evolution of the Upper Mississippi Valley, Lively, R.S. (ed.): Abstracts and Field Trip Guide, Minnesota Geological Survey, St. Paul MN, p. 27-30.

----, (ed.), 1987, Middle and Late Ordovician lithostratigraphy and biostratigraphy of the Upper Mississippi Valley: Minnesota Geological Survey, Report of Investigations 35, 232 p.

----, 1987, Tectonics, biostratigraphy and lithostratigraphy of the Middle and Late Ordovician of the Upper Mississippi Valley **in** Middle and Late Ordovician lithostratigraphy and biostratigraphy of the Upper Mississippi Valley: Minnesota Geological Survey Report of Investigations 35, p. 7-20.

Sloan, R.L., and Webers, G.F., 1987, Stratigraphic ranges of Middle and Late Ordovician gastropoda and monoplacophora of Minnesota, **in** Middle and Late Ordovician lithostratigraphy and biostratigraphy of the upper Mississippi Valley, Sloan, R.E. (ed.): Minnesota Geological Survey Report of Investigations 35, p. 183.

Sloss, L.L., 1963, Sequences in the cratonic interior of North America: Geological Society of America Bulletin, v. 74, p. 93-114.

Southgate, P.N., 1986, Cambrian phoscrete profiles, coated grains, and microbial processes in phosphogenesis: Georgina Basin, Australia, Journal of Sedimentary Petrology, v. 56, p. 429-441.

Walkden, G.M., and Berry, J.R., 1984, Natural calcite in cathodoluminescence: crystal growth during diagenesis: Nature, v. 308, p. 525-527.

Witzke, B.J., 1983, Ordovician Galena Group in Iowa subsurface in Ordovician Galena Group of the Upper Mississippi Valley - Deposition, diagenesis, and paleoecology, Delgado, D.J. (ed.): Guidebook for the 13th Annual Field Conference, Great Lakes Section SEPM, p. D1-D26.

Wright, H.E., 1985, History of the Mississippi river in Minnesota below St. Paul in Pleistocene geology and evolution of the Upper Mississippi Valley, Lively, R.S. (ed.): Abstracts and Field Trip Guide, Minnesota Geological Survey, St. Paul MN, p. 1-2.

APPENDIX 1 -- Bench Marks in Mystery Cave

The following semi-permanent points serve as bench marks for elevations in Mystery Cave. Their locations are shown on the accompanying map and are described below. Some are located on features that may change with time, such as handrails; these are generally accompanied by a nearby permanent station such as a chiseled + in the wall. Bench marks are arranged in order as they are encountered in traveling from Mystery I to Mystery II.

Bench Mark	Altitude (ft)	Feature	Location
D1	1230.37 ft.	nail in basswood tree	South of Mystery I ticket office, on east side of trees, 1 ft above ground.
D861	1228.36	+ on rock wall	Walnut Cave entrance, + chiseled in rock face 2-3 ft south of entrance:

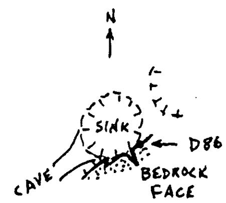

Bench Mark	Altitude (ft)	Feature	Location
D873	1244.41	+ on cliff face	Chiseled + in bedrock wall 5 ft north of north end of Old Mystery Cave entrance, one foot higher than the top of the entrance arch, and in same bed that forms the top of the entrance arch.
D863	1211.41	+ on wall	Chiseled + in northwest wall of Old Mystery Cave, 4.3 ft above floor in middle of bed DL3, 0.38 ft above old shelfstone top.
D868	1209.26	top of basin	Topmost point on south corner of artificial catch basin below waterfall near end of Old Mystery Cave:

Bench Mark	Altitude (ft)	Feature	Location
D879	1254.95	+ on cliff face	Chiseled + on smooth recessed bed on west-facing section of cliff, one foot below geode in overlying bed, and located between geode and entrance; 3 ft south of entrance arch, on right wall (facing entrance).

D456	1228.92	bottom hinge on door	Top surface of lower hinge on flood-proof door at Mystery I entrance: 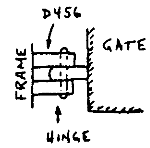
D460	1225.76	+ in concrete	1" chiseled + in concrete wall to south of inner door of Mystery I
D2	1218.56	top of stalagmite	Small stalagmite on south side of main passage in Mystery I, across from opening to Needle's Eye passage, now below level of trail.
D698	1216.26	+ on wall	In main passage of Mystery I, 1 inch below top of bed DL9, under ledge, 3 ft above trail on northwest side of opening to Needle's Eye passage.
D328	1210.46	top of stalagmite	At Needle's Eye, top of small stalagmite on southeast wall of entrance of fissure that drops to stream: 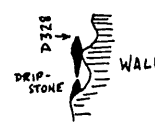
D701	1213.28	+ in artificial wall	Chiseled + in bed DL6, on south side of concrete ramp in main passage of Mystery I leading to Formation Room passage, 1.5 ft above ramp, 1 ft to west of (and 4" below) phone box.
D335	1209.54	top of railing	In passage to Formation Room: top surface of northeast end of southeast handrail on bridge across fissure, next to bedrock wall: 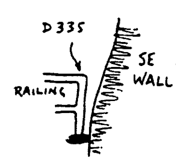
D728	1208.97	+ on wall	Chiseled + on northwest wall of passage to Formation Room, 3 ft above floor, in bed DL1, at northeast end of grate over fissure in floor.

D348	1222.96	lower tip of stalactite	Lower tip of broken stalactite with iron-oxide core -- easternmost and largest of deflected stalactites at north end of Formation Room, 6.2 ft above sediment floor:

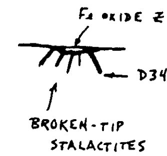

D3	1218.54	top of railing	Top of northwest elbow of handrail at west end of bridge by Frozen Falls:

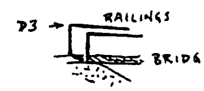

D704	1212.22	+ on wall	Chiseled + at entrance to passage to Cathedral Room, on west wall, 2 ft above trail at bottom of steps, in bed DL5.
S360	1226.07	radio location	Nail with flagging in floor at top of stairs in Cathedral Room, marking radio transmitter station.
D4	1216.93	top of railing	Top of southeast elbow of handrail at east end of bridge by Frozen Falls:

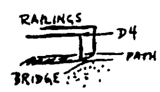

D707	1218.79	+ on artificial wall	Chiseled + in artificial rock face 1.5 ft above trail on south side of main passage of Mystery I, opposite western end of Rock Garden, about 2 ft west of western end of railing, 1.8 ft below top of flowstone cap over sediment.
D37	1220.87	top of stalagmite	Top of tiny stalagmite in Rock Garden, immediately east of small dripstone column near north wall of passage:

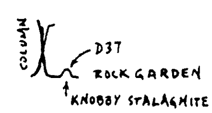

D710	1220.83	top of stalagmite	Top of stalagmite on flowstone-cemented breakdown slab on south side of main passage of Mystery I, 3.9 ft above concrete trail, just before broad flowstone mound with rippled surface on same side of passage, and 15 ft west of broken eastern end of flowstone cap over sediment.
D714	1216.25	+ on wall	Chiseled + on west wall of passage to Turquoise Lake, 6 ft from junction with main passage of Mystery I, 3.3 ft above concrete trail, in bed DL8.
S44	1214.59	top of concrete dam	Flat top of dam at Turquoise Lake.
D717	1218.39	+ on wall	chiseled + in bed DL10, 4 ft above trail on south side of main passage in Mystery I, 14 ft beyond easternmost raft cone in western group of cones.
D719	1217.19	top of raft cone	Tip of westernmost raft cone on south side of main passage of Mystery I in eastern group of cones, 2 ft west of cone that occupies middle of trail.
D53	1219.15	top of stalgmite	Top of small muddy stalagmite on east wall of Bomb Shelter, 1.4 ft above floor. During our resurvey we found that the stalagmite is loose and may shift with time.
D726	1219.19	+ on wall	Chiseled + on northeast wall of Bomb Shelter, 1.5 ft above floor at point where dirt floor begins to slope into the crawl to the door-to-door route. In bed DL9 under overhanging ledge.
D62	1214.74	top of raft cone	Topmost part of highest (and largest) raft cone (partly broken) in the group of cones just below the climb over breakdown about 250 ft northeast of Bomb Shelter on door-to-door route.
D71	1214.05	dot on breakdown	Carbide dot on small slab of rock on eastern corner of bend where narrow fissure branches to left from door-to-door route:

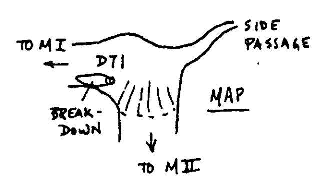

D370	1218.05	+ on wall	Penciled + on northwest wall of door-to-door route, above and just beyond crawlway opening to route leading to drop-down to stream. (Note: repeti-

tion of last digits in + elevations on door-to-door route is a result of datum-line survey with hand level, which changes datum in even numbers of feet.)

H840 1209.95 top of pyritic bed

Top of bed DT 4, at base of first significant shale in Dubuque Formation. Bed DT4 has iron oxide stains and pockets near top caused by weathering of pyrite.

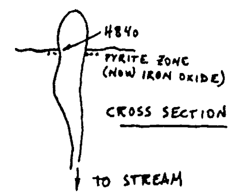

D387 1218.71 top of stalagmite

Top of flagged stalagmite on breakdown block on northeast slope of breakdown pile in door-to-door route:

D402 1218.15 flagged survey station

Old survey station marked by flagging on breakdown slope near bottom of junction at Big Fork.

H833 1224.75 top of breakdown

Top of flat slab of breakdown in floor at entrance to Wind Tunnel:

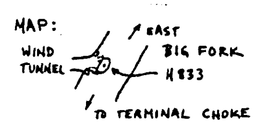

D434 1209.63 top of stalagmite

Top of highest stalagmite on crest of thin blade of breakdown in door-to-door route:

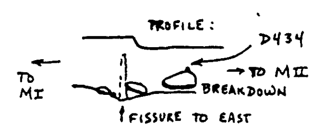

D438 1212.35 flagging tape

Upper tip of old survey station marked with flagging tape at junction with Little Fork, 2.3 ft below ceiling on high ledge along eastern wall of junction.

D581	1213.23	top of stalagmite	Top of small stalagmite at level of BP1 beneath white soda straws in door-to-door route:

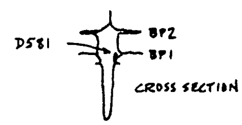

D598	1216.05	pencil line on wall	Horizontal pencil line on northeast wall at junction with Incline, 3 ft below ceiling:

D672	1215.85	+ on wall	Penciled + on ledge immediately below "CAMP" sign in Sand Camp, 2 ft below ceiling.
D676	1213.73	top of stalagmite	Top of 9" stalagmite at edge of fissure in floor, 14 ft northeast of iron oxide drapery northeast of Sand Camp.
D634	1216.57	+ on wall	Penciled + on southeast wall at SW junction with Cutoff, 1.5 ft below ceiling and 4.8 ft above edge of floor fissure, in fossil-rich limestone.
D622	1213.46	top of stalagmite	Top of larger of two stalagmites on west side of passage northeast of Cutoff, southwest of Boofer Pool. They are loose, apparently having been fractured by natural weathering, but are still in place.
D619	1213.02	top of stalagmite	Top of stalagmite in southern corner of bend next to most impressive array of stalactites and stalagmites, 6.5 ft below ceiling:

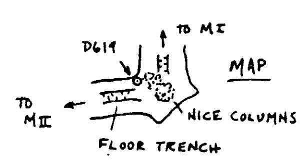

D612	1208.51	top of stalagmite	Top of stalagmite in fissure indentation in wall of floor slot at drop to Flim Flam Creek; it is the lower of two 2" stalagmites 1 ft below the

ledge overlooking the slot, and 2.5 ft northeast of slot that drops to stream:

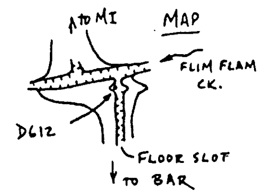

D72 1211.57 top of stalagmite

Top of stalagmite on northwest edge of fissure in floor, across from dripstone column, about 20 ft southwest of Bar:

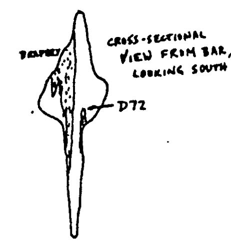

D787 1211.41 top of stalagmite

Top of highest stalagmite in cluster on northwest side of passage 11 ft northeast of Bar. There is a little nubbin at the top where a stalactitic column once touched it but has been broken away:

D77 1213.76 bottom tip of popcorn

Bottom tip of popcorn in a small cluster at junction of Angel Loop with passage to the Bar:

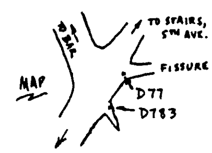

D783 1211.41 + on wall

Chiseled + on wall 2 ft above floor at northern edge of junction between Angel Loop and passage to the Bar (see above).

D794	1207.55	+ on wall	Chiseled + on wall 9" above floor at joint intersection southwest of radon monitor in Angel Loop, 6" northeast of dropoff into fissure and 6" from the angle of rock at the joint intersection:

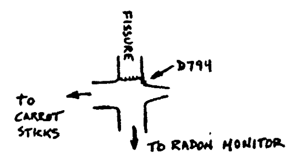

D779	1210.76	+ on wall	Chiseled + on wall at cross fissure along joint in Angel Loop, 1 ft above floor in fissure indentation in south wall of passage:

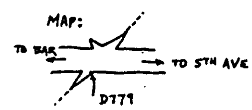

D187	1213.32	top of stalagmite	Top of highest stalagmite beneath Carrot Sticks in Angel Loop.
D111	1216.67	tip of rock pendant	Bottom of prow-shaped rock pendant projecting downward into passage at northeastern end of Angel Loop, about 20 ft from eastern junction with 5th Ave., 6.6 ft above floor:

D731	1213.17	+ on wall	Chiseled + in north wall of 5th Ave. at eastern junction with Angel Loop, 1 ft above trail, on smooth rock face 2 ft west of small dead-end joint fissure.
D104	1227.15	top of rock chip	Uppermost tip of rock-chip scar above entrance to Fat Man's Misery:

D88 1225.47 tip of breakdown

Upper tip of pointed breakdown slab along south wall of 5th Ave., 38 feet from entrance to passage to Smoking Chamber, 2.5 ft above adjacent floor:

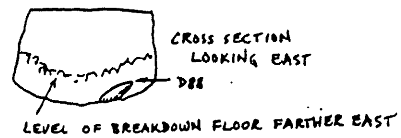

D797 1224.28 + on wall

Chiseled + on wall in bed DL2, 2.5 ft above floor and 2 ft west of rock barrier in entrance to western extension of 5th Ave.:

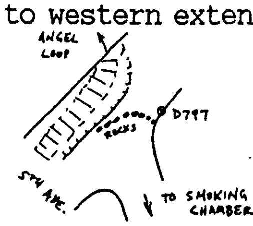

D91 1219.71 pool level

Threshold of overflow slot in drip pool in Smoking Chamber.

D99 1231.83 upper tip of chip scar

Top of scar where rock chip has been broken away, directly over entrance to crawlway in northeast wall of Base Camp, which leads to Enigma Pit, etc., about 2.4 ft above floor:

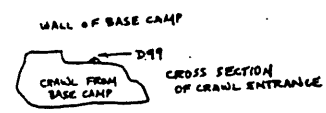

D737 1212.25 + on breakdown

Chiseled + on large breakdown slab occupying most of the floor along the north side of 5th Ave., 6" above trail, at west end of slab:

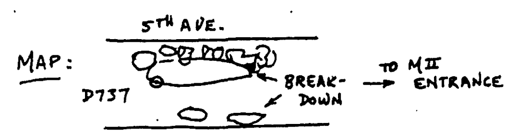

D743 1219.69 + on wall

Chiseled + in Stewartville Formation, 4.6 ft above floor on north side of 5th Ave., at contact with artificial stone wall of ramp from 4th Ave., at eastern junction with 4th Ave.

D118 1216.83 bottom of elbow

Bottom of elbow at lower end of ramp handrail at eastern junction between 5th Ave. and 4th Ave., on north side of 5th Ave.

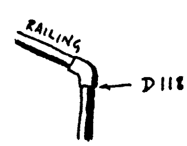

D802 1230.33 + on wall

Chiseled + on wall at southwest corner of Dome Room, above middle step leading to Diamond Caverns, 2 ft above middle step, 2" above BP2, and 2 ft from southwestern corner of intersection at Dome Room:

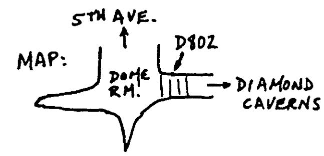

D806 1226.70 + on wall

Chiseled + on wall 6" above floor of Diamond Caverns, on south wall across from joint fissure in wall:

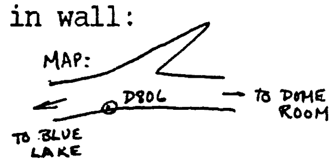

D810 1231.76 + on wall

Chiseled + on wall on northwest corner of entry to Diamond Caverns from Blue Lake area, 2.5 ft above floor at base of steps in 4th Ave.:

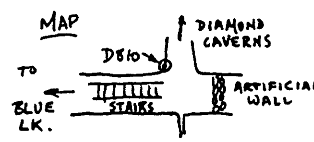

D205 1239.72 rail top

Top of railing at eastern end of Blue Lake, at southeastern elbow, 3.1 ft above floor:

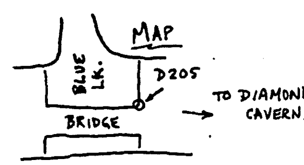

D813 1237.49 + on wall

Chiseled + on south wall of 4th Ave., 11 ft to east of bridge over Blue Lake, 10" above floor on fresh surface of shaly limestone, 2 ft east of jog in wall:

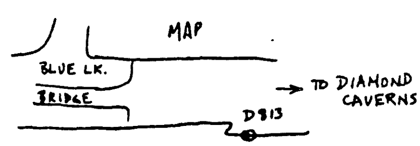

D203 1240.10 top of stalagmite

Top of small stalagmite on large flowstone mound west of Blue Lake, 4.6 ft above trail, on opposite side of flowstone from Mushroom (Cross):

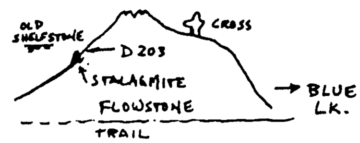

D818 1225.06 + on wall

chiseled + in south wall of 4th Ave. above breakdown pile near low point of "valley" between Hills of Rome, 2.5 ft above trail:

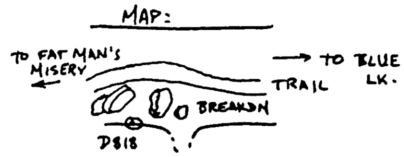

D822 1238.93 + on breakdown

Chiseled + near east tip of large breakdown slab on south side of trail above top step on western end of "valley" between Hills of Rome, 3.5 ft above trail:

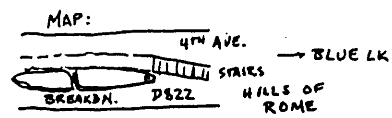

D826 1228.94 + on wall

Chiseled + on iron-oxide-stained rock face beneath overhanging ledge on southeastern corner of junction between 4th Ave. and Fat Man's Misery, 1.5 ft above top step leading from Fat Man's Misery:

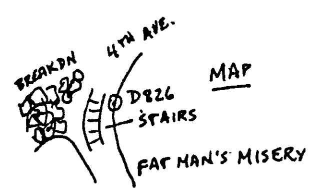

D746 1216.22 + on breakdown

Chiseled + on northeasternmost slab of breakdown in 17-Layer Rock, 1.4 ft above trail, on northwestern edge of slab:

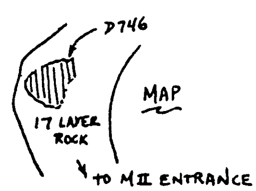

D752	1213.81	+ on wall	Chiseled + on north wall of 5th Ave., 1 ft west of junction with fissure from Mystery II entrance, 9" above floor:

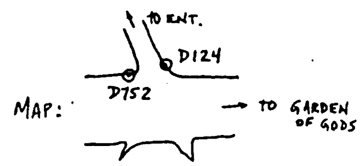

D124	1216.53	carbide dot on wall	Apparently an old survey station, at junction of 5th Ave. and fissure from Mystery II entrance; 3.2 ft above trail, on northeast corner of junction:

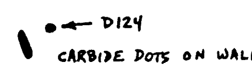

D131	1214.89	top of stalagmite	Top of stubby yellow stalagmite on ledge on southwest wall of route to Garden of Gods, 3.45 ft above trail.
D843	1210.99	+ on wall	Chiseled + on triangular face on east end of tilted undercut breakdown block, along north wall of route to Garden of Gods, 1 ft above lowest point on block and 2 ft above trail. Breakdown block is flared at bottom and rests on another larger block partly immersed in sediment fill.
D136	1213.32	top of breakdown	Topmost part of irregular breakdown block along S wall of route to Garden of Gods, just south of large semi-buried slabs called "Texas Toast":

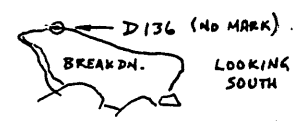

D846	1209.89	+ on breakdown	Chiseled + on south end of eastern slab of "Texas Toast" -- thin breakdown slabs partly immersed in sediment:

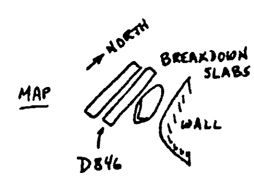

D849	1209.15	+ on wall	Chiseled + on southwest corner of fissure intersection south of Coon

			Lake in route to Garden of Gods, 3.5 ft above edge of dropoff into lower fissure, just above overhang: 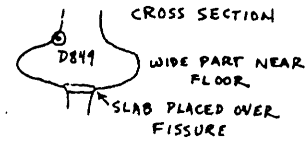
D851	1208.66	+ on wall	Chiseled + on north wall, 8" above floor on projecting rock fin at beginning of Garden of Gods loop: 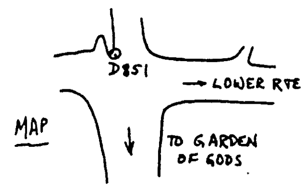
D145	1218.09	top of stalagmite	Top of large curved stalagmite beneath drip on breakdown slab in Garden of Gods, 3.4 ft above floor.
D146	1216.82	top of railing	Top of elbow in railing at top of stairs leading down from Garden of Gods.
D233	1250.49	concrete floor	Floor of entrance building at Mystery II entrance, at head of stairs.
D240	1264.61	top of signpost	Topmost point in post for "Cave Tours" sign outside ticket office at Mystery II.
D244	1272.60	nail in power pole	DNR bench mark BM15 (1272.45 ft according to DNR survey), 1 ft above ground.
D898	1271.57	top of post	top of southern post of gate at entrance of Mystery II access road.
D932	1324.12	top of bolt on sign	Top of threaded section of uppermost bolt on back side of YIELD sign at junction between north-south road leading to Mystery II (and Grabau Quarry) and east-west road near junction with Rte. 5.
D946	1330.65	top of bolt on sign	Top of threaded section of 3rd bolt upward (2nd bolt downward) on back side of "left curve" sign on south side of Rte. 5 east of junction with Mystery II access road, 875 ft east of D932.
D157	1221.13	flagging tape	Small piece of flagging tape between blocks in low cairn in middle of floor in western part of 5th Ave., 1 ft above floor: 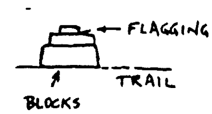

D178	1222.80	radio location	Top of nail in flagging tape at radio transmitting station.
D167	1220.10	top of stalagmite	Highest point on compound stalagmite 1.5 ft south of iron oxide powder on floor of western extension of 5th Ave.
D174	1225.07	top of stalagmite	Top of small stalagmite on ledge on east side of breakdown at western end of 5th Ave.
D175	1224.39	tip of stalactite	Tip of stalactite directly below D174 stalagmite:

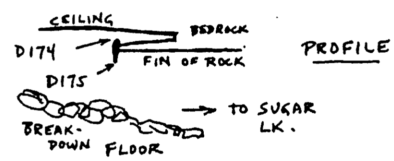

D8	1211.88	top of stalagmite	In Eureka Ave., top of small orange stalagmite 0.8 ft above floor in middle of breakdown block across entrance to passage to Rotunda. Breakdown also has an upright block on it to mark junction.
D9	1212.09	dot on breakdown	carbide dot on top of 2-ft-square block in Eureka Ave. at entrance to Discovery Route:

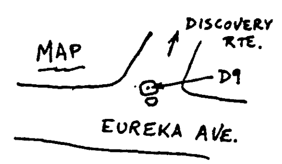

H27	1204.27	Lily Pad Lake	Top of rimstone in westernmost pool of Lily Pad Lake
D12	1212.76	top of cairn	Topmost point of cairn labeled "NO TOUCH" in Eureka Ave. at entrance to side passage to south:

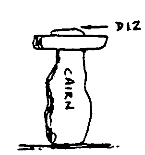

D13	1204.80	tip of soda straw	Tip of 1" soda straw on northeast corner of junction of Eureka Ave. with route to First Triangle Room, 3.7 ft above floor.

D19	1224.72	tip of stalactite	Tip of 1-ft-long corroded stalactite (with a slightly winged profile) 15 ft before western breakdown termination of Eureka Ave.
H17	1192.57	tip of breakdown block	Topmost corner of triangular breakdown block in First Triangle Room.
D31	1206.44	radio location	Head of nail holding flagging at radio location (labeled "survey point") at entrance to the Finger Passages, west of Rotunda.
D906	1227.51	dot on wall	Junction between 4th Ave. West and Under 4th Ave.; middle of old carbide dot in center of circle on south wall, in bed DS8.
H923	1225.21	former water level	Top of thin light-gray band representing former water level, on south wall of 4th Avenue West.
D929	1225.73	+ on wall	Chiseled + on north wall of 4th Ave. West next to cross-shaped cairn at beginning of Yellow Flow, above where flowstone cascade begins to drop below floor level of main passage; 1.3 ft below flat ceiling near base of bed DL12, below mud-man sculpture.
D943	1231.26	stalagmite tip	Top of stubby stalagmite with orange-brown center, located between breakdown blocks at floor level:

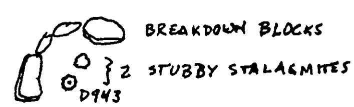

D947	1229.91	+ on wall	Penciled + on north wall above entrance to passage leading north to Enigma Pit, above small breakdown block that partly blocks opening; in middle of bed DL5, 1.0 ft above top of breakdown block.
D954	1230.54	stalagmite tip	Top of blob-shaped stalagmite on upper tip of long breakdown block along north wall of slope into Enigma Pit:

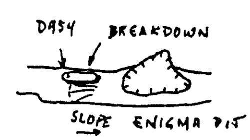

D955	1233.94	dot on ceiling	Carbide dot on flat ceiling above edge of slope into Enigma Pit.

D962	1216.46	tip of arrow	Tip of OUT arrow on south wall: 
D978	1209.21	carbide dot	Center of carbide dot on fin of rock above register jar at juction between Main Street and Labyrinth: 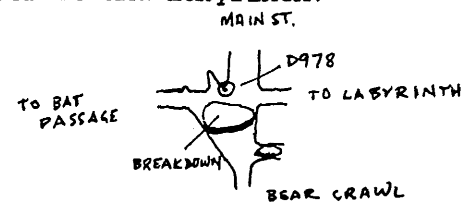
D997	1213.21	dot on ceiling	Carbide dot on flat ceiling, just after slight rise in ceiling level, above small cairn of breakdown blocks next to stream, at junction between Lily Pad Route and Helictite Route.

ADDITIONAL POINTS OF INTEREST:

Top of new well casing at house at Mystery I (cap removed): **1258.48 ft.**

Top of old well casing at house at Mystery I (cap removed): **1255.21 ft.**

Top of PVC stilling well on west bank of South Branch of Root River (installed for LCMR hydrologic study): **1230.86 ft.**

Top of PVC stilling well at Flim Flam Creek, Mystery II (installed for LCMR hydrologic study): **1194.37 ft.**

Dry bed of river at road crossing below Grabau Quarry: **1178.5 ft.**

Floor of Grabau Quarry: **1269 - 1270 ft.**

APPENDIX 2 -- Leveling Data

Survey coordinates from the geologic mapping of Mystery Cave are shown on the following pages. They are listed in the order in which they are encountered in traveling from Mystery I to Mystery II and III, with an occasional back-track into side passages. Semi-permanent bench marks are listed in Appendix 1, with locations shown on the map in Figure 1. Measurements to stratigraphic and geomorphic features are listed in the second section (which also includes bench-mark data). Station locations can be determined from the X-Y scales on the base map. Vertical coordinates were obtained with a tripod-mounted surveyor's level in large passages and with a hand level in small (or less accessible) passages.

Surveys with the tripod-mounted level consisted of alternating foresights and backsights between the instrument and a metric survey rod, with readings to the nearest 0.1 mm. Stadia readings on the rod were used to determine distance between stations, and azimuth was measured with a hand-held SUUNTO compass. Measurements to features in the cave were made from the rod with a string level. Surveys with the hand level were made by projecting a horizontal line (datum line) through the cave from one rod to another, alternating foresights and backsights and measuring up or down to significant points from the datum line. Distances were measured with a fibreglass tape and azimuths with a hand-held SUNNTO compass. The datum line was shifted up or down an even number of feet wherever the configuration of the passage prevented the original line from being continued. Both leveling instruments were frequently calibrated with closed loops on the surface, and the level survey readings were corrected for calibration error.

The overall base station for the survey data is the 1989 DNR bench mark BM10, which is the head of a spike driven into the base of a triple basswood tree south of the ticket office outside Mystery I. The DNR topographic map lists the altitude of this station as 1230.37 feet above sea level. This is the first item (D1) on the list of survey data. Coordinates are given in FEET relative to this base station.

All figures on the following pages are in FEET. Columns are as follows:

STA = survey station in level survey. D = datum (semi-permanent bench mark). T = station at tripod-mounted level. R = station at bottom of survey rod. S = same as R, except used for side shots not in sequence with the main level line. H = hand-level station (only significant ones are listed).

FROM = station from which the station listed in the first column was measured.

EAST = feet east of base station (BM10 = D1). Negative values indicate distance west of base station.

NORTH = feet north of base station (negative values indicate distance south of base station).

VERTICAL = elevation of station in feet above sea level (BM10 = 1230.37 feet used as datum). This figure is the floor or ground elevation for R and S stations. For D stations it is the exact elevation of the point. For T and H stations it is the elevation of the instrument (roughly 3.5 feet above the floor for T stations).

Elevations of various features are shown in the last two columns, as measured at or near the station. All are shown to the nearest 0.01 foot, although some could not be reliably measured to that degree of accuracy (for example, irregular bedding planes). Abbreviations of features are as follows: BM = bench mark; CEIL (or C) = passage ceiling; FLOOR (or F) = passage floor (where not otherwise indicated, the floor level coincides with R and S stations and is about 3.5 feet below T stations); BP = bedding plane; LS = limestone; SH = shale; SM = stalagmite; STAL (or ST) = stalactite; RST = rimstone; SHELFST = shelfstone; POPC = popcorn; PEND = pendant; SED = sediment; S+G = sand and gravel; ELBOW = elbow in railing pipe; DOT = carbide dot (from a previous survey?); N = north; E = east; S = south; W = west; WL = water level.

Positions of rock layers or bedding planes are noted in code as shown on the stratigraphic column. S = Stewartville Formation; D = Dubuque Formation; M = Maquoketa Formation. Contacts between beds are indicated in the following manner: D/S = Dubuque/Stewartville contact, etc. SX1 - SX 3 = granular crystalline beds near top of Stewartville. DT1 - DT4 = transitional beds at base of Dubuque, with little or no shale between them. BP1 - BP3 = major bedding planes near base of Dubuque. DL1 - DL29 = limestone beds in Dubuque sandwiched between thin shale beds. DS1-DS30 = thin shale beds in the Dubuque, separated by limestone beds. Nomenclature for these thin limestone and shale beds may seem awkward at first, but the advantage is that in the field it is possible to count quickly upward or downward from a known bed, using only the projecting limestones or the recessive shales, without having to keep track of every bed.

STA	FROM	EAST	NORTH	VERTICAL		FEET
D1	---	0.0	0.0	1230.37	BM10=NAIL	1230.37
R1	D1	0.0	0.0	1230.37		
T1	R1	6.8	15.6	1233.24		
R2	T1	-52.4	4.1	1229.24	FLOODPLAIN	1229.24
T3	R2	-151.1	22.4	1233.09		
R4	T3	-165.3	-24.0	1232.64	FLOODPLAIN	1232.64
T5	R4	-243.4	-25.4	1238.16		
R6	T5	-268.5	-28.4	1236.61	IRREG SURF	1236.61
T7	R1	7.6	17.0	1233.11		
S8	T7	68.6	-.5	1224.81	RIVER LEV	1224.81
S9	T7	115.4	1.8	1230.47	PATH	1230.47
R10	T7	46.4	41.3	1228.21		
T11	R10	27.7	116.4	1233.42	FLOODPLAIN	1233.42
R12	T11	7.9	241.5	1227.73		
T13	R12	-28.7	295.8	1231.45	FLOODPLAIN	1231.45
R14	T13	-63.1	350.7	1226.85		
T15	R14	-103.9	417.4	1230.88		
R16	T15	-141.3	497.7	1226.34	FLOODPLAIN	1226.34
T17	R16	-165.2	568.9	1229.83		
R18	T17	-184.1	657.8	1225.17		
T19	R18	-167.2	690.8	1228.81		
R20	T19	-146.1	699.4	1222.31	WL AT FORD	1222.31
T21	S9	129.3	-9.8	1231.96		
R22	T21	137.5	-11.1	1226.12		
T23	R22	165.1	-10.2	1226.12		
R24	T23	193.9	-10.2	1220.54	CEIL	1227.75
					FLOOR	1220.54
					DS18/DL17	1226.28
					DL16/DS16	1225.29
					DS16/DL15	1224.96
					DL15/DS15	1223.92
					DS15/DL14	1223.64
					DL14/DS14	1223.28
					DS14/DL13	1223.03
					DL13/DS13	1221.95
					DS13/DL12	1221.36
T25	R24	217.3	-11.8	1221.49		
R26	T25	255.5	-15.8	1215.68		
D2	R26	255.5	-15.8	1218.56	SM TOP	1218.56
T27	R26	326.1	-30.2	1220.61		
R28	T27	360.6	-34.7	1215.99	DS13/DL12	1221.96
					CEIL	1225.83
D3	R28	360.6	-34.7	1218.54	RAIL TOP	1218.54
T29	R28	401.7	-51.3	1216.52	POOL LEVEL	1204.25
R30	T29	444.3	-65.2	1213.47		
R31	D3	360.6	-34.7	1215.13		
T32	R31	400.8	-51.0	1215.96		
R33	T32	437.5	-62.9	1213.41		
D4	R33	437.5	-62.9	1216.93	RAIL TOP	1216.93
T34	R33	470.4	-61.2	1219.95		
R35	T34	500.0	-61.7	1217.47	DS13/DL12	1222.79

					CEIL	1225.35
T36	R35	570.5	-80.6	1221.36		
R37	T36	597.0	-88.2	1217.07	C=DL14/S14	1224.13
					FLOOR	1224.13
					SHELFST	1220.62
D37	R37	597.0	-88.2	1220.87	SM TOP	1220.87
T38	R37	649.1	-90.0	1221.37		
R39	T38	695.8	-101.7	1216.62	CEIL	1224.16
					SED TOP	1219.77
T40	R39	749.3	-118.0	1220.89		
R41	T40	805.4	-131.5	1217.00		
T42	R41	784.6	-140.3	1217.72		
S43	T42	790.8	-140.0	1213.82	FOLIA TOP	1219.33
					FOLIA BOT	1219.17
					DL10/DS10	1218.28
					DS10/DL9	1217.89
S44	T42	765.8	-160.5	1211.77	DAM TOP	1214.59
					WATER LEV	1214.46
					FOLIA TOP	1219.28
					CEIL	1219.32
R45	T42	805.5	-130.1	1217.00	CONE TOP	1219.36
					SHELFST	1218.94
T46	R45	846.8	-138.2	1220.08		
R47	T46	922.9	-152.3	1216.97	CONE TOP	1217.49
					OLD WL	1218.08
					CEIL	1220.87
					DL11/DS11	1220.87
T48	R47	938.7	-160.6	1218.66		
R49	T48	974.7	-164.4	1215.45	CEIL	1220.83
					OLD WL	1218.32
T50	R49	1017.4	-133.9	1218.07		
R51	T50	1058.7	-105.0	1215.08	CEIL	1220.95
					DL10/DS10	1220.95
					DS9	1218.98
					DS8	1217.83
T52	R51	1100.7	-75.6	1218.29		
R53	T52	1106.2	-86.7	1217.74	CEIL	1225.94
					DL14/DS14	1225.94
D53	R53	1106.2	-86.7	1219.15	SM TOP	1219.15
T54	R53	1100.1	-77.0	1217.87		
R55	T54	1100.5	-72.1	1214.79	CEIL	1218.40
					FLOOR	1214.13
T56	R55	1104.1	-52.7	1215.12	DL6/DS6	1215.77
					CEIL	1218.73
					LOW CEIL	1215.18
R57	T56	1125.7	-52.7	1213.69	CEIL	1219.85
					DL10/DS10	1219.36
					DS10/DL9	1219.07
					DL9/DS9	1218.08
					DS9/DL8	1217.72
					DL9/DS9	1216.28
					DS8/DL7	1215.72
T58	R57	1166.9	-24.4	1216.71		
R59	T58	1203.5	-5.3	1215.18	CEIL	1218.46
					DL9/DS9	1218.46

					FLOOR	1212.52
T60	R59	1197.5	8.9	1215.82		
R61	T60	1215.9	26.0	1213.37	CEIL	1218.92
					DL9/DS9	1218.92
					DL9/DS9	1217.82
					DL7/DS7	1216.95
					DS7/DL6	1216.56
T62	R61	1270.0	16.5	1215.31	CONE TOP	1214.74
D62	T62	1270.0	16.5	1214.74	CONE TOP	1214.74
R63	T62	1274.0	42.2	1212.61	DL9/DS9	1219.06
T64	R63	1274.1	49.0	1219.08	CEIL	1225.97
					DL14/DS14	1225.97
R65	T64	1258.2	51.0	1217.44	DS13/DL12	1224.85
					DL14/DS14	1225.90
					CEIL	1225.90
					DL12/DS12	1224.39
					DS12/DL11	1223.70
					DL11/DS11	1222.85
					DS11/DL10	1221.90
T66	R65	1222.6	57.2	1222.51		
R67	T66	1212.2	64.8	1217.91	CEIL	1225.78
					DL14/DS14	1225.78
					DS13/DL12	1224.96
					DL12/DS12	1224.27
					DS12/DL11	1223.61
					DL11/DS11	1222.83
					DS11/DL10	1221.65
					DL10/DS10	1220.50
					DS10/DL9	1220.27
					DS9	1219.35
T68	R67	1237.2	89.4	1218.57		
R69	T68	1257.9	100.0	1215.46	CEIL	1219.36
					DL9/DS9	1219.36
T70	R69	1211.4	109.8	1216.95		
R71	T70	1193.6	116.0	1211.08	CEIL	1219.94
					DL9/DS9	1219.94
					FLOOR	1209.61
D71	R71	1193.6	116.0	1214.05	DOT ON BD	1214.05
R245	D1	0.0	0.0	1229.67		
T246	R245	9.0	13.9	1233.28		
R247	T246	116.4	-2.1	1230.14		
T248	R247	129.1	-15.7	1232.10		
S249	T248	142.8	-21.4	1227.26	DL19/DS19	1229.58
					DS19/DL18	1229.10
					DL18/DS18	1228.49
					DS18/DL17	1228.17
					DS18	1227.39
					DL17/DS17	1225.19
					DS22/DL21	1230.55
					DL22/DS22	1231.07
					DS23/DL22	1231.66
					DL23/DS23	1231.87
					DS24/DL23	1233.04
					DL24/DS24	1233.92
					DS25/DL24	1234.35

					DL25/DS25	1234.68
					SH BREAK	1235.20
					SH BREAK	1235.93
					SH TOP	1236.48
R250	T248	119.4	1.8	1231.99	DL27	1237.81
					M/D	1241.11
R320	D2	255.5	-15.8	1215.48		
T321	R320	256.4	-2.2	1215.97		
R322	T321	262.7	4.8	1209.86		
T323	R322	327.0	60.7	1214.93		
R324	T323	377.0	109.0	1211.34	DS10	1216.53
					DS9	1215.41
					CEIL	1222.66
					LS/SH	1222.66
T325	R324	402.2	105.4	1213.17		
R326	T325	402.2	111.3	1209.87		
T327	R326	402.2	123.7	1210.66	D/S	1202.26
					STREAM	1180.76
R328	T327	402.2	123.7	1202.63		
D328	R328	402.2	123.7	1210.46	SM TOP	1210.46
R329	D2	255.5	-15.8	1215.53		
T330	R329	301.3	-23.9	1218.95		
R331	T330	329.1	-23.4	1210.74	SP CEIL	1215.93
					DL9/DS9	1215.93
T332	R331	352.6	-4.1	1214.36		
R333	T332	378.3	3.8	1209.46	DS10/DL9	1217.07
					CEIL	1222.81
					DL14/DS14	1222.81
					NEXT CEIL	1214.25
					DL7/DS7	1214.25
T334	R333	417.2	28.1	1211.22		
R335	T334	435.7	34.3	1206.19	DS1/DT4	1208.84
D335	R335	435.7	34.3	1209.54	RAIL TOP	1209.54
T336	R335	458.8	49.3	1209.08		
R337	T336	508.4	40.1	1206.18	DS1/DT4	1209.13
					CEIL	1213.89
					DL7/DS7	1213.89
T338	R337	552.1	65.3	1212.60		
R339	T338	583.1	85.5	1209.97	DL7/DS7	1214.40
					CEIL	1217.35
					DL10/DS10	1217.35
T340	R339	610.3	107.9	1213.75		
R341	T340	634.1	107.0	1208.92	DL7/DS7	1214.43
					CEIL	1216.20
					DL9/DS9	1216.20
					FISSURE C	1218.76
T342	R341	661.8	128.7	1212.19		
S343	T342	669.8	148.4	1206.89	DS1/DT4	1209.78
					DS4/DL3	1212.01
					DL4/DS4	1212.14
R344	T342	670.6	154.1	1211.83	DL10/DS10	1218.13
					NAUTILUS	1218.39
T345	R344	673.7	157.7	1217.80		
R346	T345	678.4	156.7	1217.74		
T347	R346	683.0	162.8	1222.37		

S348	T347	678.5	173.8	1216.72		
D348	S348	678.5	173.8	1222.96	STAL TIP	1222.96
S349	T347	687.2	167.9	1217.98	CEIL	1229.53
					DS21	1229.53
R350	D3	360.6	-34.7	1215.16		
T351	R350	375.6	-44.5	1218.62		
R352	T351	369.9	-47.2	1209.65		
T353	R352	325.9	-81.0	1211.76		
R354	T353	294.0	-106.8	1206.34	DS1/DT4	1208.99
					CEIL	1213.09
					DL6/DS6	1213.09
T355	R354	279.7	-107.6	1211.32		
R356	T355	233.2	-142.6	1211.24	DS10/DL9	1216.79
T357	R356	229.3	-146.3	1220.58		
R358	T357	226.4	-150.9	1220.41		
T359	R358	210.9	-155.0	1230.12		
S360	T359	202.8	-159.3	1225.53	RADIO LOC	1226.07
R361	T359	219.9	-164.9	1229.97	DS24/DL23	1234.56
T362	R361	187.0	-163.7	1238.05		
R363	T362	181.0	-170.6	1236.76	M/D	1242.18
					DL27	1239.13
T364	R363	177.7	-157.9	1243.19		
R365	T364	174.3	-163.9	1243.10	BD TOP	1259.51
					HIGHEST C	1249.66
H366	D71	1175.0	110.0	1212.05	DL3/DS3	1213.35
					CEIL	1216.35
					DS6	1216.35
					DS1/DT4	1211.65
					BP 3	1209.95
					FLOOR	1206.05
H367	D71	1209.4	135.4	1218.05	CEIL	1220.05
					FLOOR	1215.05
					DL9/DS9	1218.65
					DS10/DL9	1219.65
H368	H367	1244.0	161.9	1218.05	CEIL	1222.35
					DS12	1222.35
					FLOOR	1216.05
					DL10/DS10	1219.95
					DL9/DS9	1218.65
H369	H368	1250.6	181.2	1218.05	CEIL	1222.05
					FLOOR	1215.65
					DL10/DS10	1220.00
					DL9/DS9	1218.75
D370	H369	1300.8	217.6	1218.05	+ ON WALL	1218.05
H370	D370	1300.8	217.6	1218.05	CEIL	1220.05
					DL10/DS10	1220.05
					FLOOR	1214.45
					DL9/DS9	1218.80
					SP CEIL	1215.45
					DL6/DS6	1215.45
H371	H370	1353.9	259.9	1218.05	CEIL	1220.20
					DL10/DS10	1220.20
					DS10/DL9	1219.70
					DL9/DS9	1219.05
					F (BD)	1211.05

H372	H371	1402.2	290.6	1217.05	CEIL	1218.15
					FLOOR	1215.25
					DL7/DS7	1217.25
H373	H372	1399.2	307.7	1217.05	CEIL	1222.55
					DS10/DL9	1219.95
					DL9/DS9	1218.95
					DL8/DS8	1218.05
					FLOOR	1214.45
H374	H373	1341.8	311.2	1217.05	CEIL	1218.70
					DL9/DS9	1218.70
					DL8/DS8	1217.50
					DS8/DL7	1217.10
					FLOOR	1214.55
H375	H374	1366.6	332.0	1217.05	CEIL	1219.35
					DL10/DS10	1219.35
					DL9/DS9	1218.25
					FLOOR	1214.55
H376	H375	1392.4	334.2	1217.05	CEIL	1218.85
					DL9/DS9	1218.35
					FLOOR	1214.05
H377	H376	1431.2	360.4	1217.05	CEIL	1219.65
					DL10/DS10	1219.65
					DL9/DS9	1218.60
					FLOOR	1215.35
H378	H377	1461.5	383.2	1217.05	CEIL	1222.25
					DL12/DS12	1222.25
					DL9/DS9	1218.50
					FLOOR	1213.65
H379	H378	1432.6	391.8	1217.05	CEIL	1221.05
					DS10/DL9	1219.05
					DL9/DS9	1218.20
					FLOOR	1214.05
					DL6/DS6	1215.35
H380	H379	1445.6	413.0	1215.05	CEIL	1216.40
					DL7/DS7	1216.40
					F (CLAY)	1214.85
H381	H380	1445.6	413.0	1217.05	DL9/DS9	1218.25
H382	H381	1452.7	417.2	1217.05	CEIL	1219.45
					DL10/DS10	1219.45
					F (BD)	1216.85
H383	H382	1462.1	419.8	1218.05	CEIL	1219.65
					DL10/DS10	1219.65
					FLOOR	1217.65
H384	H383	1464.4	424.8	1221.05	CEIL	1225.05
					DL16/DS16	1225.05
					FLOOR	1220.75
H386	H384	1472.0	434.4	1222.05	Fe OXIDE	1223.45
					Fe OXIDE	1222.45
H387	H386	1473.9	435.4	1220.05		
D387	H387	1473.9	435.4	1218.71	SM TOP	1218.71
H388	H387	1478.1	437.6	1218.05	CEIL	1220.10
					DL10/DS10	1220.10
					DL9/DS9	1218.85
					FLOOR	1217.75
H389	H388	1526.8	478.4	1218.05	CEIL	1219.05

					DL9/DS9	1219.05
					FLOOR	1216.25
H390	H389	1541.1	493.5	1218.05	CEIL	1221.55
					DL10/DS10	1220.25
					DL9/DS9	1218.90
					FLOOR	1216.55
H391	H390	1555.7	498.8	1218.05	CEIL	1218.90
					DL9/DS9	1218.90
					FLOOR	1216.05
H392	H391	1578.8	494.5	1217.05	CEIL	1218.35
					DL8/DS8	1218.35
					FLOOR	1215.75
H393	H392	1595.8	510.7	1217.05	CEIL	1220.25
					DL10/DS10	1220.25
					DL8/DS8	1218.35
					FLOOR	1216.45
H394	H393	1616.3	522.5	1218.05	CEIL	1220.45
					DL10/DS10	1220.45
					FLOOR	1216.95
H395	H394	1694.1	585.5	1218.05	CEIL	1220.65
					DL10/DS10	1220.65
					DL9/DS9	1219.25
					FLOOR	1214.55
H396	H395	1747.2	631.7	1216.05	CEIL	1218.55
					DL9/DS9	1218.55
					DL7/DS7	1216.90
					FLOOR	1214.05
H397	H396	1779.9	625.6	1216.05	CEIL	1218.05
					DL8/DS8	1218.05
					DL7/DS7	1217.01
					DS6/DL5	1215.60
					FLOOR	1214.25
H398	H397	1798.3	644.6	1215.05	CEIL	1215.85
					DS6/DL5	1215.40
					FLOOR	1213.65
H399	H398	1812.9	659.7	1215.05	CEIL	1216.75
					DL7/DS7	1216.75
					F (BD)	1214.45
H400	H399	1816.3	668.0	1216.05	DL7/DS7	1216.90
H401	H400	1823.7	673.0	1217.05	DL10/S10 S	1219.80
					DL10/S10 N	1218.75
					DL7/DS7	1216.75
					F (BD)	1216.05
H402	H401	1822.4	680.9	1221.05		
D402	H402	1822.4	680.9	1218.15	FLAGGING	1218.15
HH402	H401	1839.9	676.4	1217.05	CEIL	1217.95
					DL9/DS9	1217.95
					DL7/DS7	1216.65
					DL6/DS6	1215.65
					F (BD)	1214.55
H403	HH402	1853.0	678.4	1215.05	CEIL	1216.05
					DL7/DS7	1216.05
					FLOOR	1213.55
H404	H403	1873.5	674.0	1215.05	CEIL	1216.60
					DL7/DS7	1216.60

					FLOOR	1214.55
H405	H404	1918.3	672.4	1215.05	CEIL	1217.30
					DL7/DS7	1217.30
					DS5/DL4	1215.15
					F (BD)	1213.05
H406	H405	1934.7	672.7	1215.05	CEIL	1215.55
					DL5/DS5	1215.55
					DS5/DL4	1215.25
					DL3/DS3	1214.85
H407	H406	1973.1	670.0	1215.05	CEIL	1216.20
					DL4/DS4	1216.20
					DS3/DL2	1215.55
					FLOOR	1213.05
H408	H407	2020.6	669.2	1215.05	CEIL	1215.75
					DL3/DS3	1215.75
					DS1/DT4	1214.05
					F (BD)	1209.75
H409	H408	2032.7	668.8	1211.05	CEIL	1213.05
					BP3	1212.45
					BP2	1209.65
					FLOOR	1207.55
H410	H409	2041.4	666.8	1211.05	CEIL	1214.05
					BP2	1212.15
					F (CLAY)	1207.95
H411	H410	2058.4	665.7	1211.05	CEIL	1213.25
					BP2 R	1210.20
					BP2 L	1209.75
					FLOOR	1209.05
H412	H411	2075.5	663.0	1211.05	CEIL	1213.85
					BP2	1209.85
					FLOOR	1209.85
H413	H412	2080.8	663.6	1211.05	CEIL	1214.05
					BP2	1209.65
					FLOOR	1209.65
H414	H413	2093.0	661.9	1211.05	CEIL	1212.65
					BP2 R	1210.25
					BP2 L	1209.75
					FLOOR	1208.65
H415	H414	2121.2	677.2	1210.05	CEIL	1212.05
					BP2	1210.25
					BP1	1208.55
					F (CLAY)	1204.55
H416	H415	2135.6	673.9	1207.05	CEIL	1211.15
					BP2	1210.05
					BP1	1208.55
					FLOOR	1205.25
H417	H416	2150.5	675.8	1210.05	CEIL	1214.55
					BP2	1210.25
					FLOOR	1206.45
H418	H417	2189.5	691.9	1210.05	CEIL	1213.55
					BP2	1210.30
					FLOOR	1206.05
H419	H418	2200.9	702.0	1210.05	CEIL	1210.65
					BP2	1210.05
					FLOOR	1207.05

H420	H419	2209.0	704.4	1210.05	CEIL	1213.15
					F (BD)	1209.55
H421	H420	2236.8	717.9	1211.05	CEIL	1215.05
					BP2	1210.40
					F (BD)	1208.05
H422	H421	2249.0	728.6	1211.05	CEIL	1214.05
					BP2	1210.60
					FLOOR	1206.55
H423	H422	2251.3	740.4	1211.05	CEIL	1214.85
					BP2	1210.45
					FLOOR	1206.55
H424	H423	2272.5	755.0	1212.05	CEIL	1214.55
					BP2	1210.55
					FLOOR	1207.75
H425	H424	2275.8	755.7	1209.05		
H426	H425	2279.7	756.5	1209.05		
H427	H426	2291.8	753.9	1209.05	CEIL	1210.65
					FLOOR	1207.05
H428	H427	2297.8	752.6	1209.05		
H429	H428	2319.0	748.1	1211.05	CEIL	1214.45
					BP2	1211.30
					F (CLAY)	1209.65
H430	H429	2322.7	755.1	1211.05	CEIL	1216.05
					BP2	1211.10
					F (CLAY)	1210.35
H431	H430	2340.2	769.3	1212.05	CEIL	1215.55
					BP2	1211.15
					FLOOR	1207.55
H432	H431	2358.1	784.5	1211.05	CEIL	1215.85
					BP2	1211.30
					BP1	1209.80
					BP3	1214.35
					FLOOR	1206.55
H433	H432	2380.0	800.5	1211.05	CEIL	1214.05
					BP2	1211.55
					FLOOR	1206.05
H434	H433	2388.0	816.2	1211.05	CEIL	1215.25
					BP2	1211.40
					BP1	1209.95
					FLOOR	1206.55
D434	H434	2388.0	816.2	1209.63	SM TOP	1209.63
H435	H434	2417.5	839.2	1211.05	CEIL	1216.05
					BP1?	1211.75
					F (CLAY)	1205.55
H436	H435	2447.6	861.6	1212.05	CEIL	1214.05
					BP1	1211.25
					F (CLAY)	1203.05
H437	H436	2453.8	864.4	1213.05		
H438	H437	2461.0	867.8	1211.05	CEIL	1214.65
					BP2	1212.35
					F (CLAY)	1204.05
					BP1	1210.95
D438	H438	2461.0	867.8	1212.35	FLAGGING	1212.35
H439	H438	2461.7	875.4	1211.05		
H564	H439	2471.8	880.3	1212.05	BP2	1212.05

					BP1	1210.65
H565	H564	2504.1	905.1	1212.05	CEIL	1214.75
					BP2	1212.25
					BP1	1210.75
					F (CLAY)	1203.75
H566	H565	2518.2	915.0	1211.05	CEIL	1214.35
					BP2	1212.15
					BP1	1210.65
					FLOOR	1204.05
H567	H566	2524.2	916.2	1207.05	CEIL	1214.05
					BP2	1212.25
					BP1	1210.65
					FLOOR	1203.55
H568	H567	2535.6	925.1	1207.05	CEIL	1214.05
					BP1	1210.85
					FLOOR	1203.05
H569	H568	2541.5	928.1	1207.05		
H570	H569	2566.9	949.0	1207.05	CEIL	1214.55
					BP2	1212.85
					BP1	1211.35
					FLOOR	1203.35
H571	H570	2568.9	952.5	1208.05		
H572	H571	2576.0	960.5	1210.05	CEIL	1214.45
					BP2	1212.35
					BP1	1210.85
					F (CLAY)	1206.55
H573	H572	2586.6	966.4	1210.05	CEIL	1214.65
					BP2	1212.35
					BP1	1210.75
					F (CLAY)	1206.95
H574	H573	2597.3	974.7	1210.05	CEIL	1215.25
					BP2	1212.70
					BP1	1211.00
					FLOOR	1206.25
H575	H574	2613.4	978.5	1211.05	CEIL	1216.05
					BP2	1212.95
					BP1	1211.45
					FLOOR	1206.25
H576	H575	2624.7	979.6	1212.05	BP1	1211.65
					FLOOR	1206.25
H577	H576	2644.6	983.5	1212.05	CEIL	1215.15
					BP2	1213.45
					BP1	1211.85
					FLOOR	1206.35
H578	H577	2661.2	983.1	1212.05	CEIL	1214.55
					BP1	1212.25
					FLOOR	1203.55
H579	H578	2680.2	984.4	1212.05	CEIL	1214.35
					BP2	1214.05
					BP1	1212.55
					BP	1211.35
					FLOOR	1201.55
H580	H579	2694.5	984.9	1214.05	CEIL	1215.65
					BP2	1214.35
					BP1	1212.85

					FLOOR	1202.05
H581	H580	2736.9	991.6	1214.05	CEIL	1216.55
					BP2	1214.60
					FLOOR	1199.95
D581	H581	2736.9	991.6	1213.23	SM TOP	1213.23
H582	H581	2769.8	999.8	1214.05	CEIL	1217.25
					BP2	1214.90
					BP1	1213.50
					FLOOR	1199.15
H583	H582	2817.8	1001.9	1214.05	CEIL	1217.25
					BP2	1215.45
					BP1	1213.85
					FLOOR	1199.55
H584	H583	2843.2	1004.6	1214.05	CEIL	1218.05
					BP2	1215.80
					BP1	1214.35
H585	H584	2867.9	1007.6	1214.05	CEIL	1219.75
					BP2	1216.05
					BP1	1214.65
					FLOOR	1199.35
H586	H585	2898.1	1013.0	1214.05	CEIL	1219.35
					BP2	1216.25
					BP1	1214.85
					FLOOR	1198.85
H587	H586	2932.1	1019.0	1214.05		
H588	H587	2936.1	1021.9	1214.05	CEIL	1218.05
					BP2	1216.35
					BP1	1215.00
					CHOCKS	1210.05
H589	H588	2942.8	1021.6	1214.05		
H590	H589	2967.0	1029.9	1214.05	CEIL	1216.55
					BP1	1215.25
H591	H590	2978.4	1032.1	1214.05	CEIL	1216.65
					BP1	1215.20
					BP	1214.05
					FLOOR	1198.25
H592	H591	2989.9	1037.5	1214.05		
H593	H592	3014.4	1041.4	1214.05	CEIL	1217.35
					BP1	1215.50
					BP	1214.95
					FLOOR	1198.05
H594	H593	3033.0	1046.4	1214.05		
H595	H594	3042.5	1049.5	1203.05	F (CLAY)	1198.05
H596	H595	3072.8	1053.7	1203.05	FLOOR	1197.75
H597	H596	3108.4	1053.4	1202.05		
H598	H597	3116.6	1053.5	1202.05	F (CLAY)	1197.55
D598	H598	3116.6	1053.5	1216.05	LINE	1216.05
					CEIL	1219.05
					BP1	1216.85
H599	D598	3143.6	1054.9	1216.05		
H635	D598	3113.6	1056.2	1216.05		
H636	H635	3114.1	1068.4	1216.05	CEIL	1217.45
					BP1	1217.05
					F (CLAY)	1207.25
H637	H636	3112.7	1079.4	1216.05	CEIL	1217.45

					BP1	1216.70
					LEDGE	1212.85
					FLOOR	1211.05
H638	H637	3122.6	1087.0	1214.05		
H639	H638	3125.7	1088.1	1214.05	CEIL	1216.05
					LEDGE	1211.85
					F=FST/S+G	1210.85
H640	H639	3127.2	1092.8	1214.05		
H641	H640	3137.1	1101.1	1214.05	C POCKET	1218.15
					CEIL	1216.05
					LEDGE	1213.25
					F (FST)	1210.25
H642	H641	3151.3	1110.0	1213.05	CEIL	1217.05
					LEDGE	1213.75
					F (S+G)	1211.25
H643	H642	3122.5	1115.3	1214.05	C FISSURE	1220.65
					BP1	1217.05
					LEDGE	1213.75
					F (FST)	1211.05
H644	H643	3099.5	1119.6	1214.05	CEIL	1217.05
					BP1	1216.80
					LEDGE	1213.00
					SHELFST	1210.49
					F (S+G)	1209.55
H645	H644	3076.9	1104.9	1214.05	CEIL	1218.85
					BP1	1216.40
					LEDGE	1212.95
					FLOOR	1210.05
H646	H645	3075.7	1101.7	1214.05		
H647	H646	3044.6	1107.2	1213.05	CEIL	1216.55
					BP1	1216.05
					LEDGE	1212.35
					F (S+G)	1208.15
H648	H647	3036.5	1109.5	1213.05		
H649	H648	3031.9	1102.0	1213.05	CEIL	1214.55
					LEDGE	1212.25
					FLOOR	1208.45
H650	H649	3010.2	1105.6	1214.05	CEIL	1215.35
					LEDGE	1212.25
					TRENCH F	1207.75
H651	H650	3001.0	1110.2	1214.05		
H652	H651	2979.3	1115.1	1213.05	CEIL	1216.05
					BP1	1215.70
					F (S+G)	1207.95
H653	H652	2968.8	1117.0	1213.05	CEIL	1216.25
					BP1	1215.45
					LEDGE	1211.75
					F (CLAY)	1207.95
H654	H653	2987.9	1133.0	1212.05		
H655	H654	2989.8	1137.4	1212.05	CEIL	1217.45
					LEDGE	1211.95
					FLOOR	1207.25
H656	H655	3011.6	1153.8	1212.55		
H657	H656	3018.3	1157.7	1212.55	CEIL	1216.55
					BP1	1216.40

					Fe OXIDE	1213.15
					F (CLAY)	1208.05
H658	H657	3024.4	1159.7	1212.55		
H659	H658	3028.5	1164.4	1213.05	CEIL	1218.05
					BP	1217.15
					BP1	1216.50
					F (BD)	1210.05
H660	H659	3008.3	1168.8	1213.05	CEIL	1216.35
					F (CLAY)	1206.25
H661	H660	3019.1	1177.6	1213.05		
H662	H661	3043.9	1197.7	1211.05	CEIL	1220.55
					BP	1218.05
					BP1	1216.55
					LEDGE	1212.75
					FLOOR	1206.15
H663	H662	3045.4	1200.4	1211.05		
H664	H663	3059.6	1211.4	1211.05	CEIL	1220.05
					FLOOR	1205.75
H665	H664	3071.6	1221.5	1209.05		
H666	H665	3059.4	1223.5	1209.05	CEIL	1216.95
					BP1	1216.55
					BP	1215.95
					F (BD)	1206.95
H667	H666	3079.8	1237.8	1209.05	FLOOR	1204.95
H668	H667	3089.5	1247.8	1209.05		
H669	H668	3102.4	1256.2	1209.05	CEIL SLOT	1221.05
					BP	1216.95
					BP	1215.95
					FLOOR	1204.45
H670	H669	3093.0	1258.7	1209.05		
H671	H670	3052.6	1267.3	1212.55	CEIL	1217.95
					CROSS JT	1220.05
					BP1	1216.35
					FLOOR	1212.55
H672	H671	3021.4	1279.9	1216.05	CEIL	1217.85
					BP1	1216.25
					MUDCRACKS	1213.75
					F (S+G)	1213.45
D672	H672	3021.4	1279.9	1215.85	+ ON LEDGE	1215.85
H673	H672	3003.4	1308.7	1216.05	CEIL	1219.55
					BP1	1216.95
					LEDGE	1212.85
					F FISSURE	1206.65
H674	H673	3040.5	1337.7	1216.05	CEIL	1219.75
					BP1	1217.25
					BP	1216.45
					LEDGE	1212.85
					F FISSURE	1207.15
H675	H674	3073.3	1352.9	1216.05	CEIL	1218.55
					BP	1217.35
					BP	1216.75
					BP	1215.75
					LEDGE	1211.55
					F FISSURE	1208.35
H676	H675	3105.2	1369.9	1216.05	CEIL	1220.65

					BP	1217.75
					BP	1216.90
					BP	1216.35
					BP	1215.45
					LEDGE	1213.05
					F FISSURE	1206.45
D676	H676	3105.2	1369.9	1213.73	SM TOP	1213.73
H677	H676	3171.0	1404.9	1216.05		
D634	H677	3171.0	1404.9	1216.57	+ ON WALL	1216.57
H634	D634	3171.0	1404.9	1216.57	CEIL	1218.07
					BP1	1215.37
					FLOOR	1211.77
					TRENCH	1203.77
H633	H634	3129.6	1419.1	1216.57	CEIL	1217.52
					BP1	1215.57
					FLOOR	1212.97
H632	H633	3128.1	1426.0	1219.57		
H631	H632	3136.4	1430.4	1219.57	CEIL	1221.27
					F (BD)	1216.57
H630	H631	3152.8	1442.7	1219.57	CEIL	1221.07
					F (BD)	1215.57
H629	H630	3161.6	1454.9	1218.57	CEIL	1219.97
					F (BD)	1217.07
H628	H629	3165.7	1458.8	1217.57		
H627	H628	3170.0	1461.7	1215.57	CEIL	1219.57
					BP1	1215.67
					F (BD)	1213.07
H626	H627	3200.6	1493.4	1215.57	CEIL	1218.77
					BP2	1216.77
					BP	1215.92
					BP1	1215.47
H625	H626	3260.6	1479.5	1215.57	CEIL	1221.67
					BP	1216.52
					FLOOR	1211.97
H624	H625	3290.8	1504.0	1213.57	CEIL	1221.87
					BP2	1217.77
					BP	1216.37
					BP1	1215.77
					GRAVEL	1212.42
					F SLOT	1210.97
H623	H624	3329.4	1536.9	1213.57	CEIL	1221.07
					BP2	1218.42
					BP1	1215.97
					WIDEST	1212.57
H622	H623	3328.7	1562.4	1213.57		
D622	H622	3328.7	1562.4	1213.46	SM TOP	1213.46
H621	H622	3336.4	1570.4	1213.57	CEIL	1221.07
					BP2	1217.72
					BP	1216.22
					BP1	1215.37
					F (CLAY)	1203.27
H620	H621	3369.5	1607.8	1212.57	CEIL	1220.07
					BP2	1217.57
					BP1	1215.62
					FLOOR	1202.07

H619	H620	3408.6	1638.4	1212.57	CEIL	1219.57
					BP	1216.47
					BP1	1215.57
					F (CLAY)	1200.57
D619	H619	3408.6	1638.4	1213.02	SM TOP	1213.02
H618	H619	3440.2	1633.1	1212.57	BP1	1215.82
					CEIL	1219.82
					BP	1212.37
					F (CLAY)	1200.07
H617	H618	3468.9	1659.9	1212.57	CEIL	1220.07
					BP2	1217.77
					BP1	1215.67
					WIDEST	1212.07
					F (CLAY)	1198.07
H616	H617	3504.6	1677.3	1212.57	CEIL	1221.67
					BP2	1218.42
					BP	1217.07
					BP1	1215.97
					WIDEST	1211.77
					F (CLAY)	1198.07
H615	H616	3522.7	1695.1	1212.57	CEIL	1221.27
					BP1	1216.47
					WIDEST	1211.57
					F (CLAY)	1197.57
H614	H615	3558.8	1728.7	1211.57	CEIL	1218.17
					BP2	1218.17
					BP1	1216.27
					WIDEST	1211.57
					F (CLAY)	1179.57
H613	H614	3576.2	1725.0	1211.57	CEIL	1220.27
					BP1	1216.57
					WIDEST	1212.27
H612	H613	3585.0	1753.7	1211.57	LEDGE	1210.07
					PVC TOP	1194.37
					STREAM	1166.00
					FLOOR	1164.57
D612	H612	3585.0	1753.7	1208.51	SM TOP	1208.51
H611	H612	3598.1	1775.5	1212.57	CEIL	1222.57
					BP1	1216.57
					LEDGE	1210.67
					F (CLAY)	1166.97
D72	H611	3639.6	1803.5	1211.57	SM TOP	1211.57
H827	H401	1818.8	677.9	1221.05		
H828	H827	1811.0	680.9	1228.05	DOME CEIL	1236.55
					CEIL	1230.55
					DL20/DS20	1230.55
					DS17/L16 S	1228.25
					DS17/L16 N	1227.95
					DS17/L16 E	1227.55
H829	H828	1762.2	686.8	1228.05	CEIL	1231.50
					DS21/DL20	1231.50
					DL20/DS20	1230.65
					F (BD)	1224.05
					DS17/DL16	1227.70
H830	H829	1715.2	689.3	1228.05	CEIL	1233.45

					DL23/DS23	1233.45
					DS17/DL16	1226.90
					FLOOR	1224.35
H831	H830	1669.0	695.0	1229.05	CEIL	1232.95
					DS17/DL16	1226.80
					FLOOR	1225.05
H832	H831	1635.0	698.6	1229.05	CEIL	1234.95
					DS17/DL16	1226.35
					F (BD)	1226.35
H833	H832	1586.8	701.9	1228.05	CEIL	1228.70
					DL20/DS20	1228.70
					DS17/DL16	1225.75
					F (BD)	1224.75
H834	H833	1513.5	704.5	1227.05	CEIL	1227.85
					DL20/DS20	1227.85
					DS17/DL16	1224.95
					MUCK TOP.	1224.05
					F (BD)	1223.05
H835	H370	1282.8	221.8	1215.05	CEIL	1215.75
					DL6/DS6	1215.75
					F (BD)	1213.05
H836	H835	1264.1	225.4	1213.05	CEIL	1214.65
					DL5/DS5	1214.65
					DS4/DL3	1213.65
					F (BD)	1212.05
H837	H836	1241.1	229.9	1213.05	CEIL	1213.85
					DL4/DS4	1213.85
					DS1/DT4	1211.45
					F (SILT)	1207.35
H838	H837	1232.5	228.2	1208.05	CEIL	1211.55
					BP3	1209.75
					F (SILT)	1206.55
H839	H838	1211.4	232.3	1208.05	CEIL	1208.85
					F (SILT)	1205.25
H840	H839	1180.8	241.6	1208.05	C POCKET	1216.55
					CEIL	1212.95
					DS3/DL2	1212.35
					DS1/DT4	1209.95
					WAVY BP	1207.85
					STREAM	1171.55
					FLOOR	1170.55
R72	D72	3639.6	1803.5	1210.75	CEIL	1223.87
					LEDGE	1210.75
T73	R72	3659.7	1818.1	1213.37		
R74	T73	3684.6	1812.4	1210.28	CEIL	1219.30
					BP1	1217.33
T75	R74	3722.3	1847.6	1215.04		
R76	T75	3743.5	1863.8	1210.71	C POCKETS	1222.19
					CEIL	1219.67
					BP1	1217.99
T77	R76	3781.5	1888.5	1212.58		
R77	T77	3781.5	1888.5	1212.58		
D77	R77	3781.5	1888.5	1213.76	POPC BOT	1213.76
R78	T77	3762.1	1892.4	1209.39	CEIL	1217.66
					BP1	1217.26

					BP	1211.59
T79	R78	3715.6	1901.9	1211.31		
R80	T79	3696.8	1940.5	1206.56	CEIL	1216.08
					BP1	1216.11
					BP	1211.29
T81	R80	3728.8	1962.1	1211.80		
R82	T81	3716.1	1991.3	1210.77	BP2	1218.19
					BP1	1216.61
					BP	1211.33
T83	R82	3728.6	1998.1	1219.72		
R84	T83	3734.9	1998.5	1217.59	BP3	1221.33
T85	R84	3737.7	2005.5	1225.81		
S86	T85	3745.3	2005.3	1221.60	BP3	1221.60
					DS1/DT4	1223.27
					DL2/DS2	1223.86
					DL3/DS3	1224.68
					DL4/DS4	1225.54
					DL5/DS5	1226.27
					DL6/DS6	1226.95
					SP CEIL	1229.28
S87	T85	3785.9	1996.6	1225.39	DL4/DS4	1226.18
					DL9/DS9	1230.41
					DL10/DS10	1231.56
					CEIL	1235.24
S88	T85	3772.5	1990.4	1222.96		
D88	S88	3772.5	1990.4	1225.47	BD TIP	1225.47
R89	T85	3763.3	2032.5	1217.98	CEIL	1228.07
					DL3/DS3	1224.71
					BP3	1221.66
T90	R89	3812.5	2062.6	1225.30		
S91	T90	3805.2	2054.2	1218.99		
D91	S91	3805.2	2054.2	1219.71	POOL LEVEL	1219.71
R92	T90	3824.1	2072.9	1224.42	CEIL	1231.80
					DS3/DL2	1226.03
T93	R92	3867.2	2107.1	1229.18		
R94	T93	3923.6	2094.1	1225.44	CEIL	1232.50
T95	R94	3998.5	2079.5	1229.14		
S96	T95	3989.7	2078.0	1224.91	DS3/DL2	1226.89
R97	T95	4054.3	2120.0	1225.84	CEIL	1233.39
					DS3/DL2	1227.75
T98	R97	4076.1	2137.1	1230.08		
R99	T98	4084.0	2153.7	1229.42		
D99	R99	4084.0	2153.7	1231.83	CHIP TOP	1231.83
R100	D88	3772.5	1990.4	1222.43		
T101	R100	3837.1	1991.5	1229.83		
R102	T101	3892.4	1991.5	1225.97	DS10/DL9	1232.79
					DS9/DL8	1231.58
T103	R102	3939.3	1978.1	1230.43		
S104	T103	3908.8	1991.0	1222.87		
D104	S104	3908.8	1991.0	1227.15	CHIP TOP	1227.15
R105	T103	3981.5	1976.6	1224.21	DL10/DS10	1234.06
T106	R105	4002.4	1971.4	1225.98		
R107	T106	4065.8	1965.9	1219.73	CEIL	1232.20
					BP3	1222.55
T108	R107	4078.9	1963.8	1221.24		

R109	T108	4102.5	1963.6	1215.10	CEIL	1227.57
					BP3	1222.98
T110	R109	4127.2	1963.2	1216.75		
S111	T110	4109.7	1941.5	1210.07		
D111	S111	4109.7	1941.5	1216.67	PEND TIP	1216.67
R112	T110	4195.1	1961.4	1212.13	CEIL	1226.89
					BP1	1222.30
					BP	1213.11
T113	R112	4275.9	1960.0	1215.91		
R114	T113	4364.6	1955.3	1211.62	CEIL	1231.31
					BP	1214.31
T115	R114	4435.4	1960.3	1216.80		
R116	T115	4507.4	1955.2	1212.39	BP	1215.18
T117	R116	4607.1	1958.7	1219.02		
R118	T117	4706.8	1955.2	1214.74	CEIL	1231.15
					BP1	1224.58
					BP	1216.45
D118	R118	4642.0	1960.9	1216.83	ELBOW BOT	1216.83
T119	R118	4737.7	1906.6	1219.36		
R120	T119	4785.7	1896.4	1215.64	BP1	1223.19
T121	R120	4832.7	1895.6	1220.18		
R122	T121	4908.1	1886.4	1214.15	CEIL	1227.27
T123	R122	4966.2	1874.0	1217.05		
S124	T123	4964.3	1879.8	1213.31		
D124	S124	4964.3	1879.8	1216.53	WALL DOT	1216.53
R125	D124	4964.3	1879.8	1213.37		
T126	R125	4977.9	1870.1	1216.53		
R127	T126	5008.4	1872.7	1211.87	POOR BP	1215.78
					BP	1213.28
T128	R127	5074.6	1910.2	1216.64		
R129	T128	5110.8	1896.6	1211.78	CEIL	1226.22
					BIOSPARITE	1219.72
					POOR BP	1216.24
T130	R129	5127.4	1864.0	1214.57		
S131	T130	5107.8	1885.8	1211.43		
D131	S131	5107.8	1885.8	1214.89	SM TOP	1214.89
R132	T130	5179.1	1859.5	1210.00	POOR BP/XT	1216.17
T133	R132	5228.0	1853.5	1214.43		
R134	T133	5270.3	1848.3	1209.07	BP=SPAR	1219.57
					BP=SPAR	1216.92
T135	R134	5295.3	1801.4	1213.30		
S136	T135	5302.7	1798.7	1208.13		
D136	S136	5302.7	1798.7	1213.32	BD TOP	1213.32
R137	T135	5353.6	1799.4	1209.16	CEIL	1225.56
					D/S	1225.56
					LOW SPAR	1217.23
					SED TOP	1212.37
T138	R137	5384.0	1790.6	1211.54		
R139	T138	5397.7	1753.0	1205.09	C SLOT	1221.83
					CEIL	1218.55
					LOW SPAR	1216.91
T140	R139	5456.1	1751.0	1211.69		
R141	T140	5512.5	1749.0	1207.16	CEIL	1220.28
					LOW SPAR S	1217.99
					LOW SPAR N	1217.33

T142	R141	5549.7	1747.7	1212.52		
R143	T142	5555.3	1730.5	1210.71	CEIL	1222.20
					UPPER SPAR	1218.75
					LOW SPAR	1216.62
T144	R143	5615.2	1729.4	1219.04		
R145	T144	5645.4	1729.4	1214.73	FLAT CEIL	1222.60
					BP	1220.17
					SED TOP	1220.14
D145	R145	5645.4	1729.4	1218.09	SM TOP	1218.09
S146	T144	5631.5	1739.8	1213.87		
D146	S146	5631.5	1739.8	1216.82	ELBOW TOP	1216.82
R147	D88	3772.5	1990.4	1223.04		
T148	R147	3739.9	2005.6	1225.68		
R149	T148	3685.9	2002.8	1218.23	DS3/DL2	1224.41
					DL1/DS1	1222.76
T150	R149	3618.8	2006.3	1223.23		
R151	T150	3580.9	2010.0	1221.74	CEIL	1232.76
					DL9/DS9	1227.96
T152	R151	3526.3	2017.6	1225.43		
R153	T152	3457.5	2020.0	1220.67	CEIL	1229.86
					DL12/DS12	1229.86
					DL9/DS9	1226.15
T154	R153	3399.7	2025.1	1223.73		
R155	T154	3348.2	2026.0	1219.41	CEIL	1228.10
					DL9/DS9	1224.56
T156	R155	3294.3	2031.7	1225.28		
S157	T156	3325.9	2027.2	1219.95		
D157	S157	3325.9	2027.2	1221.13	FLAGGING	1221.13
R158	T156	3228.8	2035.1	1219.69	CEIL	1229.77
					DL9/DS9	1223.01
T159	R158	3164.5	2032.8	1223.63		
R160	T159	3110.1	2036.2	1220.25	DL10/DS10	1222.61
					CEIL	1228.45
T161	R160	3066.3	2040.0	1226.36		
S162	T161	3064.2	2044.1	1223.21	CEIL	1231.58
R163	T161	3038.7	2039.8	1217.57	CEIL	1227.74
					DL10/DS10	1222.20
T164	R163	3003.4	2038.5	1226.49		
R165	T164	2954.5	2038.5	1220.03	CEIL	1226.95
					DS14/DL13	1226.95
T166	R165	2892.5	2048.3	1223.91		
S167	T166	2930.9	2045.0	1219.73		
D167	S167	2930.9	2045.0	1220.10	SM TOP	1220.10
R168	T166	2844.5	2046.7	1221.84	DS14/DL13	1225.68
T169	R168	2818.3	2048.5	1224.77		
R170	T169	2793.8	2052.8	1224.55	CEIL	1229.01
					DL17/DS17	1229.01
					DL16/DS16	1227.87
					DL15/DS15	1227.01
T171	R170	2729.0	2054.5	1226.05		
R172	T171	2653.8	2057.1	1223.12	CEIL	1227.17
					DL17/DS17	1227.17
					DL16/DS16	1226.14
					DL15/DS15	1224.89
T173	R172	2614.9	2064.0	1223.72		

R174	T173	2603.0	2061.9	1221.99	DL15/DS15	1224.54
D174	R174	2603.0	2061.9	1225.07	SM-ST TOP	1225.07
D175	R174	2603.0	2061.9	1224.39	STAL TIP	1224.39
S175	T173	2634.7	2062.6	1220.70	CONE TOPS	1219.78
R176	D157	3325.9	2027.2	1219.80		
T177	R176	3280.9	2030.0	1225.51		
S178	T177	3271.8	2029.1	1222.73		
D178	S178	3271.8	2029.1	1222.80	RADIO LOC	1222.80
R179	D77	3781.5	1888.5	1209.46		
T180	R179	3792.9	1884.2	1213.75		
R181	T180	3833.1	1882.8	1210.18	C FISSURE	1224.94
					BP1	1218.02
T182	R181	3916.1	1868.2	1214.08		
R183	T182	4011.4	1859.8	1209.64	CEIL	1219.49
					SPAR BED	1215.29
T184	R183	4048.4	1856.9	1213.86		
R185	T184	4070.9	1864.9	1210.43	CEIL	1219.94
					BP1	1219.94
					SPAR BED	1216.30
T186	R185	4053.6	1897.5	1214.46		
S187	T186	4055.4	1902.4	1210.57		
D187	S187	4055.4	1902.4	1213.32	SM TOP	1213.32
R188	T186	4085.8	1926.5	1210.13	CEIL	1223.26
					SPAR BED	1215.64
T189	R188	4107.5	1938.0	1214.21		
R190	T189	4117.1	1944.5	1210.06		
D111	R190	4117.1	1944.5	1216.68	PEND TIP	1216.68
R191	D104	3908.8	1991.0	1222.45	DS9/DL8	1231.73
T192	R191	3935.9	2011.0	1225.19		
R193	T192	3945.1	2020.6	1224.58		
T194	R193	3965.5	2026.5	1231.02		
S195	T194	3957.1	2022.5	1228.69	CEIL	1241.49
					DL10/DS10	1233.56
R196	T194	4003.1	2025.8	1230.83	CEIL	1241.99
					DL10/DS10	1234.28
T197	R196	4038.8	2021.7	1238.67		
S198	T197	4029.1	2022.4	1236.62	CEIL	1245.48
R199	T197	4046.8	2021.5	1231.03		
T200	R199	4052.4	2018.9	1231.68		
R201	T200	4115.1	2010.7	1230.01	DL10/DS10	1235.65
T202	R201	4155.9	2000.9	1237.23		
R203	T202	4172.3	1998.7	1235.45	FLAT CEIL	1244.17
					SHELFST	1241.50
D203	R203	4172.3	1998.7	1240.10	SM TOP	1240.10
T204	R203	4245.1	1985.9	1239.19		
S205	T204	4240.6	1989.9	1236.59	CEIL	1243.06
					LAKE LEVEL	1226.62
					CONE TOP	1229.85
D205	S205	4240.6	1989.9	1239.72	RAIL TOP	1239.72
R206	T204	4287.3	1978.4	1234.08	CEIL	1241.40
					DL10/DS10	1237.41
T207	R206	4315.1	1974.5	1234.96		
R208	T207	4329.9	1974.8	1229.83	CEIL	1236.65
					DL9/DS9	1236.65
T209	R208	4411.7	1969.1	1231.77		

R210	T209	4403.2	1982.8	1223.01	CEIL	1235.21
					BP2	1225.53
T211	R210	4384.3	2012.9	1224.72		
R212	T211	4393.9	2017.6	1221.68	CEIL	1230.76
					SED TOP	1228.89
					BP2	1225.09
T213	R212	4426.0	2012.8	1223.97		
R214	T213	4460.3	2023.2	1220.08	CEIL	1227.40
					BP2	1225.22
T215	R214	4510.2	2016.2	1222.71		
R216	T215	4541.3	2010.8	1220.14	CEIL	1226.27
					BP2	1224.14
T217	R216	4552.8	2018.3	1223.35		
R218	T217	4579.7	2015.7	1221.06	CEIL	1231.56
					BP3	1228.87
					BP	1225.64
					BP2	1224.22
T219	R218	4589.1	2021.1	1226.80		
R220	T219	4606.6	1971.6	1223.26	C 4TH AVE	1234.91
					SED TOP	1230.05
					BP	1226.12
					BP2?	1224.81
					BP1	1224.05
T221	R220	4615.5	1969.7	1224.33		
R222	T221	4642.2	1962.0	1214.74		
D118	R222	4642.2	1962.0	1216.83	ELBOW BOT	1216.83
R223	D124	4964.3	1879.8	1213.18	BP	1218.49
T224	R223	4942.1	1923.4	1218.85		
R225	T224	4931.4	1941.1	1218.04	CEIL	1227.23
					BP2	1227.23
					BP	1218.38
T226	R225	4929.9	1945.4	1225.10		
R227	T226	4923.5	1942.9	1224.92	DS1/DT4	1231.71
					SED TOP	1235.42
T228	R227	4917.2	1944.2	1233.54		
R229	T228	4913.8	1946.9	1233.23	CEIL	1243.57
					DL10/DS10	1239.96
T230	R229	4910.4	1948.4	1239.69		
R231	T230	4905.3	1950.5	1239.33	CONCR C	1249.82
T232	R231	4896.4	1952.3	1248.75		
R233	T232	4894.3	1957.3	1248.69		
D233	R233	4894.3	1957.3	1250.49	BLDG FLOOR	1250.49
R234	D233	4894.3	1957.3	1249.95		
T235	R234	4909.3	1967.0	1255.27		
R236	T235	4933.0	1999.0	1255.09		
T237	R236	4971.3	2037.3	1264.16		
R238	T237	5008.7	2078.9	1261.54		
T239	R238	5062.8	2114.0	1263.75		
R240	T239	5110.7	2115.3	1259.69		
D240	R240	5110.7	2115.3	1264.61	POST TOP	1264.61
T241	R240	5083.9	2082.8	1268.87		
R242	T241	5066.1	2076.0	1267.32		
T243	R242	5052.0	2055.8	1276.21		
R244	T243	5031.8	2049.1	1271.92		
D244	R244	5031.8	2049.1	1272.60	BM15=NAIL	1272.60

H1	D174	2535.0	2072.0	1222.07	CEIL	1232.07
					DS16/DL15	1225.32
					FLOOR	1221.67
H2	H1	2555.0	2091.0	1223.07	CEIL	1224.62
					LOW CEIL	1222.67
					SPAR TOP	1221.77
H3	H2	2585.0	2116.0	1223.07	RST TOP	1222.57
					WL 8-7-91	1222.17
					CONE TOPS	1222.37
					LAKE BOT	1218.87
H4	H3	2619.0	2150.0	1228.07	CEIL	1232.07
					F (FST)	1226.37
H5	H4	2594.0	2170.0	1228.07	CEIL	1228.97
					DL17/DS17	1225.82
					FLOOR	1223.17
H6	H5	2427.0	2180.0	1228.07	CEIL	1231.47
					DL17/DS17	1227.87
					FLOOR	1225.57
H7	H6	2299.0	2195.0	1222.07	CEIL	1226.52
					DL17/DS17	1223.12
H8	H7	2255.0	2195.0	1217.07	FLOOR	1211.07
D8	H8	2255.0	2195.0	1211.88	SM TOP	1211.88
H9	H8	2201.0	2200.0	1215.07		
D9	H9	2201.0	2200.0	1212.09	DOT ON BD	1212.09
H10	H9	2102.0	2214.0	1217.07	CEIL	1223.77
					DL17/DS17	1221.57
					F (BD)	1212.07
H11	H10	2063.0	2219.0	1202.07	DS1/DT4	1199.87
					BP3	1199.30
					F (MUD)	1195.27
H36	H11	2014.0	2234.0	1216.07	CEIL	1221.87
					DL17/DS17	1220.87
					F (MUD)	1213.72
H12	H36	1837.0	2259.0	1216.07	CEIL	1224.57
D12	H12	1837.0	2259.0	1212.76	CAIRN TOP	1212.76
H13	H12	1777.0	2268.0	1206.07	DS10/DL9	1211.07
					FLOOR	1201.07
D13	H13	1777.0	2268.0	1204.80	SSTRAW TIP	1204.80
H14	H13	1778.0	2271.0	1203.07	SP CEIL	1206.27
H15	H14	1807.0	2293.0	1200.07	CEIL	1205.47
					BP	1198.37
					CRAWL CEIL	1198.37
					FLOOR	1195.37
H16	H15	1871.0	2313.0	1198.07	CEIL	1204.07
					DL1/DS1	1200.47
					BP3	1198.77
					BP2	1196.57
					F (S+G)	1191.57
H17	H16	1925.0	2347.0	1198.07	CEIL	1200.57
					BP	1199.07
					D/S	1196.97
					ROCK TOP	1192.57
					STREAM	1170.07
H18	D13	1728.0	2278.0	1206.07	DS10/DL9	1209.92
					F (SAND)	1203.22

H19	H18	1610.0	2293.0	1226.07	CEIL	1229.57
					F (BD)	1224.07
D19	H19	1610.0	2293.0	1224.72	STAL TIP	1224.72
H20	D9	2201.0	2200.0	1215.07	DS10/DL9	1212.96
H21	H20	2250.0	2239.0	1210.07	CEIL	1219.37
					F (BD)	1207.07
H22	H21	2319.0	2288.0	1208.07	CEIL	1215.47
					DS10/DL9	1213.07
					FLOOR	1203.07
H23	H22	2378.0	2337.0	1203.07	D/S	1198.67
					FLOOR	1196.57
H24	H23	2462.0	2327.0	1201.07	CEIL	1211.07
					D/S	1198.47
					F (BD)	1195.57
H25	H24	2575.0	2421.0	1201.07	WATER LEV	1169.57
					FLOOR	1167.07
H26	H25	2580.0	2421.0	1202.07	BP3	1201.97
					BP	1200.72
					D/S	1199.27
H27	H26	2619.0	2416.0	1205.07	CEIL	1210.87
					DS2	1208.17
					DS1/DT4	1207.07
					BP3	1205.22
					WATER LEV	1202.27
H28	D8	2240.0	2180.0	1215.07	DL10/DS10	1213.47
H29	H28	2147.0	2101.0	1215.07	CEIL	1218.87
					DL10/DS10	1212.67
					F (BD)	1211.27
H30	H29	2043.0	2126.0	1219.07	CEIL	1223.97
					DS17/DL16	1220.77
					FLOOR	1213.87
H31	H30	1748.0	2150.0	1209.07	CEIL	1219.57
					SED TOP	1215.87
					DL10/DS10	1210.17
					F (SAND)	1206.07
D31	H31	1748.0	2150.0	1206.44	RADIO LOC	1206.44
H32	H31	1709.0	2111.0	1210.07	CEIL	1215.07
					FLOOR	1207.07
H33	H32	1659.0	2077.0	1210.07	DOME CEIL	1223.07
					C 6TH AVE	1216.47
					SED TOP	1214.77
					DS11/DL10	1209.73
					F (SAND)	1208.07
H34	H33	1556.0	1993.0	1212.07	HIGH CEIL	1218.77
					BD TIP	1210.35
					THRESHOLD	1209.92
					DL10/DS10	1209.47
					F (SAND)	1208.52
H35	H34	1526.0	1958.0	1213.07	CEIL	1217.37
					DL10/DS10	1209.07
					F (MUD)	1208.33
R795	D88	3772.5	1990.4	1222.41		
T796	R795	3755.6	1999.4	1225.31		
R797	T796	3735.9	2009.0	1223.18		
D797	R797	3735.9	2009.0	1224.28	BM +	1224.28

R852	D1	0.0	0.0	1229.40	
T853	R852	13.2	9.8	1233.04	
R854	T853	-25.6	63.1	1229.23	
T855	R854	-66.8	115.9	1233.69	
R856	T855	-95.5	185.1	1228.91	
T857	R856	-133.4	239.2	1233.29	
R858	T857	-176.2	282.8	1228.94	
T859	R858	-227.7	318.2	1232.22	
R860	T859	-282.2	316.8	1226.54	
D861	R860	-282.2	316.8	1228.36	+ ON ROCK 1228.36
R862	D1	0.0	0.0	1229.40	
T863	R862	15.9	-53.7	1232.85	
R864	T863	7.1	-120.5	1228.42	
T865	R864	-1.6	-190.9	1233.50	
R866	T865	-13.1	-253.2	1228.49	
T867	R866	-17.0	-317.7	1231.71	
R868	T867	28.8	-323.3	1227.38	
T869	R868	41.4	-320.1	1236.61	
R870	T869	48.7	-326.1	1235.25	
T871	R870	55.7	-334.9	1244.77	
R872	T871	58.2	-327.7	1240.86	
D873	R872	58.2	-327.7	1244.41	+ AT ENT 1244.41
R874	T871	39.9	-350.4	1235.87	
T875	R874	28.7	-392.2	1244.65	
R876	T875	33.1	-388.5	1243.46	
T877	R876	45.0	-396.4	1253.26	
R878	T877	58.0	-401.1	1252.56	
D879	R878	58.0	-401.1	1254.95	+ AT ENT 1254.95
R880	D205	4240.6	1989.9	1236.74	
T881	R880	4247.4	1987.4	1239.55	
S882	T881	4215.0	1991.4	1236.14	
D883	S882	4215.0	1991.4	1239.19	RAIL TOP 1239.19
S884	T881	4210.5	1992.6	1236.01	
D885	S884	4210.5	1992.6	1239.01	RAIL TOP 1239.01
					LAKE LEVEL 1233.21
R886	T881	4280.6	1978.5	1234.85	
T887	R886	4305.9	1975.0	1236.37	
S888	T887	4298.8	1976.8	1233.07	TOP SEEP 1233.28
					LOWER SEEP 1233.12
R889	D240	5110.7	2115.3	1259.94	
T890	R889	5143.8	2059.0	1269.59	
R891	T890	5207.9	2017.4	1267.12	
T892	R891	5275.0	1990.3	1271.76	
R893	T892	5338.5	1960.0	1267.71	
T894	R893	5408.4	1931.0	1271.47	
R895	T894	5514.3	1881.7	1266.79	
T896	R895	5577.4	1856.1	1271.00	
R897	T896	5653.0	1824.0	1266.94	
D898	R897	5653.0	1824.0	1271.57	POST TOP 1271.57
T899	R897	5696.4	1792.5	1273.09	
R900	T899	5696.9	1739.8	1272.98	
T901	R900	5695.9	1685.1	1282.55	
R902	T901	5696.9	1647.7	1282.21	
T903	R902	5695.1	1596.1	1291.84	
R904	T903	5695.6	1564.7	1291.74	

T905	R904	5694.5	1521.2	1300.71		
R906	T905	5694.2	1483.6	1300.57		
T907	R906	5692.3	1431.5	1309.37		
R908	T907	5694.1	1365.0	1309.32		
T909	R908	5694.1	1307.1	1314.46		
R910	T909	5698.5	1205.3	1310.03		
T911	R910	5700.0	1147.8	1315.98		
R912	T911	5703.6	1065.3	1315.55		
T913	R912	5706.2	1016.7	1323.31		
R914	T913	5709.1	968.7	1323.25		
T915	R914	5712.3	923.3	1331.80		
R916	T915	5714.4	874.3	1331.79		
T917	R916	5717.0	825.1	1340.66		
R918	T917	5718.6	779.6	1340.52		
T919	R918	5721.0	733.5	1349.18		
R920	T919	5724.2	659.9	1349.09		
T921	R920	5727.4	598.3	1353.77		
R922	T921	5733.2	515.5	1346.10		
T923	R922	5733.2	458.6	1347.78		
R924	T923	5736.1	376.5	1340.77		
T925	R924	5735.0	314.7	1343.55		
R926	T925	5737.3	227.2	1337.77		
T927	R926	5739.3	169.2	1340.59		
R928	T927	5740.1	87.5	1332.07		
T929	R928	5742.0	43.3	1333.55		
R930	T929	5742.6	-30.2	1324.86		
T931	R930	5742.0	-98.7	1326.19		
R932	T931	5736.1	-183.8	1320.10		
D932	R932	5736.1	-183.8	1324.12	BOLT TOP	1324.12
T933	R932	5770.4	-242.1	1323.41		
R934	T933	5821.4	-296.7	1317.99		
T935	R934	5856.7	-338.0	1322.30		
R936	T935	5913.8	-389.4	1318.99		
T937	R936	5981.5	-409.5	1324.06		
R938	T937	6054.7	-352.3	1322.43		
T939	R938	6112.4	-314.1	1328.90		
R940	T939	6195.4	-273.6	1326.52		
T941	R940	6250.5	-255.2	1331.66		
R942	T941	6340.5	-228.6	1328.77		
T943	R942	6416.1	-219.9	1332.91		
R944	T943	6460.2	-213.0	1329.77		
T945	R944	6534.3	-213.0	1333.83		
R946	T945	6610.3	-224.3	1326.98		
D946	R946	6610.3	-224.3	1330.65	BOLT TOP	1330.65
R947	D946	6610.3	-224.3	1326.97		
T948	R947	6675.6	-213.4	1333.28		
R949	T948	6758.5	-209.0	1329.42		
T950	R949	6830.3	-211.5	1332.90		
R951	T950	6934.9	-208.8	1328.48		
T952	R951	7009.5	-211.4	1332.46		
R953	T952	7103.2	-208.9	1327.89		
T954	R953	7172.4	-208.3	1332.14		
R955	T954	7277.5	-197.3	1327.50		
T956	R955	7351.7	-182.2	1331.45		
R957	T956	7448.7	-148.8	1326.29		

T958	R957	7521.4	-117.2	1330.24		
R959	T958	7611.3	-63.2	1324.74		
T960	R959	7666.5	-21.6	1328.41		
R961	T960	7734.7	42.0	1322.85		
T962	R961	7784.0	96.8	1326.33		
R963	T962	7841.7	172.0	1319.92		
T964	R963	7879.8	235.4	1325.48		
R965	T964	7914.6	315.5	1318.34		
T966	R965	7940.4	379.4	1320.23		
R967	T966	7966.9	450.0	1312.67		
T968	R967	7994.9	519.5	1313.77		
R969	T968	8025.6	599.3	1305.40		
T970	R969	8051.3	668.2	1306.56		
R971	T970	8081.1	743.9	1298.05		
T972	R971	8105.8	811.7	1299.27		
R973	T972	8132.6	881.5	1291.68		
T974	R973	8158.5	948.9	1292.94		
R975	T974	8190.1	1023.4	1284.71		
T976	R975	8217.9	1088.8	1285.96		
R977	T976	8256.3	1162.6	1277.81		
T978	R977	8291.7	1227.9	1278.92		
R979	T978	8338.9	1303.3	1270.55		
T980	R979	8379.0	1363.9	1271.94		
R981	T980	8426.2	1427.7	1263.88		
T982	R981	8470.9	1486.0	1265.26		
R983	T982	8527.6	1546.7	1256.54		
T984	R983	8577.8	1600.6	1257.86		
S985	T984	8593.5	1593.8	1249.36	DT4 PYRITE	1249.52
R986	T984	8637.1	1654.0	1249.29		
T987	R986	8691.7	1700.6	1250.03		
R988	T987	8730.7	1709.3	1240.58	BP1	1243.59
H900	D91	3805.2	2054.2	1224.71	DS1/DT4	1223.79
H901	H900	3778.9	2054.9	1228.71		
H902	H901	3756.3	2052.1	1228.71	DS10/DL9	1231.01
					CEIL	1240.11
					DL16/DS16	1240.11
					F (BD)	1226.91
H903	H902	3729.9	2058.7	1232.71	CEIL	1238.66
					DL15/DS15	1238.66
					F (BD)	1231.11
					DS13/DL12	1235.61
					DL13/DS13	1235.91
					DL14/DS14	1236.66
H904	H903	3710.9	2061.7	1232.71	CEIL	1238.21
					DL15/DS15	1238.21
					DS10/DL9	1229.89
					F (BD)	1227.21
H905	H904	3678.9	2066.2	1227.71	F (BD)	1223.71
H906	H905	3662.9	2062.4	1227.71	DS10/DL9	1229.61
					F (BD)	1222.71
D906	H906	3662.9	2062.4	1227.51	DOT	1227.51
H907	H906	3618.1	2071.9	1227.71	CEIL	1235.01
					DL14/DS14	1235.01
					DS10/DL9	1228.76
					F (BD)	1223.21

MYSTERYL

STA	FROM	EAST	NORTH	VERTICAL		FEET
H908	H907	3592.5	2075.1	1228.71	CEIL	1234.81
					DL14/DS14	1234.81
					F (BD)	1228.21
					RED SH	1228.11
H909	H908	3546.4	2080.0	1230.71	CEIL	1234.21
					DL14/DS14	1234.21
					F (BD)	1229.71
H910	H909	3497.0	2086.9	1230.71	CEIL	1231.46
					DL12/DS12	1231.46
					F (BD)	1227.71
H911	H910	3447.9	2093.0	1229.71	CEIL	1230.91
					DL12/DS12	1230.91
					DS10/DL9	1226.61
					F (BD)	1225.81
H912	H911	3399.0	2097.2	1229.71	CEIL	1230.21
					DL12/DS12	1230.21
					F (BD)	1226.31
H913	H912	3371.2	2099.7	1228.71	CEIL	1229.81
					DL12/DS12	1229.81
					F (CLAY)	1227.31
H914	H913	3326.1	2104.4	1227.71	CEIL	1229.01
					DL12/DS12	1229.01
					F (CLAY)	1225.91
H915	H914	3322.9	2104.6	1226.71	CEIL	1227.71
					F (CLAY)	1224.31
H916	H915	3316.5	2105.8	1224.71		
H917	H916	3282.0	2107.6	1224.21	C (BOXWK)	1224.91
					F (MUD)	1223.51
H918	H917	3277.0	2108.1	1224.21	C=SHELFST	1225.61
					F (CLAY)	1224.21
H919	H918	3277.0	2108.1	1227.61		
H920	H919	3227.3	2118.7	1227.61	CEIL	1229.61
					DL14/DS14	1229.61
					F (BD)	1225.81
					SIDE F	1223.61
H921	H920	3188.0	2123.5	1227.61	CEIL	1228.86
					DL14/DS14	1228.86
					F (BD)	1226.11
					NORTH F	1223.61
H922	H921	3156.2	2126.0	1227.61	CEIL	1228.61
					DL14/DS14	1228.61
H923	H922	3132.0	2131.6	1225.61	CEIL	1226.61
					DL12/DS12	1226.61
					WATER LEV	1225.21
H924	H923	3130.1	2132.0	1226.61	CEIL	1228.11
					DL14/DS14	1228.11
H925	H924	3099.1	2138.9	1226.61	CEIL	1229.21
					DL16/DS16	1229.21
					DL14/DS14	1228.11
					F (BD)	1226.61
					DEEP F	1224.11

H926	H925	3063.6	2147.1	1227.61	CEIL	1229.61
					DL16/DS16	1229.61
					F (BD)	1227.01
H927	H926	3047.5	2151.6	1227.61	CEIL	1229.51
					DL16/DS16	1229.51
					DL15/DS15	1228.76
					F (BD)	1226.21
H928	H927	2997.5	2155.5	1226.61	CEIL	1227.21
					DL14/DS14	1227.21
					F (CLAY)	1223.41
H929	H928	2977.6	2157.2	1226.61	CEIL	1227.11
					DL14/DS14	1227.11
					F (RST)	1223.61
D929	H929	2977.6	2157.2	1225.73	+ ON WALL	1225.73
H850	D873	58.2	-327.7	1242.41		
H851	H850	71.9	-340.7	1237.41		
H852	H851	79.1	-334.9	1237.41	CEIL	1246.31
					DL27/DS27	1238.98
					F (BD)	1233.41
H853	H852	94.9	-339.1	1234.41	F (BD)	1230.41
H854	H853	105.0	-344.0	1227.41	F (BD)	1226.71
H855	H854	121.3	-345.7	1227.41	F (BD)	1222.91
H856	H855	126.6	-350.0	1223.41	CEIL	1226.01
					F (BD)	1219.41
H857	H856	131.3	-348.6	1220.41	CEIL	1222.71
					F (BD)	1215.91
H858	H857	137.3	-349.4	1216.41	CEIL	1222.71
					DL14/DS14	1222.71
					DL13/DS13	1222.21
					F (BD)	1211.41
H859	H858	141.7	-344.4	1212.41	DS4/DL3	1211.51
					FLOOR	1208.91
H860	H859	146.2	-325.7	1211.41	CEIL	1214.31
					DL7/DS7	1214.31
					F (MUD)	1206.91
H861	H860	191.8	-332.1	1211.41	CEIL	1214.11
					DL7/DS7	1214.11
					F (MUD)	1206.81
H862	H861	241.3	-337.3	1211.41	CEIL	1213.41
					DS4/DL3	1211.71
					DS3/DL2	1210.66
					DS2/DL1	1209.91
					DS1/DT4	1209.31
					F (MUD)	1206.91
H863	H862	278.0	-340.5	1211.41	CEIL	1213.51
					DL6/DS6	1213.51
					DS1/DT4	1209.41
					SHELF TOP	1210.11
					F (MUD)	1206.91
D863	H863	278.0	-340.5	1211.41	+ ON WALL	1211.41
H864	D863	287.1	-325.3	1210.41	CEIL	1212.76
					DS4/DL3	1210.86
					F (MUD)	1205.81
H865	H864	327.5	-294.3	1210.41	CEIL	1211.91
					DL5/DS5	1211.91

					DS3/DL2	1210.01
					FLOOR	1205.91
H866	H865	368.7	-264.4	1210.41	CEIL	1213.41
					DS3/DL2	1210.96
					F (SAND)	1206.91
H867	H866	403.8	-242.5	1210.41	CEIL	1215.21
					SHELF TOP	1208.21
					DS1/DT4	1209.76
					FLOOR	1206.21
D868	H867	403.8	-242.5	1209.26	BASIN TIP	1209.26
H869	H867	418.4	-234.0	1210.41	CEIL	1214.71
					DS1/DT4	1209.56
					SHELF TOP	1208.14
					F (CLAY)	1207.01
H930	D99	4084.0	2153.7	1229.93	CRAWL CEIL	1231.73
					DL8/DS8	1231.73
					FLOOR	1229.33
H931	H930	4090.3	2169.0	1229.43	CEIL	1230.33
					DL7/DS7	1230.33
					F (BD)	1227.63
H932	H931	4089.7	2171.7	1228.83		
H933	H932	4090.5	2172.4	1228.83		
H934	H933	4090.9	2173.4	1228.23		
H935	H934	4091.4	2188.9	1227.73	CEIL	1230.23
					DL7/DS7	1230.23
					LOW CEIL	1228.23
					HIGH CEIL	1230.88
					DL8/DS8	1230.88
					F=BD+CLAY	1226.98
H936	H935	4098.7	2193.4	1228.73	CEIL	1233.13
					DL7/DS7	1230.08
					FLOOR	1228.43
H937	H936	4103.1	2199.0	1229.73	FLOOR	1226.73
H938	H937	4112.1	2201.9	1230.33		
H939	H938	4144.4	2195.3	1231.63	DS10/DL9	1233.53
					F (BD)	1227.13
H940	H939	4174.6	2226.1	1231.63	DL10/DS10	1234.83
					LOW CEIL	1232.53
					DL8/DS8	1232.53
					F=BD+CLAY	1227.13
H941	H940	4193.3	2239.6	1231.63	DS10/DL9	1233.98
					F (BD)	1230.63
H942	H941	4198.2	2243.8	1233.63		
H943	H942	4211.4	2244.2	1233.63	DL9/DS9	1233.78
					F (BD)	1231.13
D943	H943	4211.4	2244.2	1231.26	SM TOP	1231.26
H944	H943	4215.0	2252.8	1232.53	DL8/DS8	1233.98
					F=BD+CLAY	1228.13
H945	H944	4249.8	2287.0	1229.33	CEIL	1233.06
					DL8/DS8	1233.06
					F (CLAY)	1228.33
H946	H945	4231.8	2297.4	1230.03	CEIL	1231.63
					DL7/DS7	1231.63
					F=BD+CLAY	1227.73
D947	H946	4231.8	2297.4	1229.91	+ ON WALL	1229.91

H948	H946	4247.1	2309.2	1228.53	CEIL	1229.83
					DL5/DS5	1229.83
					F (CLAY)	1226.93
H949	H948	4267.4	2310.8	1227.63	CEIL	1230.23
					DL5/DS5	1230.23
					DS1/DT4	1226.66
					F (CLAY)	1225.63
H950	H949	4282.7	2319.1	1227.63	CEIL	1230.88
					DL6/DS6	1230.88
					F (CLAY)	1226.83
H951	H950	4293.9	2325.2	1230.63	CEIL	1232.08
					DL7/DS7	1232.08
					F=BD+CLAY	1229.63
H952	H951	4329.5	2358.3	1231.03	CEIL	1232.93
					DL8/DS8	1232.93
					F (CLAY)	1229.13
					F SLOT	1216.03
H953	H952	4350.6	2366.6	1232.03	CEIL	1233.23
					DL9/DS9	1233.23
					F (CLAY)	1231.53
H954	H953	4373.5	2354.5	1231.03	PIT FLOOR	1210.63
					BD/SED	1231.43
D954	H954	4373.5	2354.5	1230.54	SM TOP	1230.54
D955	H954	4373.5	2354.5	1233.94	CEIL DOT	1233.94
H955	D947	4208.5	2295.9	1229.91	CEIL	1231.11
					DL7/DS7	1231.11
H956	H955	4204.1	2297.4	1225.91	DS1/DT4	1226.26
					F (CLAY)	1220.61
H957	H956	4198.3	2297.9	1219.91	CEIL	1222.21
					FLOOR	1218.51
H958	H957	4172.5	2302.4	1219.91	CEIL	1221.11
					BP	1221.11
					BP1	1219.51
					WAVY BP	1218.71
H959	H958	4158.3	2305.2	1217.91	CEIL	1220.31
					BP	1220.31
					BP1	1219.21
					FLOOR	1212.51
H960	H959	4147.1	2301.6	1215.91	CEIL	1220.21
					BP1	1219.11
					F (CLAY)	1210.71
H961	H960	4098.0	2309.8	1213.91	CEIL	1219.81
					BP1	1218.41
					F (CLAY)	1209.81
H962	H961	4079.8	2313.2	1213.91	CEIL	1219.31
					BP1	1218.11
					FLOOR	1210.61
D962	H962	4079.8	2313.2	1216.46	ARROW TIP	1216.46
H963	H962	4070.9	2333.3	1213.91		
H964	H963	4068.4	2342.2	1213.91	CEIL	1218.41
					FLOOR	1210.81
H965	H964	4057.7	2362.2	1211.61	CEIL	1215.61
					FLOOR	1209.61
H966	H965	4053.0	2374.1	1211.61	CEIL	1216.51
					FLOOR	1210.86

H967	H966	4043.5	2390.0	1213.61	CEIL	1215.91
					FLOOR	1210.91
H968	H967	4016.4	2381.9	1211.61	CEIL	1215.21
					FLOOR	1210.71
H969	H968	4002.5	2378.3	1211.61	CEIL	1213.61
					FLOOR	1210.41
H970	H969	3994.1	2381.6	1211.61	CEIL	1213.61
					F (CLAY)	1210.61
H971	H970	3976.4	2384.2	1211.61	CEIL	1213.61
					F (CLAY)	1210.61
H972	H971	3960.7	2386.7	1211.61	CEIL	1213.61
					F (CLAY)	1210.51
H973	H972	3941.8	2388.7	1211.61	CEIL	1214.11
					F (CLAY)	1210.51
H974	H973	3925.8	2391.7	1211.61	CEIL	1214.11
					F (CLAY)	1210.41
H975	H974	3908.4	2394.7	1211.11	CEIL	1213.21
					F (CLAY)	1209.81
H976	H975	3898.2	2397.6	1210.61	CEIL	1213.41
					F (CLAY)	1209.51
H977	H976	3888.6	2401.8	1210.61	CEIL	1213.81
					BP	1213.66
					F (CLAY)	1207.11
H978	H977	3880.2	2401.8	1207.61	C = BP	1213.41
					BP	1209.26
					FLOOR	1203.41
D978	H978	3880.2	2401.8	1209.21	WALL DOT	1209.21
H979	H978	3858.0	2404.6	1207.61	CEIL	1212.71
					BP	1209.11
					F (CLAY)	1204.21
H980	H979	3841.3	2399.0	1208.61	CEIL	1212.91
					BP	1208.91
					FLOOR	1204.41
H981	H980	3824.0	2403.9	1209.61	CEIL	1213.11
					BP	1208.71
					FLOOR	1204.81
H982	H981	3776.8	2411.8	1209.61	CEIL	1213.31
					BP (POOR)	1208.36
					BP	1212.56
					F (CLAY)	1204.51
H983	H982	3727.1	2417.1	1209.61	CEIL	1212.31
					BP	1211.81
					F (CLAY)	1205.01
H984	H983	3697.8	2420.4	1209.61	CEIL (BP)	1212.31
					BP	1211.46
					MUCK TOP	1206.51
					F (CLAY)	1205.11
H985	H984	3676.9	2424.8	1209.61	CEIL (BP)	1212.01
					BP (WAVY)	1211.06
					FLOOR	1205.31
H986	H985	3642.1	2412.9	1209.61	CEIL	1212.11
					WAVY BP	1210.71
					BP	1211.71
					F=SILT	1204.91
H987	H986	3624.2	2412.5	1209.61	CEIL	1211.76

					BP	1211.54
					WAVY BP	1210.51
					F (SAND)	1205.01
H988	H987	3614.5	2412.6	1209.61	CEIL	1211.91
					BP	1211.41
					WAVY BP	1210.51
					FLOOR	1205.01
H989	H988	3591.1	2416.8	1209.61	CEIL	1211.71
					BP	1211.61
					BP	1210.97
					WAVY BP	1210.16
					MUCK TOP	1207.11
					FLOOR	1205.01
H990	H989	3577.0	2417.6	1207.61	CEIL	1212.81
					BP2	1211.21
					BP1	1210.81
					WAVY BP	1210.11
					F (STREAM)	1203.11
H991	H990	3528.2	2425.4	1208.61	C=BP+PYRIT	1213.61
					BP	1212.25
					BP	1211.81
					BP	1211.41
					BP	1211.01
					BP	1210.31
					WAVY BP	1209.31
					F (STREAM)	1204.81
H992	H991	3481.6	2431.5	1209.61	CEIL	1212.71
					BP	1211.81
					BP	1211.36
					BP	1210.41
					BP	1209.91
					WAVY BP	1209.01
					F (STREAM)	1206.71
H993	H992	3463.5	2436.2	1209.61	CEIL	1213.61
					CONTACT?	1211.66
					WAVY BP	1208.96
					F (STREAM)	1206.96
H994	H993	3452.2	2424.7	1211.61	CEIL	1214.91
					BP+SHALE	1214.51
					BP+SHALE	1214.08
					BP+SHALE	1214.01
					BP+SHALE	1213.71
					BP+SHALE	1213.21
					BP+SHALE	1212.94
					MAJOR BP	1211.11
					BP	1210.26
					BP	1209.71
					WAVY BP	1208.91
					F (STREAM)	1207.71
H995	H994	3433.2	2427.4	1211.61	CEIL	1213.56
					MAJOR BP	1211.11
					F (STREAM)	1207.91
H996	H995	3440.2	2438.6	1211.61	CEIL	1213.91
					MAJOR BP	1211.01
					F (STREAM)	1208.21

H997	H996	3425.0	2467.2	1210.11	CEIL	1213.21
					MAJOR BP	1210.74
					F (STREAM)	1208.41
D997	H997	3425.0	2467.2	1213.21	CEIL DOT	1213.21

END OF FILE

APPENDIX 3 -- Seismic Refraction Data

Picnic area across river from Mystery I:

1. At west end of footbridge, extending 120 feet to north (azimuth 350 deg).

X (ft)	forward time (msec)	reverse time (msec)
0	0	46.5
5	4.37	---
10	8.79	42.9
15	13.32	---
20	19.7	39.2
25	23.6	39.2
30	28.6	39.1
40	28.8	41.7
50	32.1	38.1
60	40.0	37.4
70	40.0	30.4
80	40.2	30.0
90	41.8	24.1
100	44.2	19.2
110	44.0	7.1
120	46.6	0

v1 = 1050 ft/sec (dry sediment).
v2 = 11,770 ft/sec (limestone).
Depth to bedrock approx. 18 ft.
Irregular bedrock surface.
Arrivals were indistinct in reverse shot.

2. From west end of footbridge, extending 120 ft to west (azimuth 270 deg):

X (ft)	forward time (msec)	reverse time (msec)
0	0	49.0
10	8.58	49.0
20	21.8	49.6
30	27.1	49.6
40	30.1	47.5
50	31.7	44.4
60	36.1	43.2
70	39.9	35.3
80	39.0	34.9
90	39.0	34.9
100	39.8	28.9
110	40.7	15.7
120	42.5	0

v1 = 820 ft/sec (dry sediment).
v2 = 7150 ft/sec (weathered bedrock?).
Depth to bedrock approx. 10 ft?
Slight bedrock slope toward west.

3. Continuation of #2 toward west:

X (ft)	forward time (msec)	reverse time (msec)
0	0	52.3
10	8.8	52.7
20	18.0	50.7
30	26.4	49.2
40	35.7	48.7
50	45.5	47.0
60	46.1	45.8
70	47.1	45.3
80	49.9	35.6
90	49.4	26.4
100	49.5	17.4
110	50.1	---
120	51.1	0

v1 = 1110 ft/sec (dry sediment)
v2 = 9900 ft/sec (bedrock)
Depth to bedrock = 23 ft.
Slight bedrock slope toward east.
Very little relief on bedrock.

4. Eastward from picnic grounds road, to 20 ft from western river bank (azimuth 70 deg), 250 ft south of ford (now bridge) over river:

X (ft)	forward time (msec)	reverse time (msec)
0	0	45.9
10	8.9	45.1
20	17.6	43.3
30	26.5	41.5
40	35.7	39.1
50	39.2	38.1
60	42.1	33.6
70	41.2	25.8
80	43.1	---
90	43.1	7.4
100	45.9	0

v1 = 1160 ft/sec (dry sediment).
v2 = 8450 ft/sec (bedrock).
Depth to bedrock 20 ft.
Little relief on bedrock surface.
Bedrock slopes gently toward east.

5. Northward, terminating at eastern end of #4, parallel to western river bank, 20 ft from river, azimuth 335 deg:

X (ft)	forward time (msec)	reverse time (msec)
0	0	41.9
10	8.5	42.2
20	17.6	40.6
30	26.5	39.4
40	29.6	42.0
50	32.1	37.2
60	41.8	35.0
70	40.1	26.6
80	41.4	17.6
90	40.1	8.6
100	41.2	0

v1 = 1150 ft/sec (dry sediment).
v2 = 13,300 ft/sec (limestone).
Some scatter in bedrock arrivals.
Depth to bedrock approx. 20 ft.

6. Parallel to western boundary of Park, along faint road, azimuth 0 deg, on low terrace, from southern edge of patch of woods toward Walnut Cave:

X (ft)	forward time (msec)	reverse time (msec)
0	0	—
10	13.2	40.5
20	17.5	38.4
30	23.9	37.8
40	26.7	36.6
50	32.8	32.2
60	41.8	27.2
70	43.3	23.6
80	51.0	17.8
90	52.0	8.4
100	51.8	0

v1 = 1450 ft/sec. (dry sediment).
v2 = 12,800 ft/sec (limestone).
Depth to bedrock 23 ft.
Forward arrivals indistinct.

7. Ten feet from river, parallel to west bank of river, starting 30 feet from ticket office, directly across from Mystery I entrance, azimuth 190 deg.

X (ft)	forward time (msec)	reverse time (msec)
0	0	43.3
5	7.35	---
10	12.5	37.1
15	17.5	---
20	21.3	37.1
25	25.9	---
30	31.1	38.3

35	31.3	---
40	35.3	34.9
45	40.0	---
50	44.3	30.2
60	50.5	27.2
70	53.1	26.3
80	55.1	20.6
90	55.1	11.1
100	57.8	0

Great amount of scatter.
Depth to bedrock apparently >20 ft.

8. From southern end of #7, extending toward west (azimuth 280 deg), starting 50 ft from west bank of river:

X (ft)	forward time (msec)	reverse time (msec)
0	0	39.4
10	9.1	39.1
20	18.0	38.2
30	25.9	36.4
40	30.6	38.1
50	31.5	35.5
60	32.9	32.7
70	34.3	27.3
80	36.8	18.1
90	38.9	8.9
100	41.6	0

$v1$ = 1130 ft/sec (dry sediment).
$v2$ = 7700 ft/sec (weathered bedrock).
Depth to bedrock 17 ft. on west end, 11.4 ft on east end.
Bedrock slopes toward west.

9. In Grabau Quarry parallel to west wall, 25 ft from wall, Stewartville Formation in floor of quarry:

X (ft)	forward time (msec)
0	0
5	2.96
10	5.09
20	8.57
30	13.45
50	21.3

Apparent velocity = 2460 ft/sec. Interpretation not clear.

10. Southeast of Grabau Quarry on dirt road, extending southward across dry bed of South Branch of Root River:

X (ft)	forward time (msec)	reverse time (msec)
0	0	---
10	4.4	---
20	7.3	---
30	10.7	---

40	15.9	--- readings obscure
50	21.5	---
60	23.3	---
70	26.9	---
80	31.1	---
90	31.3	19.4
100	34.2	13.7
110	35.0	5.3
120	36.6	0

Reverse shot gave indistinct arrivals beyond 30 ft.
v1 = 2400 ft/sec (compact or moist sediment).
v2 = 7270 ft/sec (weathered bedrock).
Depth to bedrock = 27 ft.

11. Parallel to dry bed of South Branch, on south side, extending west, in pulloff 100 feet south of dry bed:

X (ft)	forward time (msec)	reverse time (msec)
0	0	38.8
10	6.0	35.6
20	13.0	35.6
30	23.0	34.6
40	28.2	34.2
50	32.2	34.9
60	33.9	34.8
70	34.9	34.8
80	36.8	31.1
90	38.2	25.6
100	38.9	16.9
110	43.3	8.1
120	45.2	0

v1 = 1300 ft/sec (dry sediment).
v2 = high limestone velocity (actual value not clear).
Depth to bedrock approx. 19 ft.
Average slope on bedrock about 5.5 deg to west (in line of traverse).
Moderate relief on bedrock surface.

12. Almost directly over Garden of the Gods in Mystery II, south of driveway, extending westward just north of fence line across driveway from flagged stake (about 100 feet west of gate to Mystery II driveway):

X (ft)	forward time (msec)	reverse time (msec)
0	0	43.4
10	9.1	43.5
20	18.7	42.8
30	27.5	42.3
40	36.4	41.0
50	40.5	36.6
60	43.7	35.5
70	44.4	27.1
80	44.9	18.2
90	45.6	9.5
100	---	0

v1 = 1110 ft/sec (dry soil and sediment).
v2 = 16,570 ft/sec (limestone).
Depth to bedrock = 22 ft.
Rather uniform bedrock surface.

13. Extension of #6 toward north along faint dirt road over Walnut Cave:

X (ft)	forward time (msec)	reverse time (msec)
0	0	---
5	7.2	---
10	9.18	25.9
20	14.1	24.8
30	18.4	24.5
40	21.2	22.4
50	22.5	22.6
60	27.4?	21.3
70	25.6	20.1
80	26.5	17.4
90	30.1	9.0
95	---	4.5
100	31.7	0

v1 = 1160 ft/sec (dry sediment).
v2 = 8860 ft/sec (bedrock).
Depth to bedrock about 10 ft. over Walnut Cave.
Irregular bedrock surface.

14. Perpendicular to #13, from a point 15 ft south of southern end of #13, extending west-southwest across field:

X (ft)	forward time (msec)	reverse time (msec)
0	0	35.2
5	4.1	---
10	8.7	33.7
20	17.5	33.4
30	24.0	33.9
40	24.0	32.0
50	26.7	30.6
60	27.0	29.6
70	29.4	25.7
80	32.2	20.1
90	34.2	9.0
95	---	5.8
100	35.1	0

v1 = 1060 ft/sec (dry sediment).
v2 = 9300 ft/sec (bedrock).
Depth to bedrock 10.7 ft at east end, 14.4 ft on west end.
Bedrock surface rather flat; land rises about 3.5 degrees toward west.

15. Continuation WSW from western end of #14:

X (ft)	forward time (msec)	reverse time (msec)
0	0	---
10	9.1	40.0
20	22.9	37.9
30	32.0	37.0
40	36.1	36.8
50	36.3	29.8
60	37.3	26.7
70	39.0	26.0
80	43.3	21.4
90	44.2	7.9
100	45.1	0

v1 = 906 (loose dry sediment).
v2 = 4400 ft/sec (weathered bedrock?).
Great amount of scatter: irregular bedrock surface.

16. Continuation WSW from western end of #15:

X (ft)	forward time (msec)	reverse time (msec)
0	0	34.9
10	10.2	35.8
20	21.6	33.0
30	26.1	33.8
40	27.7	31.5
50	---	30.7
60	28.8	29.9
70	29.8	27.2
80	32.9	22.0
90	33.0	9.7
100	35.0	0

v1 = 910 ft/sec (dry, loose sediment or soil).
v2 = 8400 ft/sec (bedrock).
Depth to bedrock 11 ft.
Rather uniform bedrock surface.

17. Continuation WSW from western end of #16:

X (ft)	forward time (msec)	reverse time (msec)	
0	0	---	(wind interference)
10	8.8	---	
20	21.6	---	
30	26.8	31.5	
40	28.6	31.2	
50	30.6	31.3	
60	34.0	31.9	
70	34.5	27.2	
80	34.7	17.9	
90	36.0	8.8	
100	36.4	0	

v1 = 1030 ft/sec (dry sediment).

v2 = about 15,000 ft/sec (limestone).

Depth to bedrock about 12-15 ft.

Land rises gently toward west, but bedrock surface is rather flat.

18. Continuation WSW from western end of #17 to edge of woods, at a relatively high part of field:

X (ft)	forward time (msec)	reverse time (msec)
0	0	45.5
10	8.7	45.5
20	18.1	45.8
30	26.4	45.6
40	32.0	45.2
50	35.2	---
60	37.4	35.5
70	39.7	26.6
80	42.3	17.9
90	43.2	8.6
100	44.1	0

v1 = 1130 ft/sec (dry soil or sediment).

v2 = indistinct, but high (limestone).

Depth to bedrock approx. 15-20 ft.

APPENDIX 4 -- Location of Samples

List of samples collected for this project. Samples are listed out of numerical order so that those from the same area could be grouped together. See Figure 30 for map of sample locations.

MY SAMPLES	LOCATION + DESCRIPTION
2-4	Grabau Quarry. Bedrock.
8-12, 18, 31 138-151	Rubble pile at Mystery I, originally from route to Bomb Shelter, moved to Frozen Falls Pool, reexcavated for recent renovations and moved to rubble pile. Shelfstone.
120-122	Seven Springs. Bedrock.
131-135	Old toilet house, speleothems removed from Frozen Falls Pool area during renovations.
218a-218d	Hilltop above Mystery I, Cedar Valley Fm. Bedrock.
93-119	Cliff face at entrance to Mystery I. Bedrock.
137	Moquoketa Fm. Ceiling of Cathedral Room. Bedrock.
13	Turquoise Lake, granular raft debris.
204	Turquoise Lake, pool crust.
30	Turquoise Lake, folia.
225	Across Turquoise Lake, pool fingers, collected by Warren Netherton.
32	Bomb Shelter, flowstone.
216	Bomb Shelter, loose, recrystallized raft cone material.
33	Door-to-Door Route, raft cone material.
34	Door-to-Door Route, loose, raft cone material.
214	Door-to-Door Route, broken stalagmite.
210-213	Door-to-Door Route, flowstone and sediment at iron formation.
35-37	Garden of the Gods, sediment.
16-17	Blue Lake, botryoidal crust broken for trail building.
220-223	Blue Lake, Rugged Cross, for Rich Lively to date.
217	Angel Loop, silt.
38-47	Below the bar. Bedrock.
89-92	Fifth Avenue West. Bedrock.
205	Enigma Pit, projecting burrow.
206	Enigma Pit. Rafinesquina fossil.
49-77 77-88	Fifth Avenue. Bedrock.
15	Fifth avenue. Weathered bedrock.
6	Just before Dragon Jaw Lake, broken, iron-filled stalactite.
7	Just before Dragon Jaw Lake, broken soda straw.
20	Sugar Lake, granular material in drip cone.
152	Sugar Lake, flowstone over sediment.
200	Dragon Jaw Lake, pool crust.
128	Fireball Falls, broken stalactite.
130	Tar Pits, broken stalactite.
202	Tar Pits, western deep pool, shelfstone.
203	Tar Pits, shallow pool, pool crust.
123-124	Tar Pits, bedrock and silt.
219	Tar Pits, black flowstone
201	Tar Pits, western deep pool, pool crust
125	Lily Pad Lake, shelfstone
126	Lily Pad Lake, pool crust

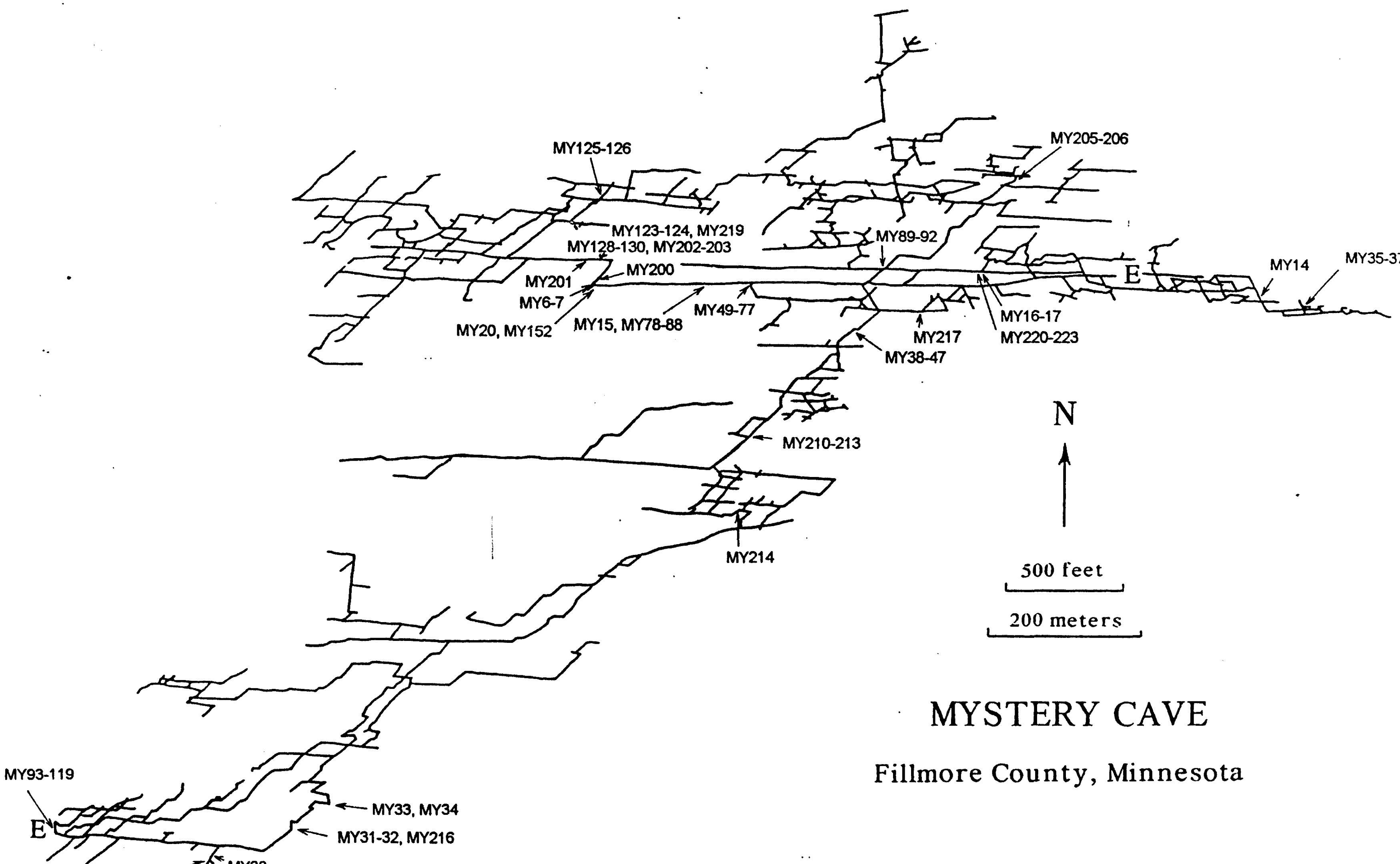

Figure 30: Location of bedrock and speleothem samples analyzed for this project.

APPENDIX 5: Description of Bedrock Samples Analyzed for this Project

SAMPLE #	DESCRIPTION	INSOLUBLE % if measured
	STEWARTVILLE FORMATION	
MY38	23 ft below top of Stewartville. Massive, mottled medium brown, burrowed, dolomitic fossiliferous limestone. Dolomite in burrows is sugary textured. Fossils float in patches of spar.	
MY39	20 ft below top of Stewartville. Massive, black mottled, burrowed, dolomitic limestone. Dolomite in burrows is sugary textured.	
MY40	18 ft below top of Stewartville. Massive, sparry, dolomitic limestone.	
MY41	13 ft below top of Stewartville. Massive, mottled-brown, burrowed, dolomitic, orange limestone wackestone. Dolomite in burrows is sugary textured and weathering out.	
MY42	10 ft below top of Stewartville. Massive, brown-mottled, burrowed, pinkish, dolomitic limestone wackestone. Scattered patches of spar. Dolomite in burrows. Some dolomite is partly altered to calcite. Stylolites.	
MY43	Bed SX1. Resistant, granular, mottled burrowed, medium brown, dolomitic limestone wackestone. Dolomite is dissolved at cave wall.	
MY44	Bed SX2. 1-2 inch thick, friable, granular, orange-mottled burrowed, light gray, dolomitized limestone wackestone. Dolomite in burrows is sugary. Stylolites. Dolomite is partly altered to calcite and is dissolved at cave wall. Spar replaced some fossils.	
MY45	Topmost bed of Stewartville. Resistant, dark brown, mottled, burrowed, dolomitic fossiliferous limestone. Dolomite partly altered to calcite. Dissolved at cave wall. Spar fossils weather outward and make the wall feel gritty. Burrow was recrystallized to spar - (gypsum?) Top of MY45 = Bedding Plane 1, the top of the Stewartville Formation.	
MY46	Bed SX3. Granular, brown "marker bed" sometimes defined as the top of the Stewartville Fm. Marker bed grades laterally into wavy disconformity with up to half a foot of relief. Dolomitized limestone wackestone with iron oxide after pyrite lined spar after gypsum in vugs and cracks. Dolomite is partly assimilated in spar.	
MY47	Topmost bed in Stewartville. Granular, yellow-mottled, dolomitic limestone wackestone, just below bedding plane 1. Bedrock has been brecciated and clasts float in spar after gypsum. Spar is concentrated along joints.	
	DUBUQUE FORMATION	
MY49	Bed DT1. Knobby, orange, dolomitic wackestone. Dolomite is partly altered to calcite and is dissolved at cave wall.	
MY52	Bed DT2. Brown dolomitic wackestone. Dark concentrations of iron and manganese oxides associated with dolomite. Overgrowths on some fossil fragments.	
MY50	Bed DT3. One of several closely spaced, .3 foot-thick, undulose beds. Medium gray dolomitic limestone mudstone and wackestone. Black-mottled iron oxide in dolomite.	
MY53	Bed DT3. One of several closely spaced, 0.3 foot-thick, undulose beds. Massive brown dolomitic limestone wackestone. Dolomite is partly altered to calcite. Overgrowths on some fossil fragments. Bedding plane 3 is at the top of the sequence of undulose beds.	
MY55	Bed DT4. Light gray, slightly dolomitic limestone wackestone. Black iron oxide. Dolomite is partly altered to calcite and is dissolved at cave wall.	
MY54	Bed DT4. Gray, slightly dolomitic limestone wackestone with large balls of iron oxide after pyrite. Dolomite is partly altered to calcite and is dissolved at cave wall.	
MY56	Bed DS1. First significant shale. Shaly, dolomitic limestone.	49%
MY57	Bed DL1. Medium crystalline, light gray-brown dolomitic limestone wackestone. Dolomite is corroded at cave wall.	
MY58	Bed DS2. Calcitic shale. Phosphatic fossil fragments. Iron oxide. Trace glauconite.	57%
MY59	Bed DL2. Gray mudstone to wackestone. Spar replaced some fossils.	

MY60	Bed DS3. First major shale bed. Some dolomite, phosphate and iron oxide.	52%
MY61	Bed DL3. Light brown limestone wackestone. Slightly dolomitic weathering to pores at cave wall. Spar has replaced some fossils. Some iron oxide.	
MY63	Bed DL4. Gray-brown, slightly dolomitic limestone mudstone to wackestone. Dolomite weathers to pores at cave wall. Some iron oxide and phosphate grains.	
MY65	Bed DL5. Slightly shaly, yellow-gray limestone wackestone. Some iron oxide and phosphate grains.	
MY66	Bed DS6. Slightly dolomitic, fissile, shaly limestone wackestone. Phosphate grains, some iron oxide.	34%
MY67	Bed DL6. Slightly dolomitic, unlaminated, brown-gray limestone wackestone. Fe oxide	
MY68	Bed DS7. Unlaminated, shaly, light gray limestone wackestone. Phosphate grains and iron oxide.	46%
MY69	Bed DL7. Massive, yellow-gray, shaly limestone wackestone. Iron oxide.	
MY70	Bed DS8. Dolomitic, shaly, nonlaminated, medium gray limestone wackestone. Iron oxide and phosphate grains. Poorly recessed, shaly zone.	52%
MY71	Bed DL8. Orange-brown, shaly limestone wackestone. Iron oxide and phosphate grains.	
MY72	Bed DS9. Yellow, calcitic shale. Iron oxide and phosphate grains.	65%
MY73	Bed DL9. Slightly dolomitic, shaly gray limestone wackestone. Spar fills voids between grains. Iron oxide and phosphate grains. Dolomite is dissolved next to cave.	
MY74	Bed DS10. Slightly dolomitic, calcitic shale. Iron oxide and large amount of phosphate grains. Dolomite looks detrital with corroded edges.	49%
MY75	Bed DL10. Shaly, medium brown, limestone wackestone. Spar filled some fossils. Iron oxide and some phosphate grains.	
MY76	Bed DS11. Slightly dolomitic, shaly, yellow-gray, fissile, laminated limestone wackestone. Iron oxide and phosphate grains.	
MY78	Bed DS11. Large masses of gypsum and iron oxide from the oxidation of pyrite in shale. Much iron oxide is moldic after euhedral gypsum crystals.	
MY77	Bed DL12. Shaly, fissile, limestone wackestone with yellow laminae. Iron oxide and phosphate grains	
MY79	Bed DL13. Shaly, brown, limestone wackestone. Iron oxide and phosphate grains. Trace dolomite.	
MY80	Bed DS14. Laminated, slightly dolomitic, calcitic dark brown shale. Iron oxide and some phosphate grains. Candidate for bentonite (still investigating).	
MY81	Bed DS14. Brown finely laminated, calcitic shale with fossils, iron oxide, phosphate.	72%
MY82	Bed DL14. Shaly, light brown limestone wackestone. Iron oxide and phosphate grains. Trace dolomite that has dissolved next to cave.	
MY83	Bed DS15. Dolomitic, shaly yellow-gray limestone wackestone. Iron oxide and phosphate grains.	
MY84	Bed DL15. Slightly dolomitic, shaly, yellow limestone wackestone. Some iron oxide and phosphate grains.	
MY85	Bed DS16. Thick, gummy dolomitic, calcitic, brown massive shale. Iron oxide and phosphate grains. Dolomite is altered to calcite.	69%
MY86	Bed DL16. Slightly shaly, light tan limestone wackestone. Trace dolomite. Iron oxide and phosphate grains.	
MY87	Bed DS17. Dolomitic, shaly, unlaminated limestone mudstone. Phosphate grains. Dolomite is altered to calcite.	77%
MY88	Bed DL17. Shaly, gray, limestone wackestone. Iron oxide and some phosphate grains. Trace dolomite.	
MY93	Bed DS18. Medium gray-brown shale. Trace dolomite. Few large fossil fragments. Phosphate.	79%

MY94	Bed DS19. Dolomitic, shaly, medium gray-brown limestone wackestone. Iron oxide and phosphate grains.	
MY95	Bed DL19. Dolomitic, shaly, brown-gray wackestone. Iron oxide and phosphate grains.	
MY96	Bed DS20. Dolomitic, shaly, light brown limestone wackestone. Iron oxide.	
MY90	Bed DS20. Gummy, dolomitic, yellow-brown, calcitic shale. Strong limonitic stain near base. Dolomite is altered to calcite. Iron oxide and phosphate grains.	58%
MY91	Bed DL20. Dolomitic, yellow, calcitic shale. Some fossils contain spar.	48%
MY97	Bed DL20. Brown, fossiliferous limestone wackestone. Trace dolomite and shale. Dolomite is dissolved to pores. Iron oxide and spar bind clusters of fossils.	
MY92	Bed DS21. Soft, yellow-gray, massive, calcitic shale with infrequent laminations of shell fragments and iron oxide. Phosphate grains and trace dolomite.	68%
MY99	Bed DL21. Shaly, white, massive limestone wackestone. Iron oxide.	
MY100	Bed DS22. Dolomitic, calcitic, dark gray shale. Iron oxide and phosphate grains. Concentration of fossil fragments at shale/limestone contact.	72%
MY101	Bed DL22. Shaly, yellow-orange, limestone wackestone. Iron oxide and phosphate grains. Burrow filled with spar (fossil floating in spar) after gypsum.	
MY102	Bed DS23. Dolomitic, dark gray, calcitic shale. Iron oxide, phosphate, chitinozoans.	
MY103	Bed DL23. Massive, dolomitic, light brown limestone wackestone. Spar has replaced scattered large fossils. Phosphate.	
MY104	Bed DS24. Dolomitic, thick, dark gray, shaly limestone wackestone. Phosphate grains, iron oxide and chitinozoans.	49%
MY106	Bed DS25. Thick dolomitic, brown, calcitic shale. Large amount of tiny, phosphatic fossils. Chitinozoans.	60%
MY107	Bed DL25. Dolomitic, gray-brown limestone wackestone. Phosphate grains and iron oxide. Some dolomite is altered to calcite.	
MY108	Bed DS26. Dolomitic, shaly, gray to yellow limestone wackestone. Nodules of spar. Phosphate grains and iron oxide.	37%
MY109	Bed DL26. Dolomitic, shaly, brown, limestone mudstone to wackestone. Phosphate grains and iron oxide.	
MY110	Bed DL27. Brown shale with flecks of organic material along bedding. Iron oxide and chitinozoans.	
MY111	Bed DS28. Dolomitic, calcitic, dark gray-brown shale. Iron oxide and chitinozoans.	80%
MY112	Bed DL28. Incompetent, dolomitic, shaly, light gray limestone wackestone. Iron oxide, phosphate grains and chitinozoans.	
MY113	Bed DL28. Dark brown, shaly dolomite. Fossils, iron oxide, some phosphate grains and chitinozoans.	28%
MY114	Bed DL29. Incompetent, brown, shaly dolomite. Scattered fossils. Irregular clusters of fossils cemented by overgrowths and spar.	
MY115	Bed DS30. Mottled, gray-brown, shaly dolomite. Scattered fossils. Iron oxide and chitinozoans. Some dolomite is altered to calcite. This is the last definite shale bed at the top of the Dubuque Formation.	
	MAQUOKETA FORMATION	
MY116	Base of Maquoketa. Yellow, shaly, dolomitic limestone wackestone. Scattered large fossils. Some phosphate. Some fossils replaced by spar. Undulatory bedding at base.	
MY117	3 ft above base of Maquoketa. Dolomitic, calcitic, yellow shale. Some phosphate grains and iron oxide.	
MY118	5 ft above base of Maquoketa. Medium gray, fissile, shaly dolomitic wackestone. Phosphate grains and iron oxide.	
MY119	9 ft above base of Maquoketa. Flaggy, medium-thin bedded, burrowed, light tan, shaly dolomitic mudstone. Iron oxide.	

APPENDIX 6: Grain Composition of Bedrock Samples

Point-count results for thin sections of bedrock samples are shown here. "Pores" in the dolomite column represent rhombic pores that were once dolomite but have since dissolved. They were not counted in the percentages. See Figure 2 for exact locations in the stratigraphic column.

SAMPLE	% SPAR	% CALCITE MUD	% DOLOMITE	% FOSSILS	% NON CARBONATE
MY38 (S'ville)	15	10	40	35	1
MY39 "		42	36	21	
MY40 "		24	56	21	
MY41 "		29	50	18	3
MY42 "		42	19	39	
MY43 (SX1)		34	41	25	.5
MY44 (SX2)	3	48	6	42	
MY45 (S'ville)		44	6	41	9
MY46 (SX3)	38	8	30	23	
MY49 (DT1)		7	67	27	
MY52 (DT2)		22	27	51	
MY50 (DT2)		33	52	15	
MY53 (DT2)		48	19	33	
MY55 (DT4)		64	pores	34	
MY54 (DT4)		50	12	38	
MY57 (DL1)		75	pores	25	
MY58 (DS2)		13	trace	27	60
MY59 (DL2)		74		26	
MY60 (DS3)		17	trace	17	67
MY61 (DL3)		81	trace	19	
MY63 (DL4)		47	pores	38	16
MY65 (DL5)		63	trace	7	29
MY66 (DS6)		43	10	13	34
MY67 (DL6)		88		9	3
MY68 (DS7)		25		25	50
MY69 (DL7)		73		9	18
MY70 (DS8)		37	pores	26	37
MY71 (DL8)		62		12	26
MY72 (DS9)		22		26	52
MY73 (DL9)		68	pores	25	8
MY74 (DS10)		16	trace	38	46
MY75 (DL10)		62		28	10
MY76 (DS11)		45	pores	50	5
MY77 (DL12)		77		12	11
MY79 (DL13)		13		33	54
MY80 (DS14)		6		21	73
MY81 (DS14)		5		24	71
MY82 (DL14)		58		27	15
MY83 (DS15)		9	9	55	27
MY84 (DL15)		72		16	12
MY85 (DS16)		40	3	6	51

MY86 (DL16)		70		24	6
MY87 (DS17)		54	trace	3	43
MY88 (DL17)		64		30	6
MY93 (DS18)		1		2	97
MY94 (DS19)		67	3	15	15
MY95 (DL19)		54	18	15	13
MY96 (DS20)		16	13	38	34
MY90 (DS20)	--	33	3	6	58
MY91 (DL20)		69		24	6
MY97 (DL20)		53	pores	45	2
MY92 (DS21)		5		9	86
MY99 (DL21)		74		12	14
MY100 (DS22)		6	3	3	88
MY101 (DL22)		69		16	15
MY102 (DS23)		5	26	13	57
MY103 (DL23)		37	27	36	
MY104 (DS24)		23	14	30	33
MY106 (DS25)		4	6	27	63
MY107 (DL25)		9	8	82	1
MY108 (DS26)		20	9	48	23
MY109 (DL26)		9	45	15	31
MY110 (DL27)				3	97
MY111 (DS28)		3	10	19	68
MY112 (DL28)		26	24	41	9
MY113 (DS29)			55	33	12
MY114 (DL29)			64	16	20
MY115 (DS30)			41	33	26
MY116 (M'keta)	6	45	29	15	5
MY117 "			44	4	52
MY118 "		5	69	18	8
MY119 "			91	1	8

APPENDIX 7: Clay Content of Bedrock Samples (from X-ray Diffraction)

SAMPLE	QUARTZ	ILLITE	MUSCOVITE	CHLORITE	KAOLINITE
MY56	x	x	x		
MY58	x	x	x		
MY60	x		x		
MY66	x	x	x		
MY68	x	x	x		
MY70	x	x	x		
MY72	x	x	x		
MY74	x	x	x		
MY81	x	x	x		
MY85 clay		x		x	x
MY85 coarse	x	x	x		x
MY87	x	x	x		
MY90	x	x		x	x
MY91	x	x	x		
MY92	x	x	x		
MY93 coarse	x	x	x		
MY98	x	x	x		
MY100	x	x	x		
MY104	x	x	x		
MY105	x				
MY106 clay	x	x		x	x
MY108	x	x	x		
MY113	x	x	x		
MY131	x		x		
MY137	x	x	x		

APPENDIX 8: X-ray Analysis of Speleothem Samples

Sample	Calcite, deg. 2-theta	Silica (SiO_2)	Description
MY8	29.50	2%	needles and blades from chenille spar, Mystery I
MY12	29.50	0	outer bladed crystals on ice, Mystery I
MY13	29.54	0	granular drip cone precipitate on floor of Turquoise Lake
MY14	0	aragonite	wall near Garden of Gods. Bedrock = dolomite
MY16	29.50 29.53	0 0	acicular crust on botryoids twinned pyramidal crystals Blue Lake pool crust
MY17	29.57	0	both inner yellow layer and outer layer, Blue Lake acicular pool crust
MY19	29.51 29.50	0 0	tiny bladed crystals on shrub-like stalk orange acicular crust Mystery I
MY30	29.52	0	folia, Turquoise Lake
MY32	29.52	0	Flowstone (twinned blades), Bomb Shelter
MY33a	29.52	0	raft cone fragments, Door-to-Door Route
MY33b	29.54	0	raft cone fragments, Door-to-Door Route
MY34	29.56	2%	cave ice from raft cone station T62 Door-to-Door Route
MY38	29.54	aragonite	Below the Bar, Stewartville bedrock, Mystery II
MY82	29.50 29.51	46% 7%	weathered, yellow bedrock unweathered, gray bedrock
MY86	29.47	5%	Bedrock
MY95	29.50	7%	Bedrock
MY116	29.47	0	Moonmilk on dolomite bedrock
MY129	29.52 29.58	0 1%	yellow inside soda straw outer white crust Tar Pits
MY131	29.49 29.495	12% 8%	limestone bedrock white crust on limestone
MY132	29.45 29.46	0 0	white, chalky crust on stal yellow center of stal Old Toilet House
MY143	29.52 29.55	0 1%	acicular flowstone layer over shrubs shrubs Mystery I
MY154	29.52 29.52	0 6%	acicular flowstone layer shrubs Mystery I
MY155	29.50 29.52	8% 0	shrubs below flowstone flowstone Mystery I
MY201	29.54	1%	subaqueous stacked plates to needles, Tar Pits deep lake
MY202	29.56	1%	shelfstone, vertical rhombs and silt, Tar Pits deep lake
MY203	29.575	0	botryoidal crust, vertical, stacked rhombs, Tar Pit shallow lake
MY204	29.505	0	chenille spar, bladed to stacked needles, Turquoise Lake

MY214	29.52 29.53	1% 0	outer edge, stalagmite center, stalagmite Door-to-Door Route
MY225	29.50	1%	pool fingers, stacked to radiating needles Input side of Turquoise Lake

APPENDIX 9: Speleothem Ages

Speleothem ages determined by Richard Lively, Minnesota Geological Survey, including measurements made for the LCMR Geology Project, arranged by age from youngest to oldest. See Figure 31 for map of sample locations.

SAMPLE	AGE (ka)	ERROR (years)	SITE DESCRIPTION
MC28d	.5	.1	Mystery III, base of mud pit, east of Eureka Ave.
MC28c	2	.1	Mystery III, base of mud pit, east of Eureka Ave.
MC28b	3.4	.1	Mystery III, base of mud pit, east of Eureka Ave.
MC28a	6	.4	Mystery III, base of mud pit, east of Eureka Ave.
MC9	7.7	.4	Mystery I, Bomb Shelter, top of flowstone layer
MC24	8.6	.5	Door-to-Door route, Big Fork, west of entrance to Wind Tunnel
MC8	9.6	.5	Mystery I, Bomb Shelter, middle layer of flowstone, shrubs
MC8609	10.3	.6	Mystery III. Just before entrance to second crawl. Small joint on right side of passage going in
MC1	11.98	1.3	Mystery II, Angel Route
MC25	12	.4	Door-to-Door route, entrance to Wind Tunnel, Big Fork area
MC7	12.2	.4	Mystery I, Bomb Shelter, base of thick flowstone overlying gravel deposit, shrubs
MC29	12.2	.4	Mystery I, main commercial passage about 150 feet west of entrance to Turquoise Lake
MC25a	12.3	.7	Door-to-Door route, entrance to Wind Tunnel
MC1	12.3	.3	Mystery II, Angel Route
MC1	12.6	.7	Mystery II, Angel Route
MC25b	12.7	.6	Door-to-Door route, entrance to Wind Tunnel
MC27	13	.6	Mystery III, Formation Route Creek
MC1	14.4	.8	Mystery II, Angel Route just east of Carrot Sticks
MC8603	14.5	.4	Mystery III. Along Helictite route just before boxwork
MC30	15	.2	Mystery III, above entrance to Helictite Route
MC1	15.4	1	Mystery II, Angel Route
MC8503	15.5	.3	Mystery II, area beyond Garden of the Gods
MC8605	16	.5	Mystery III. Boxwork area, after first crawl, and near second crawl; left side going in
MC1	16.8	3.1	Mystery II, Angel Route
MC8503	18	.5	Mystery II, area beyond Garden of the Gods
MC1	19.6	1.3	Mystery II, Angel Route
MC1	26.2	1.7	Mystery II, Angel Route
MC8505	34	1	Mystery II, top of side passage, entrance to Garden of Gods area, may not be original location
MC19d	36	2	Mystery II, west end of 5th Ave.
MC26a	38	1	Mystery II, 4th Ave., 1/2 to 2/3 distance from Wishing Well
MC19c	38	2	Mystery II. west end of 5th Ave.
MC21	41	1	Mystery III, Eureka Ave. entrance of passage going to Rotunda Room
MY222	49	2.4	Mystery II, Blue Lake, top half of uppermost part of more recent flowstone next to lake
MC8505	57	2	Mystery II, top of side passage, entrance to Garden of Gods area, may not be original location

MC19b	57	5	Mystery II, west end of 5th Ave.
MC19a	61	5	Mystery II, west end of 5th Ave, growing on top of breakdown, covered by newer breakdown
MC222	77.9	3.5	Mystery II, Blue Lake, lower half of uppermost, more recent flow-stone next to lake
MC8501	81	4	Mystery II, left side passage off commercial tour just prior to Garden of the Gods
D2	85	5	Mystery II, Dome Room, east of Blue Lake
MC5	85	3	Mystery II, west end of 5th Ave.
MY223	89	3.4	Mystery II, Blue Lake, botryoidal calcite below flowstone mound, subaqueous.
MC5	93	3	Mystery II, west end of 5th Ave.
MC5	97	4	Mystery II, west end of 5th Ave.
MC5	97	8	Mystery II, dig site opposite Dragon's Jaw Lake
MC13	101	4	Mystery II, layer capping sediment
MC5	101	4	Mystery II, west end of 5th Ave.
MC5	101	5	Mystery II, west end of 5th Ave. dig site
MC5	104	8	Mystery II, west end of 5th Ave. dig site
MC5	104	21	Mystery II, west end 5th Ave. dig site
MC20b	106	5	Mystery II, west end of 5th Ave., near Dragon's Jaw Lake
MC17	109	6	Mystery II, 4th Ave.
MC5	113	9	Mystery II, west end of 5th Ave., dig site
MC26b	116	7	Mystery II, 4th Ave., 1/2 to 2/3 of the way from Wishing Well to end of passage
MC10a	117	11	Mystery II, Enigma Pit, top of sediment, left side
MC26	119	5	Mystery II, 4th Ave., between Wishing Well and west end
MC18	121	6	Mystery II, 4th Ave., between wishing well and west end
MC8502	121	8	Mystery II, area beyond Garden of the Gods
MC14	122	11	Mystery II, Enigma Pit, middle flowstone layer
MC26d	123	5	Mystery II, 4th Ave., 1/2 to 2/3 from wishing well to end of pas-sage
MC4hg	124	7	Mystery II, dig site opposite Dragon Jaw Lake
MC3	126	11	Mystery II, west end of 5th Ave., near Dragon Jaw Lake
MC11b	128	6	Mystery II, Enigma Pit, on wall above sediments
MC3g	136	12	Mystery II, west end of 5th Ave. near Dragon's Jaw Lake
MC8504	137	7	Mystery II, base of broken stal on N side at east end of Garden of the Gods before entrance to Beyond Garden of the Gods
MC8601b	138	8	Mystery III. Along Lily Pad Route just up from Helictite Route
MC20a	141	11	Mystery II, west end of 5th Ave. near Dragon's Jaw Lake
MC3c	142	11	Mystery II, west end of 5th Ave. near Dragon's Jaw Lake
MC11a	142	9	Mystery II, Enigma Pit, north side of wall above sediment
MC16	146	10	Mystery II, Enigma Pit, 30 cm below top of sediment
MC16a	147	6	Mystery II, Enigma Pit, 30 cm below top of sediment
MC10b	150	19	Mystery II. Enigma Pit, top of sediment, north side
MC2	151	13	Mystery II. Enigma Pit, embedded upright in flowstone layer
MC5	151	32	Mystery II, west end of 5th Ave. dig site
MC8601a	152	8	Mystery III. Lily Pad Rte. west of junction with Helictite Route
MC6	158	10	Mystery II, entrance to Dragon's Jaw Lake, from ceiling of crawl
MC8601c	158	11	Mystery III, Lily Pad Route just beyond entrance to Helictite Rte.
MC4a	161	14	Mystery II, Tar Pits west end of 5th Ave.

MY220	179	10	Mystery II, oldest flowstone at mound by Blue Lake, same age as "Mushroom"
MC2a	183	16	Mystery II, Enigma Pit, flowstone
MR1	258	28	Mystery II, pit west of Blue Lake
MY221	>350		Mystery II, Blue Lake, topmost shelfstone on west end of flowstone mound, shrubs
MC3h	>350		Mystery II, west end of 5th Ave. near Dragon's Jaw Lake
MR1	>350		Mystery II, next to Blue Lake

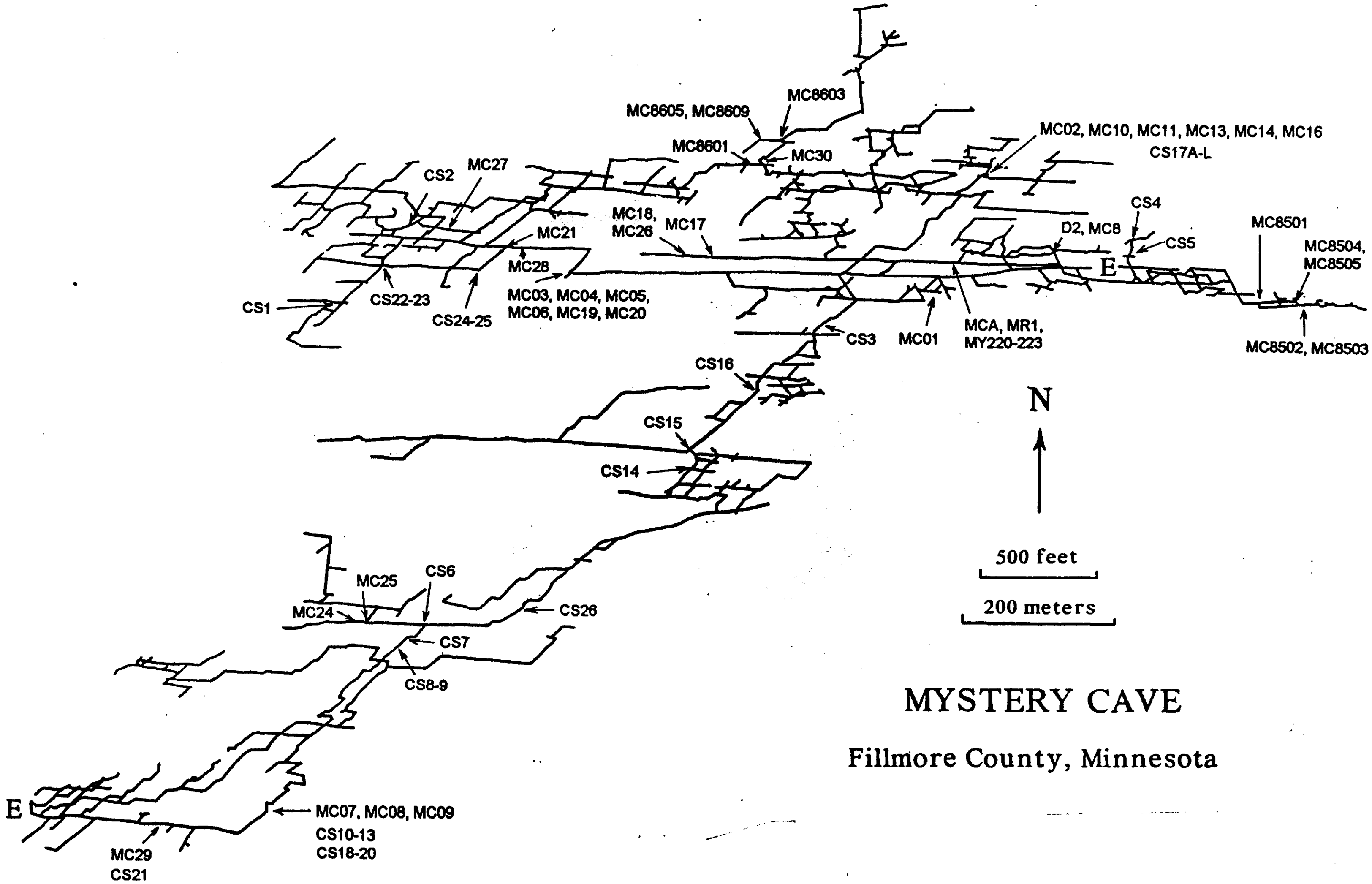

Figure 31: Location of speleothem samples used for radiometric dating by Richard Lively, (Minnesota Geological Survey) and for this project, and sediment samples (labeled CS) analyzed by Milske 1982).